Proceedings of the IAEA Symposium
on

CURRENT DISRUPTION

IN

TOROIDAL DEVICES

Garching, February 14-16, 1979

K. Lackner and H.P. Zehrfeld, Editors

IPP ~~3/51~~ III/51 Juli 1979

Max-Planck-Institut für Plasmaphysik
Garching, Germany

PREFACE

Attempts at raising the density or the plasma current in a tokamak above certain critical values generally result in termination of the discharge by a disruption. This sudden end of the plasma current and plasma confinement is accompanied by large induced voltages and currents in the outer structures which, in large tokamaks, can only be handled with considerable effort, and which will probably only be tolerable in reactors as rare accidents.

Because of its crucial importance for the construction and operation of tokamaks, this phenomenon and its theoretical interpretation were the subject of a three-day symposium organized by the International Atomic Energy Agency and Max-Planck-Institut für Plasmaphysik at Garching from February 14 to 16. Thirty-five papers of 20 or 30 minutes duration were presented during the first two days to an audience of 61 official participants and observers. The last day was dedicated to three summarizing panel discussions on

- Precondition for Disruption - Experimental Observation (Chairman: H.Wobig)
- Precondition for Disruption - Theory (Chairman: P. Rutherford)
- Dynamics of the Disruption (Co-chairman: H.Furth and B. Kadomtsev)

The scientific programme was organized by the Scientific Directors of the symposium

- H. Furth
- B. Kadomtsev
- D. Pfirsch

My particular thanks are due to the administrative secretary of the meeting, Ms. Riedl, and her colleague, Ms. Weinfurtner, who made the local organizing committee superfluous.

Garching, February 1979 K. Lackner

SYMPOSIUM ON CURRENT DISRUPTION IN TOROIDAL DEVICES

Session A: B.Waddell Memorial Session

Chairman: M.N.Rosenbluth

A 1 MULTIPLE HELICITY TEARING MODE CALCULATIONS: MAJOR DISRUPTIONS
B.Carreras, H.R.Hicks, J.A.Holmes and B.V.Waddell

A 2 ANOMALOUS RECONNECTION IN DISRUPTIVE PROCESSES IN TOKAMAK LIKE PLASMAS
D.Biskamp, H.Welter (rapporteured by B.Carreras)

A 3 PHENOMENOLOGICAL APPROACH TO THE DISCRIPTION OF CURRENT TERMINATION
B.B.Kadomtsev

A 4 REVIEW OF DISRUPTIVE PHENOMENA IN PULSATOR
F.Karger, W.Engelhardt, G.Fußmann, J.Gernhardt, E.Glock, S.v.Goeler, N.Gottardi, M.Kick, O.Klüber, G.Lisitano, H.-M.Mayer, K.McCormick, O.Meisel, H. Murmann, S.Sesnic and F.Wagner

A 5 DISCHARGES WITH AC-MODULATION
S.v.Goeler, J.Gernhardt, W.Engelhardt, F.Karger, O. Klüber, K.McCormick, H.-M.Mayer, D.Meisel, H.Murmann, F.Pohl and S.Sesnic

A 6 DISRUPTIVE INSTABILITY CAUSED BY IMPURITY ACCUMULATION
W.Engelhardt, O.Klüber, K.Lackner, S.Sesnic

Session B:

Chairman: E.Maschke

B 1 DYNAMICS OF DEVELOPMENT OF INTERNAL PERTURBATIONS DURING DISRUPTIVE INSTABILITY IN A TOKAMAK
S.V.Mirnov

B 2 STRUCTURE OF MAGNETIC FIELD PERTURBATIONS DURING DISRUPTIVE INSTABILITY IN A TOKAMAK
V.G.Mereshkin

B 3 ECONIMIC THEORY OF THE DISRUPTIVE INSTABILITY
H.P.Furth

B 4 ERGODIZATION OF RUNAWAY DRIFT SURFACES AND MAGNETIC SURFACES
G.Fußmann and H.P.Zehrfeld

B 5 VERY LOW-Q DISCHARGES FREE FROM MAJOR DISRUPTIONS IN DIVA
K.Odajima, M.Nagami, S.Yamamoto, H.Ohasa, S.Sengoku, H.Kimura, T.Yamauchi, K.Kumagai, A.Funahashi, H.Maeda,and Y.Shimomura

B 6 EXPERIMENTAL STUDY ON LIMIT OF THE SAFETY FACTOR IN JFT-2 TOKAMAK
M.Maeno, N.Suzuki, S.Konoshima, T.Yamamoto, M.Shimada,and N.Fujisawa (rapporteured by K.Odajima)

B 7 SURVEY OF MHD MODES AND THEIR EFFECTS IN ORMAK, ISX-A, and ISX-B
J.L.Dunlap, R.D.Burris, H.H.Harris, A.P.Navarro, and V.K.Paré

B 8 LOW-q(a) DISCHARGE BY CURRENT-DENSITY-PROFILE CONTROL IN THE RESISTIVE-SHELL TOKAMAK, JIPP T-II
K.Toi, S.Itoh, K.Kadota, F.Kawahata, N.Noda, K. Sakurai, K.Sato, S.Tanahashi and S.Yasue

Session C:

Chairman: D.Pfirsch

C 1 POLOIDAL ROTATION AS THE CAUSE OF THE m=1 MODE IN TOKAMAKS
A.A.Ware

C 2 NEOCLASSICAL THEORY OF THE SAWTOOTH OSCILLATIONS: AN m=O, n=O, POLOIDAL ROTATION INSTABILITY
A.A.Ware, R.D.Hazeltine, J.C.Wiley

C 3 VARIATIONAL CALCULATIONS OF THE NON-LINEAR GROWTH OF THE Q=1 ISLAND
A.Samain and M.Dubois

C 4 QUASI MHD NONLINEAR DISSIPATION AND THE MAJOR DISRUPTION
E.Minardi

C 5 INTERNAL AND EXTERNAL DISRUPTIVE INSTABILITIES IN THE PLT TOKAMAK
N.R.Sauthoff, S.v.Goeler, D.R.Eames, and W.Stodiek

C 6 SOME ASPECTS OF DISRUPTIVE INSTABILITIES IN ALCATOR A
I.H.Hutchinson and D.O.Overskei

C 7 ON THE STABLE REGIONS IN CURRENT V DENSITY PARAMETER SPACE WITH OHMIC AND ADDITIONAL HEATING
J.Hugill and A.J.Wootton

C 8 MHD MODEL OF CURRENT DISRUPTIONS IN TOKAMAK DISCHARGES
G.Lisitano

Session D:

Chairman: A.Gibson

D 1 SIMULATION OF TOKAMAK DISRUPTIONS
R.Pollard, M.Turner, A.Sykes and J.A.Wesson

D 2 STABILIZATION OF TEARING MODES: FEEDBACK STABILIZATION AND PROFILE TAILORING
H.R.Hicks, B.Carreras, J.A.Holmes, and B.V.Waddell

D 3 SINGLE HELICITY TEARING MODE EVOLUTION: MIRNOV OSCILLATIONS, SOFT AND INTERNAL DISRUPTIONS
B.Carrereas, J.D.Callen, H.R.Hicks and B.V.Waddell

D 4 HIGH BETA TEARING AND BALLOONING MODES IN TOKAMAKS
R.B.White, W.Park, D.A.Monticello, and H.Strauss

D 5 MHD-INSTABILITY OF OHMICALLY HEATED PLASMAS IN URAGAN II
J.K.Kuznetsov and U.M.Tonkoprjad

D 6 EFFECTS OF THE STELLARATOR FIELD ON THE MHD MODE BEHAVIOUR CLOSE TO THE DISRUPTION LIMIT IN W VII-A
W VII-A Team, presented by R.Jaenicke

D 7 DISRUPTIONS IN THE STELLARATOR W VII-A
- PART I -
W VII-A Team, presented by P.Smeulders

D 8 DISRUPTIONS IN THE STELLARATOR W VII-A
- PART II -
W VII-A Team, presented by P.Smeulders

D 9 SAWTOOTH OSCILLATIONS AND MAGNETIC ISLANDS IN THE TOSCA TOKAMAK

D.C.Robinson and K.M.McGuire

D 10 TOROIDAL PUMPING OF AN INTERNAL (m=1, n=1) MODE BY A TEARING MODE (m=2, n=1)

D.Edery, R.Pellat and J.L.Soulé

MULTIPLE HELICITY TEARING MODE CALCULATIONS: MAJOR DISRUPTIONS*

B. Carreras†, H. R. Hicks, J. A. Holmes, and B. V. Waddell††
Oak Ridge National Laboratory, Oak Ridge, Tennessee 37830

ABSTRACT: A dynamical mechanism to explain major disruptions in tokamaks is presented. It is based on the nonlinear interaction of tearing modes of different helicity.

The nonlinear evolution of tearing modes is being studied both numerically and analytically using the following three dimensional equations that are valid in cylindrical geometry in the low β limit[1]

$$\frac{D\psi}{Dt} \equiv \frac{\partial\psi}{\partial t} + \underline{v}_\perp \cdot \underline{\nabla}_\perp \psi = \eta J_\zeta - E^w_\zeta - \frac{\partial\phi}{\partial\zeta}$$

$$\frac{DU}{Dt} \equiv \frac{\partial U}{\partial t} + \underline{v}_\perp \cdot \underline{\nabla}_\perp U = -S^2 \nabla_\parallel J_\zeta$$

where the subscript ∥ denotes parallel to the total magnetic field, ⊥ denotes perpendicular to the toroidal direction, ψ is the poloidal flux function, ϕ is the velocity stream function, $J_\zeta = \nabla_\perp^2\psi/\mu_o$ is the toroidal current density, and $U = \nabla_\perp^2\phi$ is the ζ component of the vorticity. The parameter S is the ratio of the resistive diffusion time, $\tau_R[\equiv \mu_o a^2/\eta(o)$, where $\eta(o)$ is the resistivity at the plasma center] to the poloidal MHD time, $\tau_{Hp}[\equiv R_o/V_A$, where R_o is the major radius and V_A is the Alfven velocity].

The resistivity evolution has been incorporated through the electron heat conduction equation

$$\frac{DT}{Dt} \equiv \frac{\partial T}{\partial t} + \underline{v}_\perp \cdot \underline{\nabla}_\perp T = \hat{\chi}_\parallel \nabla_\parallel^2 T + \hat{\chi}_\perp \nabla_\perp^2 T + Q$$

where T is the electron temperature which we relate to the resistivity through Spitzer's formula. All these equations are in dimensionless form. A code RSF[2] using Fourier series expansions in ζ, toroidal, and θ, poloidal, angles has been developed to numerically advance these equations.

For profiles observed prior to major disruptions,[3,4] the m=2/n=1 and m=3/n=2 tearing modes are linearly unstable where m and n are the poloidal and toroidal mode numbers, respectively. We have been able to follow their nonlinear evolution with RSF. The essential result is that the 3/2 mode and other modes are nonlinearly destabilized on a rapid time scale ($t^{-1} \approx \gamma^0_{21}$) by the 2/1 mode [Fig. 1]. Due to the development of islands of different helicity the toroidal current density is severely deformed [Fig. 2]. These islands overlap and field lines become stochastic in a sizeable plasma volume [Fig. 3a], flattening the

temperature profile in this region through parallel heat transport [Fig. 3b]. The current deformation produces a rapid decrease in the self inductance of the plasma and the voltage at the limiter drops, becoming increasingly negative at the end of the run [Fig. 1], in agreement with the "negative voltage spikes" observed experimentally.

These results have been obtained for an ample range of parameters. The results shown in the figures are for the PLT equilibrium q profile prior to a major disruption[3] with $S = 10^6$, $\hat{\chi}_\parallel = 10^7$ ($\chi_\parallel = 10^{11}$cm^2/sec for PLT parameters) and $\hat{\chi}_\parallel/\hat{\chi}_\perp = 2.7 \times 10^8$.

We have studied a wide spectrum of equilibrium q profiles to have a better understanding of the characteristics of this nonlinear interaction. A very general result is that the strong destabilization of the 3/2 mode happens when

$$r_{21} - r_{32} < 1/2(W_{21} + W_{32})$$

where r_{mn} is the radial position of the singular surface for the m/n mode and W_{mn} is its single helicity saturated width. For all the cases we consider, the rapid destabilization of the 3/2 mode by the 2/1 starts when both magnetic islands touch. Apparently the usual resistive flow effects that reduce the mode growth from exponential to linear[5] are not operative in this explosive growth phase because the magnetic flux surfaces are being destroyed.

These results confirm the ones obtained when resistivity evolution is not taken into account,[1] except that here the disruption proceeds twice as fast. This time scale compares well with the experimentally observed time scale for the major disruption[7] [Fig. 4].

*Research sponsored by the Office of Fusion Energy (ETM), U.S. Department of Energy under contract W-7405-eng-26 with the Union Carbide Corporation.
†Visitor from Junta de Energia Nuclear, Madrid, Spain.
††Deceased September 14, 1978.

REFERENCES

1. H. R. Hicks, et al., ORNL/TM-6096, December 1977 (to be published).
2. H. R. Hicks, et al., Proc. 8th Conf. on Numerical Simulation of Plasmas, June 1978.
3. N. R. Sauthoff, et al., Nucl. Fusion 18 (1978) 1445.
4. S. V. Mirnov, et al., in Plasma Physics and Controlled Nuclear Fusion Research (Proc. 6th Int. Conf. Berchtesgaden, 1976) 1 (1977) 291.
5. P. H. Rutherford, Phys. Fluids 16 (1973) 1903.
6. B. V. Waddell, et al., Phys. Rev. Letters 41 (1978) 1386.
7. B. Carreras, et al., ORNL/TM-6175, March 1978 (to be published; J. D. Callen, et al., ORNL/TM-6564, September 1978 (to be published in the Proc. 7th Int. Conf. Innsbruck, 1978).

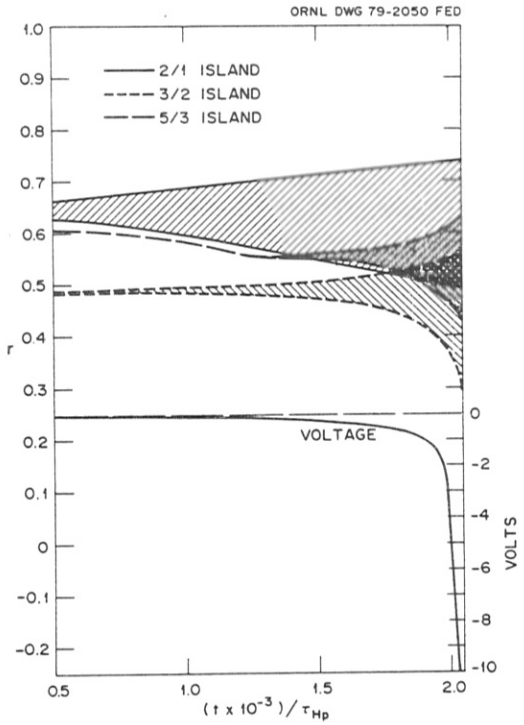

Fig. 1 The overlap of the 2/1 and 3/2 magnetic islands leads to an explosive growth. This is accompanied by a negative voltage spike.

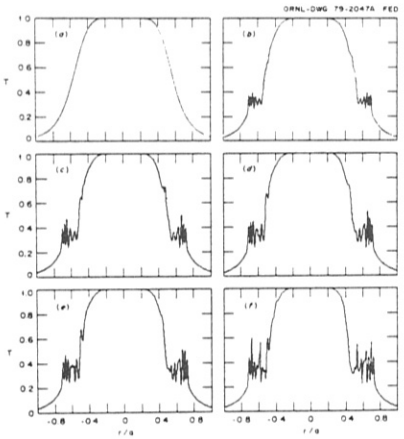

Fig. 2. Nonlinear evolution of the electron temperature profile.

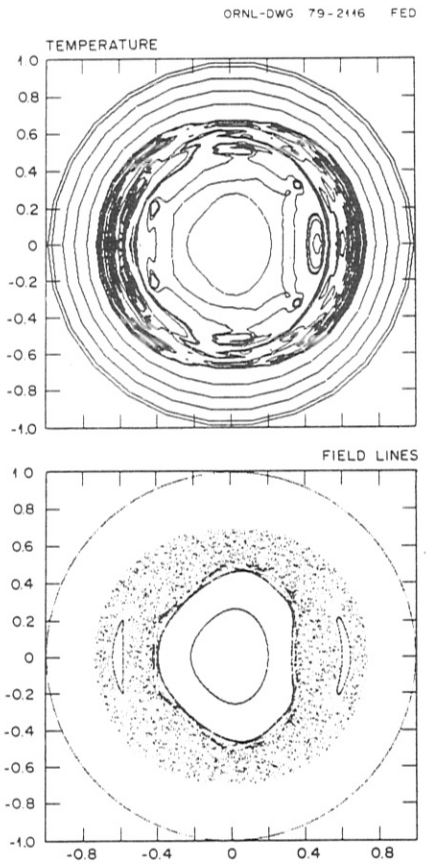

Fig. 3. Temperature contours and field line plot at t = 200 τ_{Hp}

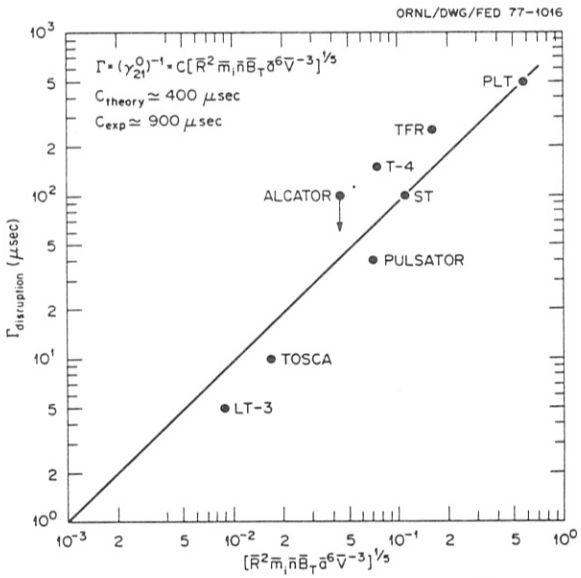

Fig. 4. Experimental time scale for the major disruption versus the theoretical time scale ($\Gamma \sim (\gamma_{21}^{0})^{-1} \sim \tau_R^{3/5} \cdot \tau_{Hp}^{2/5}$).

ANOMALOUS RECONNECTION IN DISRUPTIVE PROCESSES IN TOKAMAK LIKE PLASMAS

D. Biskamp,* H. Welter

Max-Planck-Institut für Plasmaphysik, 8046 Garching bei München

Abstract: A picture is given of the mechanisms that lead to rapid expansion of magnetic flux during disruptive processes in tokamaks. The competing role of resistivity and electron viscosity in the rapid growth of a (m,n) = (3,2) tearing mode in the presence of large (2,1) magnetic islands is studied quantitatively. When viscosity is dominating, the nonlinear growth rate scales as $\gamma \propto \mu^{1/6}$.

In present day low β tokamaks the only major source of free energy capable of driving instabilities to large amplitudes appears to be associated with the poloidal magnetic field, i.e. the current distribution. Since in a highly conductive plasma the magnetic field is essentially frozen in, the main difficulty in a theory of the disruptive processes observed in tokamaks is to explain the fast time scales, i.e. to give a mechanism for anomalous field penetration or, more pictorially, an anomalous rate of magnetic field reconnection. If reconnection takes place the electron temperature being essentially constant along field lines is changing on the same time scale.

The internal disruption, the steep part of the sawtooth oscillation, is conveniently explained in terms of the (m,n) = (1,1) tearing mode. Computer simulations show rapid growth to large amplitudes with nearly the linear growth rate, $\gamma \propto \eta^{1/3}$, in contrast to usual tearing modes (as in a plane configuration or $m \geq 2$ in a cylinder), which nonlinearly grow on the slow resistive time scale. The origin of this fast nonlinear process is, that the (1,1) mode is quasi MHD unstable, the MHD motion constituting the driving mechanism which enforces the high reconnection rate by pushing the plasma toward the x-point and generating a layer of large current density.

The external or major disruption is primarily located in the outer region of the plasma where q>1 and has to do with modes $m \geq 2$, which are usually strongly MHD stable and hence develop nonlinearly only on the resistive diffusion time scale. Thus a single tearing mode by itself cannot account for the major disruption. Since, however, prior to a disruption a (2,1)-magnetic perturbation grows to large amplitude, the equilibrium state immediately before the disruption is no longer axisymmetric but helically distorted, which is likely to give rise to MHD instability of other modes with different helicity. It has been shown that in this configuration the (1,1) mode is MHD unstable, driving a (3,2)-mode outside the q=1 surface [1]. It is therefore indicated to investigate the growth of (1,1)- or (3,2)-tearing modes in the presence of a large amplitude (2,1)-mode.

These mode coupling processes have been studied numerically using a 3D code to solve the reduced set of MHD equations for the vector potential ψ, $\nabla z \times \nabla\psi$ = poloidal magnetic field, and the stream function ϕ, $\nabla z \times \nabla\phi$ = perpendicular plasma velocity:

$$(1)\quad \frac{\partial\psi}{\partial t} - \underline{B}\cdot\nabla\phi = \eta j - \mu\nabla_\perp^2 j$$

$$(2)\quad \left(\frac{\partial}{\partial t} + v_\perp\cdot\nabla\right)\nabla_\perp^2\phi = \underline{B}\cdot\nabla\underline{j}\ , \qquad \nabla_\perp^2\psi = j.$$

Here η is the normalized resistivity = $\eta\tau_A$, μ the normalized perpendicular (anomalous) electron viscosity = $\mu_e(\tau_A/a^2)\,(c/\omega_{pe}a)^2$, a = plasma radius.

The coupling to the (3,2) mode is particularly effective, if the spatial separation of q=1.5 and q=2 is small, i.e. if both surfaces are located in the steep flanks of the current profile. Numerical simulations show the rapid growth of the (3,2) mode [2]. In contrast to the (1,1) internal disruption the fast reconnection process is not connected to isolated intense currents at the x-points of the (3,2) mode, but is due to stochastic field line behavior. As soon as the islands of the (3,2) and (2,1) modes have reached a certain size ("islands overlap"), field lines become ergodic instead of forming smooth surfaces, starting around the x-points and soon filling a large area as the modes continue to grow. Within the ergodic regions the concepts of magnetic flux or topology conservation have no meaning and reconnection can proceed at a fast rate. Stochastic field line behavior per se,however, is not connected with dissipation (apart from the irreversible temperature relaxation). Dissipation seems to enter through the response of the current density to the random magnetic field line behavior. Since the current tends to flow along field lines, $B\cdot\nabla j \simeq 0$ in (2), it necessarily breaks up into filaments of increasingly fine scale in the ergodic regions, thus strongly enhancing resistive and viscous effects. This current filamentation is a dominant feature observed in the numerical simulations.

We have studied in detail the competing dissipative effects of resistivity and electron viscosity. The current profile chosen is rather square shaped, $j \propto (1+r^8)^{-5/4}$, with q(0) = 1.15 and 1.4, so that both (2,1)- and (3,2) tearing modes are strongly unstable and lead to particularly large single mode island widths. The values of $\eta(r_s)$ were 2×10^{-5}, 2×10^{-6}, 0, $\eta(r) \propto j(r)^{-1}$, and those of μ 10^{-8}, 10^{-7}, $\mu(r)$ = const. We usually adopted the boundary condition of fixed axial electric field E_0 (loop voltage $U = 2\pi RE_0$), so that $E_0 = \eta j$ in equilibrium. The relative importance of the η and the μ terms in (1) are most easily read off from their contributions to the energy balance

$$(3)\quad \frac{d}{dt}\int dx^3\left(\frac{|\nabla\psi|^2}{2} + \frac{|\nabla\phi|^2}{2}\right) + P_\eta + P_\mu = UI,$$

where $P_\eta = \int dx^3 \eta j^2$, $P_\mu = \int dx^3 \mu\,(\nabla j)^2$. We find that in the phase of maximum growth of the (3,2) mode typically, $P_\mu > P_\eta$ as soon as $\mu > 3\times10^{-3}\eta$. This gives a conservative estimate of the importance of μ, since the growth rates are already dominated by viscosity at still smaller values of μ, $\mu > 10^{-3}\eta$. The dependence of the growth rate on μ is weak, $\gamma_{32} \propto \mu^{1/6}$, as compared with $\mu^{1/3}$ for the linear viscosity driven tearing mode [3]. Comparing P_μ for different μ we obtain an estimate of the scaling of the spatial dimensions of the current filaments, $k \simeq k_r \propto \mu^{1/4}$. The scalings for both $\gamma(\mu)$ and $k(\mu)$ are

consistent with the balance

$$\frac{\partial \psi}{\partial t} \sim \mu \nabla^4 \psi \ .$$

The total increase of the plasma current $\Delta I/I$ is about 2-3% in the most violently unstable cases, somewhat more than observed in Pulsator [4], where part of the change of the plasma inductance is accounted for by the negative voltage spike U

$$-\dot{L} = \frac{\dot{I}}{I} L - U$$

To obtain a significant change of the total plasma current the resistivity must be sufficiently high in the outer plasma region to prevent induction of strong reversed currents as the current channel broadens rapidly. Although the value $\mu = 10^{-3}\eta$ necessary to make the viscosity dominant appears to be quite small, it is still larger by a factor of at least 10^2 than the collisional value $\mu_e \sim \rho_e^2 \nu_e$. On the other hand this is an absolute lower limit, and there are various mechanisms that could strongly increase the effective value of μ_e taking it above the threshold indicated, e.g. driven by the strong gradients in the current density [5]. Once in the viscosity dominated region, the dynamical behavior is very insensitive to the magnitude of μ.

References

1. D. Edery, G. Laval, R. Pellat, F.L. Soulé, Phys. Fluids 19, 260 (1976).

2. B.V. Waddell, B. Carreras, H.R. Hicks, J.A. Homes, D.K. Lee, Phys. Rev. Letters 41, 1383 (1978).

3. H.P. Furth, P.H. Rutherford, H. Selberg, Phys. Fluids 16, 1054 (1973).

4. F. Karger et al., Plasma Physics and Controlled Nuclear Fusion Research, Vienna 1977, Vol. I, p. 267.

5. W. Horton, Jr., Phys. Rev. Letters 28, 1506 (1972).

Figure Captions

Fig. 1 Destruction of magnetic surfaces. $q(0) = 1.15$, $\eta = 2 \times 10^{-5}$, $\mu = 10^{-7}$.

Fig. 2 Local current profile for $q(0) = 1.15$, $\eta = 2 \times 10^{-6}$, $\mu = 0$.

Fig. 3 Current profile as in Fig. 2, but $\mu = 10^{-8}$.

* Present address: The Fusion Research Center, Physics Department, The University of Texas at Austin, Austin, Texas 78712

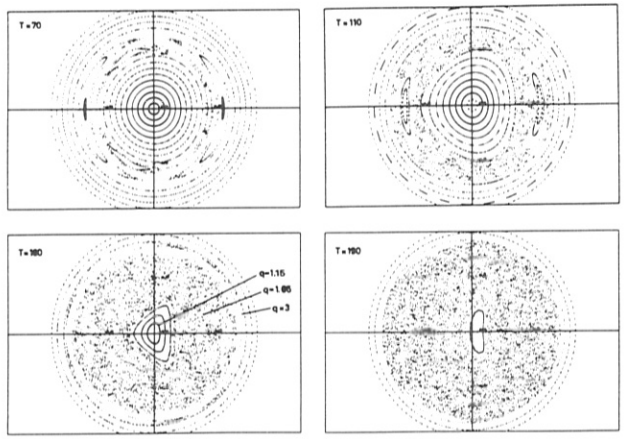

Fig. 1

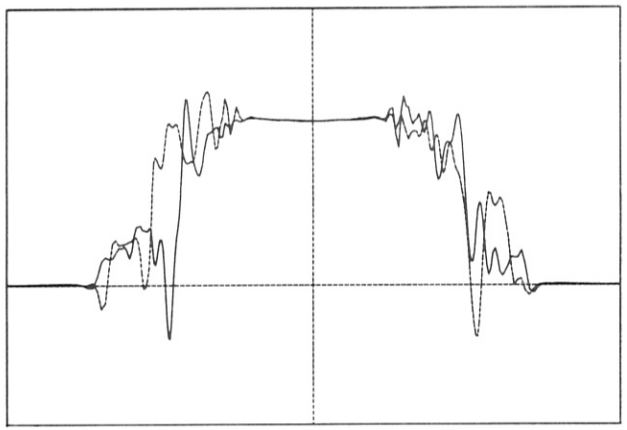

Fig. 2

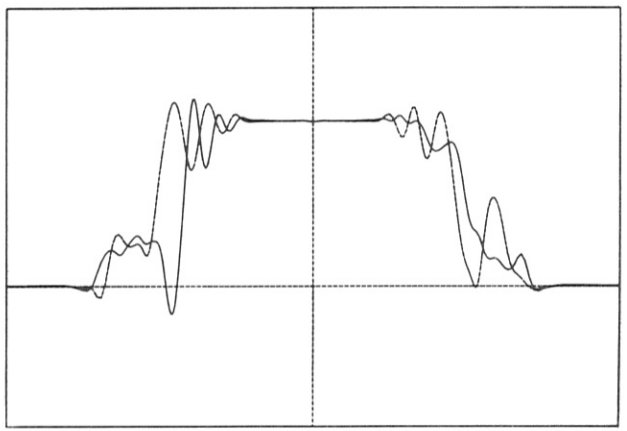

Fig. 3

Phenomenological Approach to the Description of Current Termination

B.B. Kadomtsev
I.V.Kurchatov Institute of Atomic Energy
Moscow, USSR

Experimental data and numerical simulations both show that the current disruption in tokamaks starts with low m-number helical MHD modes and leads to the reconnection of magnetic field lines. The final stage usually terminates with a total current drop. Experiments suggest that in this stage the MHD activity looks like small-scale turbulence of field lines. We shall discuss here some features of this turbulence. In tokamak ordering $B_z \gg B_\theta$ and hence B_z remains approximately constant. For the averaged azimuthal component B_θ we have

$$\frac{\partial B_\theta}{\partial t} = c \frac{\partial E_z}{\partial r} \tag{1}$$

where E_z is the averaged z-component of the electrical field. Averaging the z-component of Ohm's law one gets:

$$E_z + \frac{1}{c} \left\langle \tilde{v}_r \tilde{B}_\theta - \tilde{v}_\theta \tilde{B}_z \right\rangle = \frac{j_z}{\sigma} \tag{2}$$

If the MHD turbulence is of small-scale nature, the averaged value in (2) should be related to the local characteristics of the magnetic field - its own value and its radial derivative:

$$\left\langle \tilde{v}_r \tilde{B}_\theta - \tilde{v}_\theta \tilde{B}_z \right\rangle = vB_\theta - D \frac{\partial B_\theta}{\partial r} \tag{3}$$

with v and D proportional to the level of turbulence. The quantity v has the meaning of a transport velocity of magnetic field lines, and D looks like a diffusion coefficient. For $\sigma \to \infty$ and after substitution of E_x from equation (2), equation (1) becomes

$$\frac{\partial B_\theta}{\partial t} = \frac{\partial}{\partial r} \left(D \cdot \frac{\partial B_\theta}{\partial r} - vB_\theta \right) \tag{4}$$

Now we can try different assumptions on the functional dependence of D on v. The most natural is to suppose that equation (4) leads to flattening of the $\mu(r)$ distribution, where $\mu(r) = 1/q(r)$ is proportional to the pitch of the magnetic field lines. This corresponds to the assumption $v = D/r$, which leads to

$$\frac{\partial B_\theta}{\partial t} = \frac{\partial}{\partial r} \left(rD \frac{\partial}{\partial r} \left(\frac{B_\theta}{r} \right) \right) \qquad \frac{\partial \mu}{\partial t} = \frac{1}{r} \frac{\partial}{\partial r} \left(rD \frac{\partial \mu}{\partial r} \right) \tag{5}$$

On the other hand, as was argued by J.B. Taylor, the reconnection should conserve the invariant

$$K_o = \int \vec{A} \cdot \vec{B} \, d^3 r$$

for given $\chi(a)$, where $\chi = \int_a^r B_\theta dr'$, with a being the radius of the copper shell, this invariant may be written as $K_o = \int_o^a B_\theta r^2 dr$. Multiplying (4) by $r^2 dr$ and integrating it by parts we obtain (assuming $D = 0$ at $r = a$):

$$\int_o^a \left(vr + \frac{\partial}{\partial r} (Dr) \right) B_\theta \, dr = 0 \tag{6}$$

For arbitrary B_θ this implies $v = -\frac{\partial}{r \partial r}(rD)$. In this case, after integration over r, equation (4) can be written in the form

$$\frac{\partial \chi}{\partial t} = \frac{1}{r} \frac{\partial}{\partial r} \left(rD \frac{\partial \chi}{\partial r} \right) \tag{7}.$$

This equation would lead to $\chi = \text{const.}$ for the final state. In fact, however, this may not be so, because D should be different from zero only when MHD turbulence is fed by energy. In other words, reconnection should take place only if $\partial \varepsilon / \partial t < 0$, where ε is the energy of the poloidal magnetic

field. Multiplying (4) by $B_\Theta r dr$ and integrating it over r we obtain:

$$\frac{\partial \mathcal{E}}{\partial t} = - \int_0^a (D \frac{\partial B_\Theta}{\partial r} - v B_\Theta) j_z r dr \qquad (8)$$

We suppose, that $B_\Theta > 0$, $j_z > 0$. In addition to this we assume, that in the final state of the disruption the current distribution is more or less flattened so that $B_\Theta \sim r$. We see from eq.(8) that the assumption $v = D/r$ leads for $B_\Theta \sim r$ to the relation $\dot{\mathcal{E}} = 0$. In this case therefore the energy is not given to the field so that turbulence may exist. The relation $v = - \frac{1}{r} \frac{\partial}{\partial r} (rD)$ consistent with K_o-conservation gives $\dot{\mathcal{E}} < 0$, i.e. feeding of turbulence only if D decreases with r not steeper than $1/r^2$. For $D = \text{const.}/r^2$ both K_o-conservation and flattening of u are consistent.

The assumption $D = \text{const.}/r^2$ implies that MHD turbulence is maintained over the whole plasma column at some self-consistent level. A drop of D near the wall would lead to a stabilizing effect.

In conclusion we can say:

1. The description of current decay in terms of magnetic field line diffusion and convection produced by local MHD turbulence leads us to the conclusion that self-consistent turbulence covers the whole plasma column, so that D const/r^2 for a flattened current distribution.
2. MHD turbulence seems to be able only to maintain the current distribution flat, but not to reduce the total current (because diffusion of fields is compensated by convection with $v = D/r$.). This means that the real decay of current may be controlled by the resistivity in the boundary layer of the plasma.
3. If D drops near the wall due to the stabilizing effect of a copper shell, $\dot{\mathcal{E}}$ may change sign and the turbulence may be damped. This means that a copper shell may help to increase the current decay time during its termination phase.

Review of Disruptive Phenomena in Pulsator

F.Karger, W.Engelhardt, G.Fußmann, J.Gernhardt, E.Glock, S.v.Goeler, N.Gottardi, M.Kick, O.Klüber, G.Lisitano, H.-M.Mayer, K.McCormick, O.Meisel, H.Murmann, S.Sesnic and F.Wagner

Max-Planck-Institut für Plasmaphysik, EURATOM-IPP-Assoc. 8046 Garching, Fed.Rep.of Germany

Introduction

There is a sharp limit to the electron density obtainable in Pulsator /1/. It corresponds to 27 fringes of the microwave interferometer or to a central density of $1.8 \times 10^{14}\,cm^{-3}$ for a parabolic profile. This value has been reached in many discharge series, but the current disruption always occurs before the 28th fringe. The main aim of the disruption investigations in Pulsator is therefore to understand and possibly exceed this density limit.

Symptoms of Disruptions

The disruption, which limits the density in Pulsator, was described in detail in /2/. The disruption is preceded by two coupled modes which grow within several ms. When their amplitude is high enough, the disruption occurs on a much faster time scale. First many of the runaways hit the limiter, thus producing a burst of hard X-rays. Within 20 ... 200 µs the loop voltage decreases, the temperature in the centre drops and negative voltage and positive current spikes occur together with a fast inward motion and expansion of the plasma column. The following current decay again has a slower time scale and is accompanied by several of the mentioned fast disruptions with different strength.

Often one observes for some periods before the first negative voltage spike a pattern in the soft X-ray signals which can be interpreted as an m=2 mode modulated by an m=1 mode. This is shown in Fig. 1 for the case of a soft disruption preceding the main disruption. During the last (weak) sawtooth the m=1 oscillations on positions a/6 and a/3 are still almost exactly in phase. In contrast,the oscillations during the following soft external disruption show a monotonically increasing phase shift going from top to bottom as indicated by the dotted lines, the shape of which continues until the outermost channels (not shown in the picture). Sometimes the mode stops rotating for several periods before the main disruption. This is also illustrated in Fig. 1.

During the slow current increase, especially in low-q operation, there may be a current disruption preceded by many small spikes (soft external disruptions) which apparently do not affect the current until the main disruption (Fig. 2). In this case the soft disruptions and also the main disruption are preceded by an m=2 oscillation (Fig. 3) the frequency and growth rate of which are more than an order of magnitude larger than in the case of the above mentioned disruption which limits the density (Fig. 1).The plasma parameters are not very different.

In some cases, during the first rise of the density, one can observe a phenomenon which resembles one of the last mentioned spikes, but which is not followed by a current disruption (Fig. 2 in /3/). A fourth type of disruption can be externally induced by a resonant helical m=2, n=1 field. In this case the action of the m=2 mode is replaced by the external m=2 field. Beginning with the hard X-ray burst it shows the same pattern as the spontaneous disruption.

Causes of disruption

There are three indications that flatter current profiles which produce steeper gradients on the q=2 surface and which should thereby give rise to unstable tearing modes, are more susceptible to disruption.

1. The internal disruption periodically produces this type of profile. In fact, one observes especially for low-q discharges a modulation of the m=2 mode by the sawtooth relaxation (Fig. 4). The external disruption occurs then in most cases a short time after the internal disruption. With an external helical field resonant to the q=1 surface it was possible to influence the q=1 surface and induce disruption. The harmonic islands produced on the q=2 surface, however, are also large enough to explain the disruption /4/.
2. In Pulsator an impurity accumulation in the centre of the discharge, followed by disruption, can be observed at medium densities /5/. This accumulation is connected with flattening of the temperature and hence current profiles, which again turns out to lead to instability.
3. It is more difficult to reach the highest densities for low q(a) than for $q(a) \sim 4$ because the low-q profiles are flatter in the centre and apparently more unstable.

There are still results which do not fit into the picture of destabilising tearing modes. During both the increase of density by gas puffing and the modulation of the plasma current by low frequency /6/,profiles occur which theoretically should be unstable, but experimentally are not. In addition, the current profile cannot be the only explanation for the high density limit. It is possible, that the higher degree of ergodization, which arises when, with increasing ß, islands on rational surfaces are pressed together on the outside, is an explanation of the observation, that a mode with a certain amplitude is more likely to trigger a disruption in the case of high densities /7/.

Means of Avoiding Disruption

Besides the rates of plasma current increase and gas puffing Pulsator has still another means of influencing the current profile. By activating the m=2, n=1 windings with a DC current the profile can be flattened locally on the q=2 surface /8/. This results in a reduced amplitude of the m=2 and postponing of the disruption /2/, /9/.

By means of this effect it was attempted to extend the above mentioned density limit of 27 fringes in th low-q(a) case (Fig.5). Without a resonant helical field the discharge reaches between 20 and 27 fringes. With the helical field a density of 34 fringes was obtained corresponding to a peak density of 2.2 x 10^{14} cm^{-3} for a parabolic profile. An indication of the profile change by the resonant helical field is the increase of the sawtooth amplitude, when the helical field is switched on (Fig. 5). The increase in density is not very large, but it shows, that the gradient in the current profile is at least one determining factor in the density limit. It can be assumed that feedback control of the m=2 winding can extend the density limit even more.

In this low-q discharge sometimes the disruption during current increase with fast growing m=2 (Fig. 2 and 3) occurs. This disruption cannot be suppressed by the resonant helical field or changing the rate of current increase. But it has been found that the plasma can be stabilized when, before the point of disruption, it is displaced about 1 cm to the inside of the limiter for a few ms by an appropriately high pulse in the vertical field and then allowed to expand freely back to the normal position. Even though it is not yet clear how this "hammer" works, it is nevertheless very reliable.

References

/1/ W.ENGELHARDT et al., 7th Int.Conf.Plasma Phys.and Contr.Nucl. Fus.Res., Innsbruck,1978,IAEA-CN-37/A5

/2/ F.KARGER at al., 6th Int.Conf.Plasma Phys. and Contr.Nucl. Fus.Res., Berchtesgaden,1976,IAEA-CN-35/A7

/3/ G.FUSSMANN et al., 7th Int.Conf.Plasma Phys. and Contr.Nucl. Fus.Res.,Innsbruck,1978,IAEA-CN-37/T4

/4/ F.KARGER et al., 7th Int.Conf.Plasma Phys. and Contr.Nucl. Fus.Res.,Innsbruck,1978,IAEA-CN-37/T4 Extended synopses,pg.40

/5/ W.ENGELHARDT et al., this symposium

/6/ S.v.GOELER et al., this symposium

/7/ G.FUSSMANN et al., this symposium

/8/ F.KARGER et al., 8th Europ.Conf.Contr.Fus. and Plasma Phys., 1, Prague (1977) 3

/9/ F.KARGER et al., 5th Inf.Conf.Plasma Phys.and Contr.Nucl.Fus. Res.,Tokyo,1974,IAEA-CN-33/PD 2

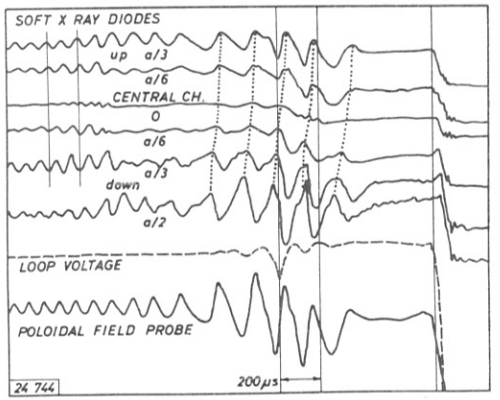

Fig. 1 Oscillogram showing the oscillations before disruption

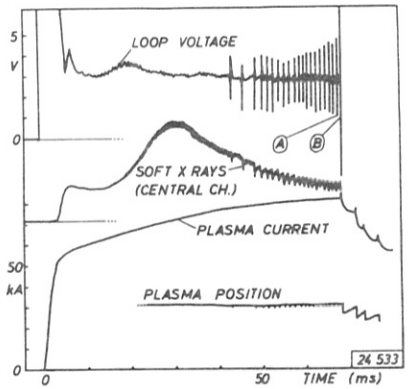

Fig. 2 Discharge with external disruptions during the current rise

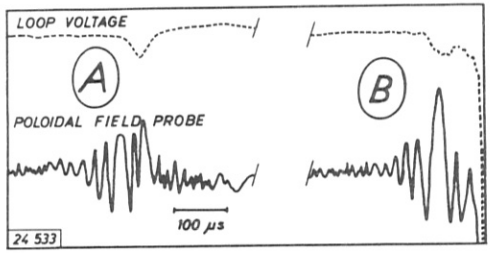

Fig.3 Expanded views at the two times A and B of Fig. 2

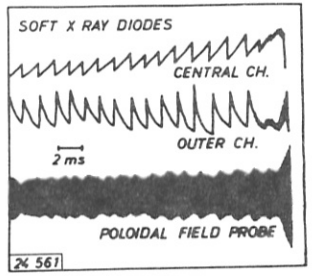

Fig.4 Oscillogram showing modulation of the m=2 mode amplitude by internal disruptions

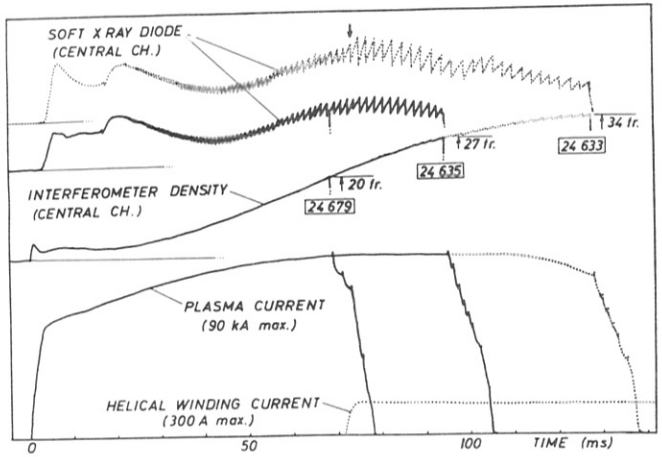

Fig.5 Low-q high density discharges without (solid line) and with (dotted line) stabilizing helical field

Discharges with AC-Modulation

S.von Goeler[+], J.Gernhardt, W.Engelhardt, F.Karger, O.Klüber, K.McCormick, H.M.Mayer, D.Meisel, H.Murmann, F.Pohl and S.Sesnic.

Max-Planck-Institut für Plasmaphysik, EURATOM-IPP Association
8046 Garching, Fed.Rep.of Germany

Practically all major disruptions in tokamaks are preceded by growing precursor oscillations with poloidal and toroidal mode numbers m=2 and n=1, and these oscillations are in general thought to be tearing modes. According to tearing mode theory /1,2,3/, growth of the instability depends mostly on the radial distribution j(r) of the plasma current, and it is therefore of interest to do experiments in which the current profile of a tokamak discharge is drastically changed. For this reason we started an experimental program on Pulsator two months ago to modulate the plasma current with an ac-component. In this case the change in the current distribution stems from the skin effect. Experiments on the skin effect with small ac-modulations were already performed earlier on the ST-tokamak /4/ and on TFR /5/ in order to study the conductivity profile and the radial Z_{eff} distribution. Our experiments aim at the disruptive instability and we report here our first and still somewhat preliminary results on these investigations.

The ac-modulation is produced on the primary side of the OH-transformer by an LC-circuit, which consists of a 10.5 mF/7 kV condensor bank and a 400 µH inductance. The frequency of the modulation is varied from 60 Hz to 800 Hz by changing the capacity of the LC-circuit. The oscillations (Fig.1) are slightly damped due to the L/R-time of the circuit. No measurement of the current distribution produced by the ac-modulation is available at present, but we hope to obtain such data in the near future with the lithium beam diagnostic. In the meantime, we rely on computer calculations of the skin effect, in which the plasma is treated as a motionless conductor with a time independent resistivity profile. Typical computer output from this code is shown in Fig.2: The ac-modulation produces an inward travelling wave, the envelope of which rises from the plasma edge to a maximum and then drops sharply towards the plasma center. There are considerable uncertainties in these predictions because the skin effect depends sensitively on the conductivity near the plasma edge which is unknown at present.

[+] On leave from the Plasma Physics Laboratory of Princeton University

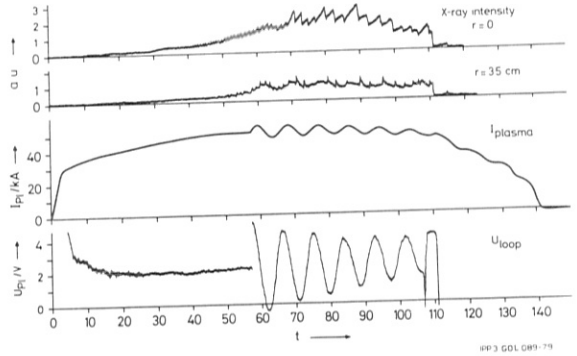

Fig.1: AC-modulation with 110 Hz. The soft X-ray emission, the plasma current I_{pl} and the loop voltage U_{pl} are plotted as a function of time. At low frequencies the skin current can penetrate to the center of the discharge, where it modulates the amplitude, frequency and radial extend of the sawtooth oscillations.

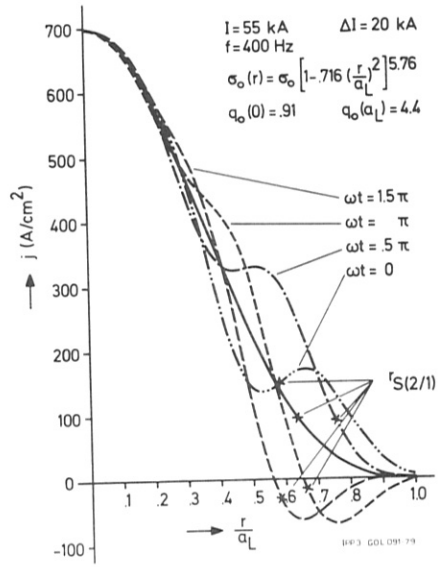

Fig.2: Radial profiles of the current density j(r) during the ac-modulation according to the skin effect code. The phase ωt is taken in respect to the maximum of the applied voltage.

In the Pulsator experiment the amplitude of the ac-modulation was turned up until the discharge disrupted. The onset of the disruption with increasing amplitude ΔI was not very sharp: At first there appeared some MHD activity on the B_θ loops. This MHD activity leads then to minor disruptions which were registered on the soft X-ray and voltage traces. Finally after a further increase in ΔI, a large current disruption was produced. The amplitude, ΔI_{crit}, where disruption occurred, depended strongly on discharge conditions and frequency. In 55 kA discharge of moderate density and with q(a)=4.5 we were able to produce a 300 Hz-modulation with 38 kA (peak to peak) amplitude. On the other hand, near the high density limit and at low-q, modulation of only a few kA was sufficient to trigger a disruption.

Figure 3 shows some typical B_θ-loop traces during the critical situation where the ac-modulation causes MHD activity but not yet a major disruption. It should be pointed out that B_θ loops pick up the ac-modula-

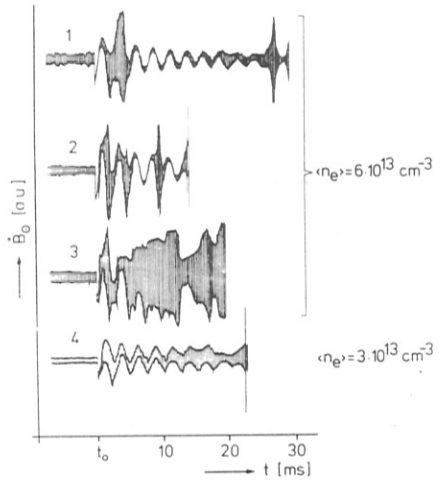

Fig.3: Typical B_Θ-loop traces during a 380 Hz modulation of the plasma current.

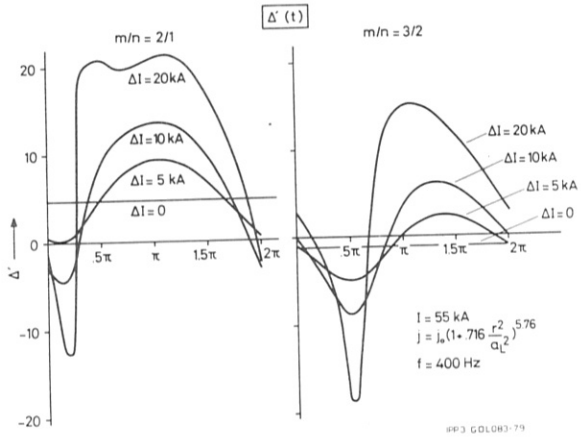

Fig.4: The instability parameter Δ' is computed for current profiles from the skin effect code and plotted as a function of time during one period of the ac-moculation. The current profiles for the case ΔI=20 kA are shown in Fig.2.

tion as well as the m=2 mode. The traces demonstrate two trends that occurred equally often in the experiment. Firstly, the instability seemed to grow in phase with the ac-current, i.e. growth occurred near the minimum of the applied ac-voltage. Such behaviour is particularly evident on traces 1 and 2. Secondly, ac-modulation seemed to make the plasma more unstable in general. This trend is illustrated by traces 3 and 4.

In order to compare the experimental results with theoretical predictions, we have computed the instability parameter Δ' of Ref./1/ for the current profiles calculated by our skin effect code. Typical results are shown in Fig.4, where Δ' is plotted as a function of time for one period of the ac-modulation. For small ac-currents $\Delta'(t)$ oscillates almost sinusiodally around the Δ' value associated with the dc-part of the current distribution. The maximum of Δ' occurs at the phase angle π, i.e. at the minimum of the applied electric field. For large ac-currents, Δ' becomes nonsinusoidal and $\langle \Delta' \rangle$ averaged over a period is much larger than the dc-value, indicating that the overall instability of the profile is increased. The computation is then in agreement with the experiment, which is surprising, because it is not clear that Δ' is relevant under so rapidly changing conditions as encountered in this experiment.

An important question is whether the ac-modulation always causes a destabilization on the average. We do not have a definite answer to this question. However, some simple arguments indicate that nonsinusoidal modulation with an inverted sawtooth might actually lead to stabilization on the average. This "dynamic stabilization" of the m=2 mode (proposed by Dr.Engelhardt) depends clearly on the exact shape of current profile, which might make practical implementation of the scheme difficult.

An open question is still why the discharge is so sensitive to any kind of current perturbation when the high density limit is approached. A series of experiments were conducted to stabilize the disruption near the high density limit by suddenly raising the current shortly before the disruption, thereby creating a current pedestal as proposed in Ref./3/. The theoretical analysis of this experiment has not yet been done, but we have the definite impression, that the current rise triggers rather than stabilizes this disruption.

Acknowledgement:
We are grateful to Dr.K.Lackner for making his computer code for the computation of Δ' available. We thank J.Stadlbauer and J. Ernesti for excellent technical assistance.

References:
/1/ H.P.Furth, P.Rutherford, H.Sellberg: Phys.Fluids 16, 1054 (1973).
/2/ A.Glasser, J.Greene, J.L.Johnson: Phys.Fluids 19, 567 (1976).
/3/ A.Glasser, H.P.Furth, P.Rutherford: Phys.Rev.Letters 38,234 (1977).
/4/ A.N.Dellis, J.Hosea: Princeton Report MATT-969 (1973)
/5/ P.Plinate and TFR Group: Proc.7th Europ.Conf.Contr.Fus.and Plasma Physics, Lausanne, Vol. I, 11, (1975)

Disruptive Instability Caused by Impurity Accumulation

W.Engelhardt, O.Klüber, K.Lackner, S.Sesnic
Max-Planck-Institut für Plasmphysik, EURATOM-IPP Association
8046 Garching, Fed.Rep. of Germany

I. Introduction

Neoclassical inward diffusion should result in peaked impurity profiles of the shape:

$$n_{imp} \propto n_i^Z$$

for vanishing temperature gradients. n_i is the proton density and n_{imp} is the density of impurities with ionic charge Z. In most tokamaks these profiles are not observed. One of the reasons is that anomalous transport leads to flat profiles /1/ of the form:

$$n_{imp} \propto n_i^{Z/\left(1+\frac{D_{anom.}}{D_{neocl.}}\right)}$$

The ratio of the anomalous to the neoclassical diffusion coefficients (D_{anom}/D_{neocl}) is of the order of 10 - 100 at low density. In high density tokamaks D_{neocl} is increased proportionally to n_e, whereas D_{anom} probably decreases, so that D_{anom}/D_{neocl} is lowered to the order of 1 - 10. In this case neoclassical inward diffusion can again lead to peaked profiles. In fact, in the high density regime of Pulsator we have observed strong emission of soft X-rays coming from the center of the plasma, which has been interpreted as an accumulation of impurities. The experimental evidence of this effect has been published in /2/ and will not be repeated in this paper.

II. Disruptive Instability

The connection of the accumulation effect with the disruption instability is an indirect one: the resistivity of the central plasma is increased due to the accumulation of impurities changing the current density profile to a flat shape with steep gradients at the q=2 surface. These profiles are susceptible to unstable tearing modes /3/ that finally trigger the disruption.

This qualitative picture is supported by the experimental findings: whenever the accumulation is detected by the soft X-ray diodes, the sawteeth are reduced or even disappear, indicating that now q(0) is greater than unity. The m=2, n=1 mode is observed to grow exponentially and the disruption sets in not later than 10 ms after the last detectable sawtooth.

III. Conditions for Accumulation

A systematic exploration of the conditions which lead to accumulation has shown that this effect occurs very reproducibly depending on the centering of the plasma column, on the absolute density, and on the influx of neutral hydrogen. The result for a well centered discharge with I = 60 kA, B = 2.7 T is summarized in Fig.1. The hydrogen influx is programmed in a way to yield constant $d\bar{n}_e/dt$. The maximum density $\bar{n}_{emax}$ is defined as the density which is reached before the disruption terminates the discharge. It is found that below a certain threshold density of $6 \cdot 10^{13} cm^{-3}$ neither accumulation nor a disruption occurs. If $d\bar{n}_e/dt$ is increased, the threshold density can be reached during the discharge time and accumulation with a following disruption is observed. A further increase of $d\bar{n}_e/dt$ results in a disruption at a higher density, $\bar{n}_{emax}$ being proportional to $d\bar{n}_e/dt$. After a threshold in $d\bar{n}_e/dt$ no accumulation occurs anymore, the X-ray signal of the central channel decreases with continuing sawteeth and the discharge disrupts at the high density limit of Pulsator /2/. Two typical discharges in these different regimes are displayed in Fig.2. Discharge a corresponds to $d\bar{n}_e/dt = 1.5 \cdot 10^{15} cm^{-3} s^{-1}$ showing accumulation on the central X-ray channel. Discharge b reaches the density limit with $d\bar{n}_e/dt = 1.67 \cdot 10^{15} cm^{-3} s^{-1}$. If $d\bar{n}_e/dt$ is further increased the maximum attainable density drops again and the discharges disrupt without accumulation.

It has been mentioned above that these results are only obtained with a well centered plasma column. A shift in the position by more than 0.5 cm either inward or outward prevents accumulation. Nevertheless the discharges disrupt also in this case, but at a density which is somewhat lower than it would have been reached with better positioning. A systematic investigation of the maximum density as a function of the plasma position and $d\bar{n}_e/dt$ has not been done yet.

IV. Qualitative Transport Model

The measured dependence of $\bar{n}_{emax}$ on $d\bar{n}_e/dt$ may be understood by the following qualitative explanation. There are two forces acting on the impurities: neoclassical inward diffusion and turbulent transport outwards due to the sawtooth activity. When the electron density is sufficiently high, neoclassical diffusion overcomes the outward transport and leads to accumulation which in turn stops the sawtooth instability. From this moment on the impurities can go unhampered to the center and a sudden increase of the X-ray intensity is observed. Furthermore, also the higher threshold at an increased hydrogen influx is explained in terms of this model. A strong influx cools the edge of the plasma and forces the current density to a peaked profile. q(0) drops and the sawtooth activity is enhanced. Now, a higher density is necessary, so that neoclassical transport can again drive the impurities to the center. A similar effect is produced by additional influx of krypton cooling predominantly the edge plasma. It was reported in /2/ that a puff of krypton stops also the accumulation like an increased influx of cold hydrogen.

V. Conclusion

The experimental results give a phenomenological explanation for the occurrence of disruptions below the high density limit of Pulsator. Accumulation is inevitable and leads to a disruption whenever the slope of the density rise is too small. They provide no explanation for the disruption at the high density limit and for the disruption at relatively low density when the plasma is not sufficiently centered. These conditions have to be investigated in more detail. Furthermore, it is desirable to study theoretically the influence of the sawtooth instability on the impurity transport. Because of the accumulation effect there may arise a severe restraint on the attainment of stationary high density plasmas in tokamaks.

References

/1/ W.Engelhardt, APS-Meeting, Atlanta 1977.

/2/ W.Engelhardt et al., 7th Int.Conf.on Plasma Physics and Contr. Nuclear Fusion Research, Innsbruck 1978, IAEA-CN-37-A-5

/3/ B.Carreras et al., this conference

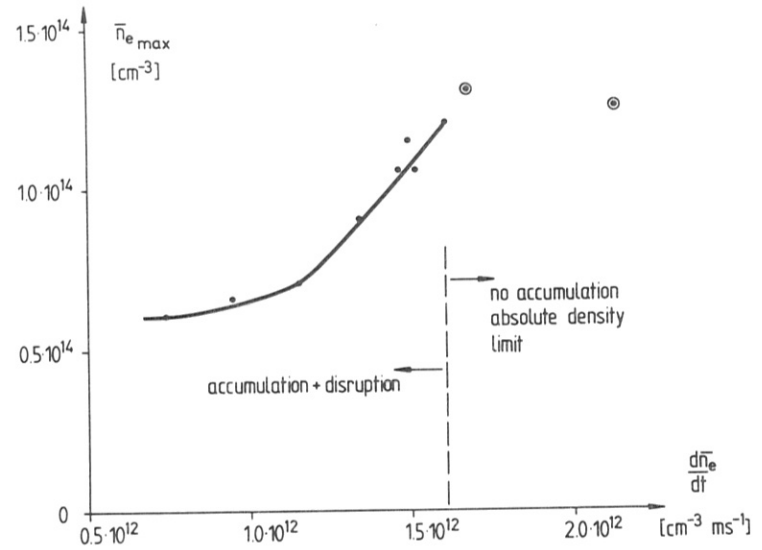

Fig.1: Dependence of the maximum attainable electron density $\bar{n}_{emax}$ on the density rise $d\bar{n}_e/dt$.

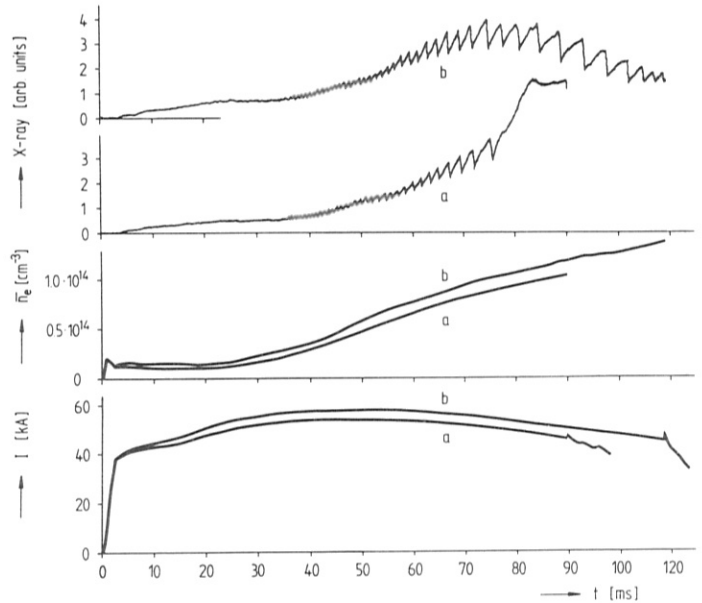

Fig.2: Soft X-ray signal (central channel), electron density and current evolution of two discharges in different regimes:
a) intermediate density discharge with accumulation, $d\bar{n}_e/dt = 1.5 \cdot 10^{15} cm^{-3} s^{-1}$.
b) high density discharge disrupting at the density limit without accumulation, $d\bar{n}_e/dt = 1.67 \cdot 10^{15} cm^{-3} s^{-1}$.

Dynamics of the Development of Internal Perturbations During the Disruptive Instability in a Tokamak

S.V.Mirnov
I.V.Kurchatov Institute of Atomic Energy, Moscow,
Union of Soviet Socialist Republics

Usually three types of MHD-activity are distinguished, which are considered to be manifestations of the disruptive instability in Tokamaks /1-13/. The characteristic feature for all of them is a symmetric expansion of some region or of the whole column. Their schemes are given in Table 1. First, there is the internal disruptive instability /10,13/; development of the perturbation m=1, n=1 transformed to m=0, n=0. It is located near the centre and is not dangerous for the plasma column in the whole. Secondly, there is the pre-disruption or small disruption; development of helical perturbations m=2,3, et al., which occurs mainly in some ring near the resonance point $q(r_s)=m$ /3,10,11,5/. And, at last, there is the disruption itself (or strong disruption) - a large-scale process along the whole plasma column resulting in turbulization of the central regions.

Experiments which were made previously in the T-4 /5,7/ allow us to point out two main features of the strong disruption. They give reasons to assume that the strong disruption is an interaction of a pre-disruption m=2, n=1 and an internal disruption m=1, n=1. The first feature is the fact that the pre-disruption usually precedes the development of a strong disruption. In Fig. 1 there are several typical oscillograms of the voltage V(t) during disruptions. The dotted lines show the behaviour V(t) in a typical predisruption. Oscillogram (g) represents the rare case of a very deep pre-disruption when all phases of disruption took place successively, except turbulization. The second feature is the flattening of the profile $T_e(r)$ before a strong disruption as a result of the development of internal perturbations with odd m.

To control the behaviour of the internal perturbation soft X-ray emmission of the central regions of the plasma column was

observed in a range of $h\nu$ = 3-10 keV. In this range the plasma glow depends on the electron temperature to such great extent that all fluctuations of it actually were determined by fluctuations of T_e which, in their turn, should follow the magnetic surface perturbations.

In order to determine the structure of the perturbations, on the T-4 the scheme was used which is shown in Fig. 2. It consisted of 2 symmetric vertical (I and II) measuring X-ray channels and 2 horizontal (III and IV).

Let us assume the case when plasma has a cylindrically symmetric form and the signals amplitudes of all channels are equal.

If now in the colums cross-section the perturbations with odd m (1,3 ...) appear, they will be found by the signals difference $U_1=X_I-X_{II}$ and $U_2=X_{III}-X_{IV}$. If the even perturbations m(2,4 ...) appear, they will be found by the sums difference $U_3=(X_I+X_{II})/2 - (X_{III}+X_{IV})/2$. The sum of signals $U_4=(X_I+X_{II}+X_{III}+X_{IV})/4$ is proportional to the value of the full glow. Its change allows to estimate the scale of the symmetric expansion of the profile T_e or, which is the same, the amplitude of the perturbation m=0, n=0.

Besides, when comparing the behaviour U_1 and U_2, it is possible to make some additional conclusions on the character of the perturbations with even m.

First, if the perturbation rotates in direction of φ, the phase difference $\pi/2$ between U_1 and U_2 should appear. Secondly, some possibilities arise to distinguish the rotating perturbations m=1 and m=3. Namely, there is a special feature in the described measuring scheme. If the direction of the perturbation rotation is given, then the visible rotation of the perturbation m=1 should coincide with the given one but the visible rotation m=3 is observed in the opposite direction (Fig. 2a).

In Fig. 3 (T-4 /7/) the values of U_4 and U_1 are shown for the cases of disruption and pre-disruption (dashed). For comparison there are also plotted the corresponding oscillograms of the external perturbations - of the field component B_φ and voltage V(t).

The first conclusion on the basis of these curves is that already at the initial stage (moment AA) disruption differs form pre-disruption by a higher level of MHD-activity in the center of the column.

According to the external characteristics of the discharge the perturbation m=0, n=0 (flattening of the profile) obviously precedes the development of the disruption. This important feature was also observed in experiments at PULSATOR /6/.

The second conclusion is that the development of the perturbation m=0 is accompanied by the increase of the odd perturbation amplitude in the center of the column. If one makes measurements only in one direction such a perturbation may be interpreted as an asymmetry in the initial X-ray signals, caused, for example, by the ordinary displacement of the plasma column /12/.

In Fig. 4 for the T-4 and for PLT /12/ the values of X_I, X_{II}, X_{III}, X_{IV} and of U_1, U_2 are plotted. It is possible to make the conclusion that for these two devices the processes which take place in the disruption are very close to each other in nature.

In the case of T-4 the comparison of U_1 and U_2 allows to find out that the odd perturbation rotates by φ. This visible direction of rotation (assuming m=1) coincides with the direction of rotation of the external perturbation m=2 /7/. It is quite natural to assume that perturbations outside and inside of the column rotate in the same direction. Then it is possible to state that the structure of the observed odd perturbation corresponds to m=1 and not to m=3 (n=2).

What is the behaviour of the even perturbation m=2 in the disruption process? One could anticipate that in the course of the development of the m=0 perturbation and of flattening of the current profile the perturbation m=2 will penetrate to the center of the column.

The experimental results are not in contradiction with such an assumption. In Fig. 5 the values of U_4, U_2, U_3 and $\tilde{B}_\varphi$ are presented for one of the disruptions (T-4 /7/), as well as the relative values of perturbations U_2/U_4 and U_3/U_4 (the difference between them is denoted by vertical shading).

On the basis of these data it is possible to make the conclusion that the development of a disruption is accompanied by the definite increase of perturbations m=2 in the center. Unfortunately, the low level of the X- ray signal at the final stage of the disruption does not allow to observe, up to the end, the stage of turbulization and the dynamics of perturbation-m=2 development.

Thus, referring again to table 1, we consider it as possible that the following sequence of events, ultimately resulting in a disruption, takes place /5/. At first a slow compression of the current channel, caused, for example, by cooling of the periphery, decrease in q near the boundary up to 2 and at the center up to 1. Then the beginning of the pre-disruption at the boundary of the column, excitation of m=1, n=1 perturbations in the central regions. Further, the initiation of the internal disruption with m=0, n=0, flattening of the current profile and, as a consequence, nonlinear increase of perturbations m=2 in the whole column. And finally, during the expansion of the plasma column, excitation of the helical mode m=3, m=4 /4,11/ and generation of large negative voltage spike.

References

1. Gorbunov E.P., Razumova K.A., At.Energ. 15 (1963) 363
2. Artsimovich L.A., Mirnov S.V., Strelkov V.S., At. Energ. 17 (1964) 170
3. Hosea I.C. et al. Proc. IV Int. Conf. Madison. 1971, IAEA-CN-28/F-7
4. Vlasenkov V.S. et al, Proc. 5th Int. Conf. IAEA, Tokio (1974) 33
5. Mirnov S.V., Semenov I.B., Preprint UAE-2723 (1976)
6. Karger F. et al. Proc. 6th Int. Conf. Berchtesgaden, IAEA-CN-35/A-7
7. Mirnov S.V., Semenov I.B. VIII Eur. Conf. Prague 1 (1977) 45
8. Vershkov V.A., Mirnov S.V., Nucl. Fusion 14 (1974) 383

9. Akulina D.K. et al. In Plasma Physics 5 (1978) 1022
10. von Goeler S., Proc. 7th Int. Conf. Lausanne 2 (1975) 71
11. Merezhkin V.G., Plasma Physics 5 (1978) 275
12. Sauthoff N.R., von Goeler S., Stodiek W., PPPL-1379 (1978)
13. von Goeler S. et al. Phys.Rev.Lett. 33 (1974) 120.

	I	II	III
V(t) voltage	t	t	t
ΔV	–	–1 ÷ –10 V	–10÷–500V
X(t) soft x-ray			
ΔX	10÷20%	30÷80%	10÷50(times)
Δn_e	–	~10%	~30%
$\Delta T_e(0)$	~10%	20÷50%	2÷3 (times)
$\tilde{B}_\varphi / B_\varphi$	–	~5%	~15÷20%
m	1,0	(3),2,1,(0)	(3),2,1,0,2,3,4

Table 1

IPP3 LKN 431-79

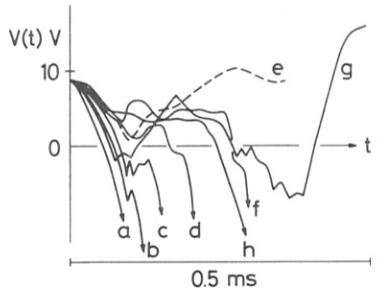

Fig. 1

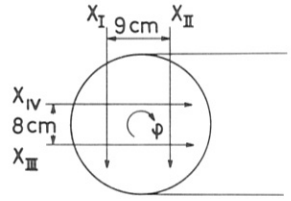

Fig. 2

IPP3 LKN 432-79

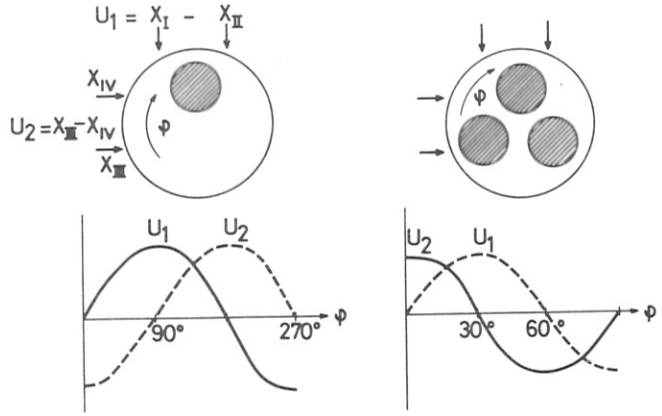

Fig. 2a

IPP3 LKN 427-79

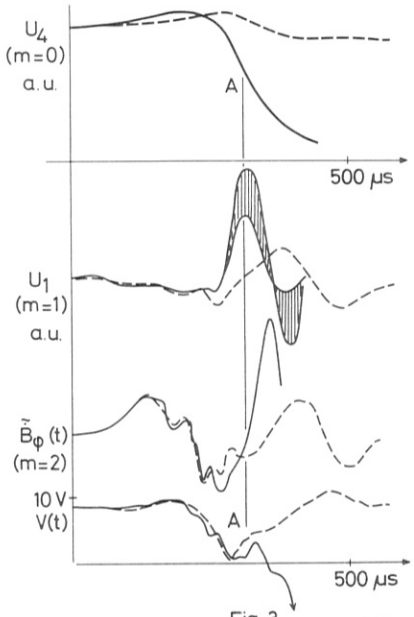

Fig. 3

IPP3 LKN 428-79

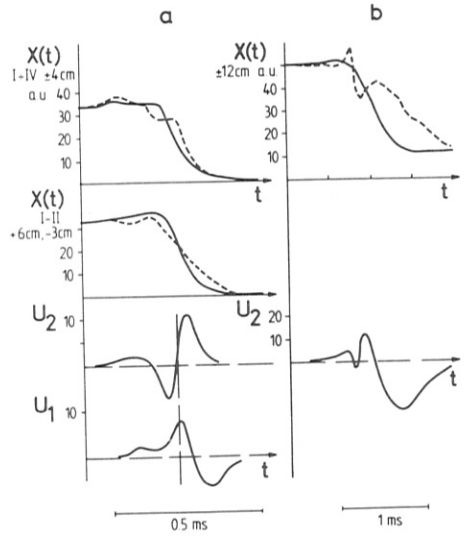

Fig. 4

IPP3 LKN 429-79

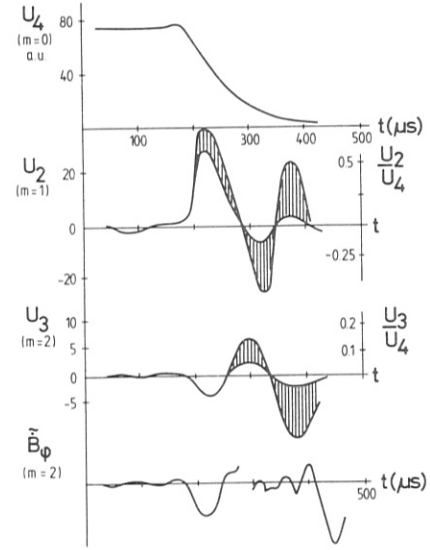

Fig. 5

IPP3 LKN 430-79

STRUCTURE OF MAGNETIC FIELD PERTURBATIONS DURING DISRUPTIVE INSTABILITY IN A TOKAMAK

V.G.Merezhkin
I.V.Kurchatov Institute of Atomic Energy ,Moscow,USSR

Detailed analysis of the magnetic field perturbations in two cross sections of the plasma column with time resolution $\sim 1\,\mu s$ during the disruptive instability in the T-6 Tokamak is presented.

The measurements were made by a system of a Rogovsky belt and 24 magnetic probes wound over it.This system was put into a stainless steel tube located inside the liner.Analogous system of six probes was located in the other cross section of the chamber 90° away from the first one over the major azimuth φ .

The probe signals were integrated with 10 ms time constant. The Rogovsky belt signal was subtracted from the probes signals at a certain weight. The resulting signals $\tilde{H}_\omega(\omega,t)$ did not have to include in the first approximation the plasma current perturbations.The vertical ΔH_v and the horizontal ΔH_R components of the magnetic field perturbations connected with the plasma column displacement were determined from the measured distribution using common equations

$$H_v = \frac{1}{\pi}\int_0^{2\pi} \tilde{H}_\omega(\omega)\cos\omega d\omega \ , \quad H_R = \frac{1}{\pi}\int_0^{2\pi} \tilde{H}_\omega(\omega)\sin\omega\, d\omega .$$

We believe that the difference $H_m(\omega) = \tilde{H}_\omega(\omega) - H_v\cos\omega - H_R\sin\omega$ is associated with the higher harmonics ($m \geq 2$).

Reproducible discharge regime with one major disruption in the middle of the discharge was studied in the T-6 Tokamak at the plasma current $I \sim 50$ kA and toroidal magnetic field $B_0 = 5.5$ kG. The vertical magnetic field was regulated so that the plasma column displacement Δ was $\lesssim$ 1cm.

The major disruption appeared after the limitation of the plasma column cross section by a tungsten target located at the radius $a_L \sim 15$ cm at $q(a_L) \simeq 1.8$ (the target was installed from the outer side of the torus). The following plasma parameters were observed before the disruption: $n_e = 5\cdot10^{12}\,cm^{-3}$, $T_e \simeq 280$ eV, $T_i \simeq 140$ ev, $\beta_p \simeq 0.25$, $l_i(a_L) \sim 0.6$. Fig.1 illustrates the regular perturbation structure with dominant m= 2,3,4 harmonics observed at its middle stage (m =3 or m=4). The m= 3,4 harmonics have a notable asymmetry: they are compressed in the inner side of the torus and rarefied in the outer region. Such asymmetry may be explained by the coupling of the perturbation structure with the geometry of the magnetic field lines. It was assumed that the ratio of the slopes of the helical harmonics and magnetic field lines at the plasma edge should be constant. Following this assumption we approximated the shape of regular magnetic perturbations with m =2 by the expression $C_m(\cos m\omega^* - \varphi_m)$ where $\omega^* = \omega - \lambda\sin\omega$ and $\lambda = \frac{a}{R}(1 + l_i/2 + \beta_p)$.

Choozing the value of λ in the range of 0.3 -0.4 we generally found a good agreement between the observed shape of magnetic field perturbations with $m \geq 2$ and this model. As a rule we have not observed the first harmonic δH_R , $\delta H_v \sim C_1^*(\cos\omega - \varphi_1)$ which could be expected to exist at the supposed shape of the higher harmonics. This means that a real helical perturbation appears as a superposition of two types of perturbations: $\cos(m\omega^* - \varphi) + \alpha\cos(\omega - \varphi - \pi)$ with $\alpha \sim \lambda$ at m =2. During the decay of the perturbations the presence of the first harmonic was manifested by vertical displacement of the plasma column with an expected amplitude C_1^* .

The results of the perturbation analysis within the accepted model are given in Fig.2 for the typical major disruption. The major disruption is seen to develop in two stages. The m= 2 harmonic appears in the beginning of the disruption corresponding to m = 2,n = 1 mode. As soon as the amplitude of this harmonic reaches approximately a half of the top value the higher harmonics m =3 and m = 4 appear. However, m =2 harmonic remains to be the dominant during the whole first stage of the disruption. The behavior of the perturbations during the first stage of the major disruption appears to repeat all the features of the minor disruption /1,2,3/.

The typical peculiarity of the minor disruption is the appearance of small deviations in the loop voltage $\Delta U \sim 2$V and the plasma current $\Delta I / I_0 \lesssim 1\%$ with a relatively large amplitude of perturbations of the dipole componen $\Delta H_v / H_{\omega o} \sim 4\%$. These perturbations can be explained by plasma energy losses.

The m = 4 harmonic dominates in the second stage of the major disruption during the second increase of the perturbations. A low weght of m= 2 mode in this stage of the disruption makes

it is possible to assume m = 4 harmonic corresponding to m = 4, n = 1 kink mode.

Under the same initial conditions the m = 3 harmonic may develop during the second stage of the disruption instead of the m = 4 harmonic with the same or even higher level ($C_4/H_{\omega o}$~10%; C_3/H ~ 15 %; the radius of the measurements was b_m = 22.5 cm). The direct measurements have shown that the m = 3 harmonic corresponds to the m = 3, n = 1 helical mode /1/.

The magnetic field structure is given in Fig.3 during one of the disruptions registrated in the abovementioned discharge regime without the target whithin the plasma (the plasma column was restricted by the rail limiter at the a_L~18cm radius). The m = 3 mode appearing in the second stage of the disruption may exist during a rather long time ~100 μs not cousing the strong destructions of the plasma column. The lowest variation of the dipole component ΔH_v was observed in this disruption pointing out lower energy losses in comparison with other disruptions.

In all the studied major disruptions fast variations of the loop voltage and the plasma current were synchronized with fast incriasing of the upper harmonic amplitudes during the second stage of the disruption. Similar variation of the current and higher harmonics were also observed during the minor disruption with m = 3, but this phenomenon was less noticeable in the case of m = 2 minor disruption.

The comparison of perturbations in the number of disruptions makes it possible to conclude that the proportionality factor between the current and higher harmonic may depend on the degree of nonresonant helical perturbation. Correlation of the current perturbations and the value $\frac{C_m}{H_{\omega o}}(a)[m - q(a)]$ is shown in Fig.4. In calculations of q (a) and $C_m/H_{\omega o}$(a) we have used the value of a, which was obtained in the adaption of λ parameter for the best description of asymmetry of the m ≥ 2 harmonics.

Thus certain notable peculierities should be pointed out in the behavior of the perturbations during the major disruption:

1. High level of helical perturbations of the magnetic field up to 20 -30 % at the plasma edge;

2. Change in the perturbation structure takes place during the disruption with increasing m/n ratio. The following transfers have been obtained in the experiments:

m=2, n=1/m=3, n=1 — q(a) ~ 1.6÷1.8

m=2, n=1/m=4, n=1? — q(a) ~ 1.8 ÷2.4

m=3, n=2/m=2, n=1 — q(a) ~ 1.

3. Notable non-resonant helical perturbations are possible in the second stage of the disruption with $m - nq \sim 1.2 \div 1.6$.

Figure captions

Fig.1- Structure of regular magnetic field perturbations observed at the major disruptions

Fig.2. Magnetic field perturbations in a typical major disruption with the dominant m=4 harmonic in the second stage of the disruption (B_0= 5.4 kG, J= 50 kA, λ = 0.33).

Fig.3- Perturbation structure in the major disruption with the dominant m=3 harmonic (B_0= 5.3 kG, J =55 kA, λ = 0.33).

Fig.4- $\Delta J/J$ as a function of $[m - q(a)]\frac{C_m}{H_{\omega o}}(a)$ for the foreront of perturbations in typical disruptions:

△▲-m=3 minor disruption; ·-m=2 minor disruption and the first stage of the major disruption; △▲ - m=3 ■-m=4 the second stage of the major disruption. The points ▲ ▲ ■ - correspond to the top levels of the perturbations.

References

1. Mezezhkin V.G. Физика плазмы, 4, №2, 1978.

2. Vlasenkov V.S. et al. In Plasma Phys. and Contr. Nucl. Fusion Res. (Proc. 5 th Internat Conf. Tokyo, 1974) IAEA, Vienna, 1975, p.33.

3. Vlasenkov V.S. et al. 6 th European Conf. on Controlled Fusion and Plasma Phys. (Proc. Conf. Moscow 1973) V.1, Moscow 1973, p.55.

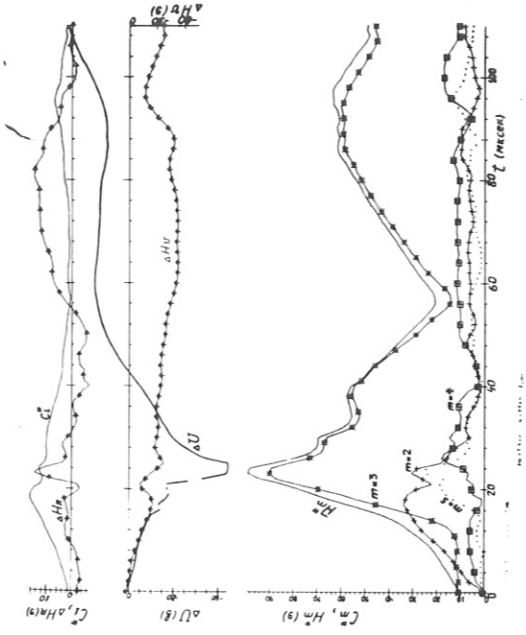

Fig. 3

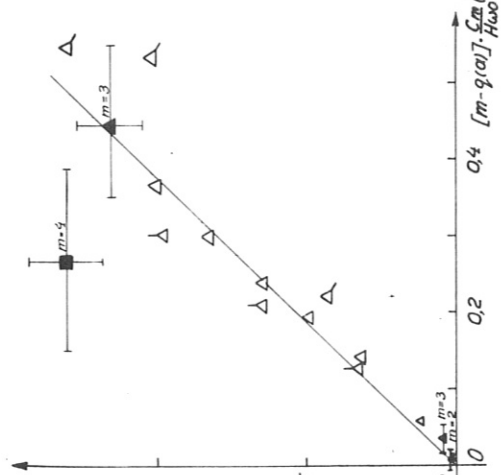

Fig. 4

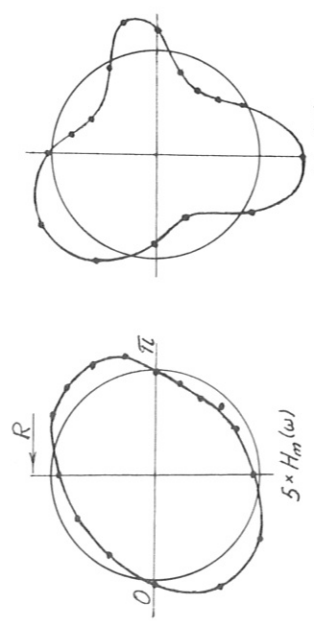

Fig 1

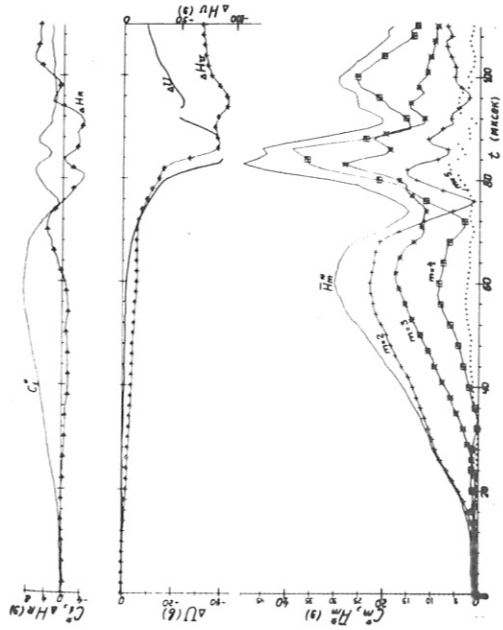

Fig. 2

Economic Theory of the Disruptive Instability

H. P. Furth
Plasma Physics Laboratory, Princeton University
Princeton, New Jersey 08540

ABSTRACT

Attempts to understand the disruptive instability in simple mechanistic terms have been frustrated by the sheer variety of the experimentally observed phenomena. For example, in Ref. 1 the disruption is reported to be a nearly symmetric ($n = 0$, $m = 0$) expansion, while in Ref. 2 it is visualized in terms of large-amplitude kink modes. Some other observations[3,4] are consistent with the symmetric expansion concept, while still others support the idea that large kinks — in various assortments of mode numbers — are present during disruption.[5]

In view of this diversity of experimental data, it is logical to look for a generalized explanation of the disruptive instability, rather than for a specific disruption mechanism. This logic is reinforced by the discovery that, in addition to the familiar "external" disruptive instability[6], there is also an internal disruption[7] and a skin-current disruption[5] — all involving different mode numbers, but all having basically similar characteristics.

The present paper proposes a speculative general theory of the disruptive instability. This theory takes as its starting point some suggestive features of the linear resistive-MHD stability analysis for large-aspect-ratio tokamaks.[8] We will assume, for the moment, that $q(r)$ is monotonically increasing from a central value q_o to a limiter value q_L. The $n = 1$, $m = 1$ mode is stable for $q_o > 1$, and becomes unstable for $q_o < 1$. Stabilization of the higher-m modes, conversely, is facilitated if $q_o < 1$, and made more difficult when q_o is raised, or when q_L is lowered. For fixed boundary values q_o and q_L, the $q(r)$ profile can still be drawn in such a manner as to stabilize any <u>finite</u> set of modes having specified m and n-numbers, by an appropriate reduction of the slope dq/dr at

the singular points r^s_{mn} of these modes, where $q(r^s_{mn}) = m/n$. Whenever the q-profile is flattened at some singular point to stabilize a particular mode, it must, of course, be steepened at some other singular point, with a resultant destabilization of some other mode. For a q_L-value that is sufficiently large and/or for a sufficiently close-fitting conducting shell, it is possible to find $q(r)$-profiles of special shape that stabilize all kinks simultaneously[8], including the $n = 1$, $m = 1$ mode; in general, however, at least one mode will remain unstable. Such residual instability is virtually inevitable in actual tokamak experiments, where radiation cooling or heat transport tends to prevent a $q(r)$ profile of optimal shape from being established.

If $q_o < 1$, so that the $n = 1$, $m = 1$ mode is left unstable, its nonlinear behavior is to grow until a large-scale magnetic reconnection[9,10] takes place, restoring q_o to the vicinity of unity. The nonlinear behavior of the higher-m modes differs in detail, but is basically similar in its consequences: each mode creates a magnetic island around its own singular point, producing a local flattening of the average $q(r)$ profile that tends to stabilize the mode in question while increasing the difficulty of stabilizing all the other modes. A detailed computer analysis[11] reveals that the mutual destabilization that occurs through the average $q(r)$ profile is supplemented by other nonlinear effects that act even more strongly in the same direction. Only in the highly nonlinear phase of this process does there appear to be a mechanism whereby individual mode amplitudes are reduced through mode-interaction: namely, modes of similar helicities m/n may absorb each other.

When attempting to describe these phenomena in generalized terms, one is led to concepts such as "free mode competition," which are reminiscent of another science dealing with the nonlinear consequences of random events, namely, economics. The "economic theory of the disruptive instability," which is tentatively proposed here, takes the following form:

1. The nonlinear behavior of every mode is generally such as to improve its own stability, while destabilizing other modes with different helicities (and tending to absorb modes with similar helicities.)

2. In normal tokamak operation at low q_L-values, at least one mode is linearly unstable. If the q_L-value is lowered further, or if non-MHD effects (such as radiation cooling) are allowed to deform the $q(r)$ profile, the unstable mode seeks to improve its own situation by destabilizing other modes, which in turn act to destabilize still others.

3. Up to some critical point, this competitive behavior serves to prolong the overall stability of the tokamak discharge, since the most precarious modes are continuously restabilized at the expense of less precarious ones. Thus an entire group of modes is brought to a highly precarious state.

4. Beyond the critical point, the benefits to be derived from destabilizing new modes are outweighed by the mutual destabilizing effects of already existing modes, and a collective, explosive instability occurs.

The preceding discussion applies specifically to the external disruptive instability, but could be rephrased to fit the other disruptions as well. Finally, it seems likely that the extreme suddenness that characterizes the onset of experimental disruptions of all three types cannot be explained satisfactorily in purely macroscopic terms. A sharply enhanced local resistivity or electron viscosity within the singular surface[12] (i.e., a change of the quality, not merely the quantity, of the finite-resistivity MHD disturbance) may be manifesting itself at the instant of disruption.

REFERENCES

1. R. A. Jacobsen, Plasma Physics 17, 547 (1975).
2. V. Vlasenkov, et al., in Plasma Physics and Controlled Nuclear Fusion Research (Proc. 5th Int. Conf., Tokyo, 1974) I, IAEA, 33.
3. S. V. Mirnov, I. B. Semenov, in Plasma Physics and Controlled Nuclear Fusion Research (Proc. 4th Int. Conf., Madison, 1971) 2, IAEA, 401.
4. S. von Goeler in Controlled Fusion and Plasma Physics (Proc. 7th Europ. Conf., Lausanne, 1975) II, 71.
5. N. R. Sauthoff, S. von Goeler, W. Stodiek, Nuclear Fusion 18, 1445 (1978).
6. L. A. Artsmovich, Nuclear Fusion 12, 215 (1972).
7. S. von Goeler, W. Stodiek, N. Sauthoff, Phys. Rev. Lett. 33, 1201 (1974).
8. A. H. Glasser, H. P. Furth, P. H. Rutherford, Phys. Rev. Lett. 38, 234 (1977).
9. B. B. Kadomtsev, O. P. Pogutse, Sov. Phys. JETP 38, 283 (1973).
10. B. V. Waddell, et al., Nuclear Fusion 16, 528 (1976).
11. J. D. Callen, et al., in Plasma Physics and Controlled Nuclear Fusion Research (Proc. 7th Int. Conf., Innsbruck, 1978) Paper CN-F-1-1, to be published by IAEA.
12. P. J. Baum, et al., Phys. Fluids 16, 1501 (1973); J. Plasma Physics 15, 259 (1976).

Ergodization of Runaway Drift Surfaces and Magnetic Surfaces

G.Fußmann and H.P.Zehrfeld
Max-Planck-Institut f. Plasmaphysik, EURATOM-IPP Assoc.
8046 Garching, Fed.Rep.of Germany

1. Introduction

In a recent paper we reported modulated losses of runaway electrons that have been observed in the high density discharges in PULSATOR /1/: There are enhanced losses correlated with the internal disruptions leading to inversed sawteeth in the hard X-rays. Prior to the current disruption, intensity oscillations and also hard X-ray bursts have been observed. The question whether these observations can be explained in terms of an ergodization of the magnetic field was investigated by means of code calculations where toroidal effects are fully taken into account. As an important result it was found that, at least for a certain type of helical perturbation, runaway drift surfaces are more stable against ergodization than the magnetic surfaces. Only in the case of very strong magnetic ergodization was an ergodized motion of the runaways found. Whereas these calculations suffered from the fact that the plasma current had been idealized by a filament, we present in this paper calculations with realistic current and pressure distributions which also enable us to study the influence of finite pressure. This is of particular interest with regard to the density limits of tokamak discharges.

2. Magnetic field calculations

We consider distributions of toroidal plasma current I_T and pressure p of the form

$$I = I_T\cdot(1-(1-\rho^2)^{\mu+1}) \quad , \quad p = p_0\cdot(1-\rho^2)^{\nu} \tag{1}$$

where ρ is the normalized radius of the magnetic surfaces, and μ and ν are parameters. The poloidal magnetic field produced by these distributions is

$$B_p = \frac{\mu_0 I R_0}{2\pi a \rho R}\,(1-\Delta_p'\cos\theta)\,\hat{e}_\theta \quad , \tag{2a}$$

where

$$\Delta_p = \Delta_p(\rho, \beta_{pol}, \mu, \nu, R_0/a) \quad , \quad \Delta_p' = \partial\Delta_p/\partial\rho \, . \tag{2b}$$

R is the distance from the main axis, R_0 the major torus radius and Δ_p the plasma displacement. Although distributions with $\Delta_p' \neq 0$ are not compatible with toroidal plasma equilibrium, it was assumed that they reflect the basic topology for the study of ergodization. Computations using equilibrium fields (being much more time consuming) will be discussed in Sec.6.

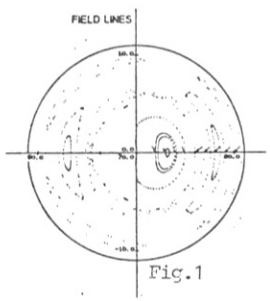

Fig.1

In all calculations we refer to PULSATOR data: I_T=60 kA, a=11 cm, R_0=70 cm, B_0=27 kG, q(a)=3.9. For the case μ=3, which fits best to the experiments, we obtain q(0)=0.98.

As in the former calculations, the helical perturbations are produced by a partial helical dipole winding outside the plasma which is available on PULSATOR /1/. This winding was chosen in particular because it produces large islands on the q=1 and q=2 surfaces -which are known to be present in the experiments - and because, in addition, it induces smaller islands on all other rational q-surfaces, which can be assumed to be also present in reality.

For a helical perturbation current of 20 kA the intersection points of the magnetic field lines with the meridional plane φ =0 are shown in Fig.1. In the Figure, nine lines (starting points marked by arrows, torus axis to the left) were followed for 100 toroidal revolutions.

3. Runaway trajectories

For the magnetic configuration described in the preceding paragraph the motion of runaways was also calculated by integrating the guiding center equation

$$\frac{dx_G}{dt} = v_\parallel \frac{B}{B} + v_D \tag{3a}$$

The drift velocity in terms of the relativistic parameter $\gamma = (1-v^2/c^2)^{-1/2}$ is given by

$$v_D = \frac{m_0\gamma}{eB^2}\, B \times \left\{ \frac{v_\parallel^2}{B^2} B\cdot\nabla B + \frac{v_\perp^2}{2B}\nabla B \right\} \tag{3b}$$

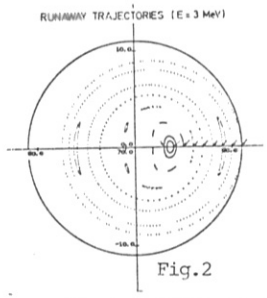

Fig.2

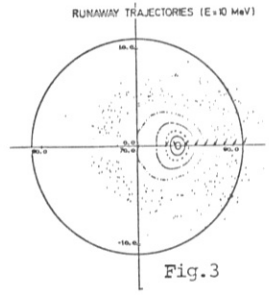

Fig.3

In the calculations we assumed $v_{\perp 0}/v$=.1. It was found, however, that the results only depend very weakly on this ratio as long as it is kept below ~ 0.3. In Figs.2-3 we present results for runaway energies of 3 and 10 MeV. In the first case all intersection points of the trajectories appear to be arranged on smooth toroidal or island drift surfaces (no ergodization), whereas in the second case drastic radial scattering (ergodization) is observed. In addition, we note that the "path island" corresponding to the m=2/n=1 magnetic island is turned by $\Delta\theta = 90^\circ$ when the energy changes from 3.5 to 4 MeV. At 3.75 MeV an intermediate state is obtained where the island width seems to be minimum.

4. A magnetic field analogy to runaway motion

Neglecting terms of higher order, the drift velocity given in eq. 3b is a vector pointing in the vertical direction $\vec{v}_D \sim v_D\hat{e}_z$. Since $v_\parallel \sim v$, the equation for the runaway trajectories can then be written as

$$\frac{dx_G}{ds} = \frac{B/B + v_D\hat{e}_z/v}{|B/B + v_D\hat{e}_z/v|} \tag{4}$$

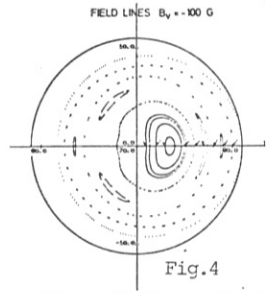

Fig.4

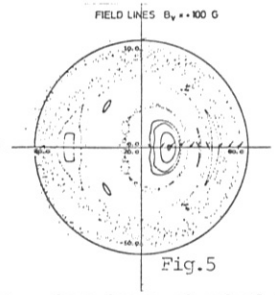

Fig.5

with s being the length of arc. This equation is equivalent to the equation of the magnetic field lines when an additional vertical field $\vec{B}_V = B_V\hat{e}_z$ is taken into account. Therefore it is to be expected that calculations of field lines with $B_V = B\, v_D/v$ show the essential features of the runaway motion. This prediction has been checked by adding vertical fields varying in sign and magnitude. Two results are given in Figs.4 and 5 (to be compared with Fig.1). The case B=-100 G corresponds

to the runaway case and shows reduced ergodization, whereas in the opposite case B=+100 G a high degree of ergodization is to be noticed. Since the shift of both magnetic and drift surfaces is proportional to q to lowest order,

$$\Delta = \Delta_0 q(r) \quad , \quad \Delta_0 = R_0 B_v / B_0 \quad \text{or} \quad \Delta_0 = m_0 c^2 \sqrt{\gamma^2 - 1} / eB_0 \quad , \qquad (5)$$

the shift of the outer surfaces is larger than that of the inner surfaces. Hence a compression of the surfaces at the inner side (runaway case) or outer side of the torus occurs. According to the calculations described, a certain compression at the inner side of the torus is favourable in suppressing ergodization, whereas compression on the outside considerably increases the degree of ergodization. In order to prove that this effect is not only specific to the chosen type of perturbation, similar calculations were performed for m=2/n=1 and m=3/n=1 helices.

5. Discussion of vertical field effects

When discussing the influence of vertical fields, one has to consider the possibility of overlapping of islands and the change of the island widths. In the examples shown, the islands are coupled at the outside of the torus. For this reason this region is most critical with respect to compression of the surfaces, and the touching of the islands at the outside can rather easily be accomplished. Due to the uniqueness of the vectors $\vec{B}$ and $\vec{\nabla}$, however, a touching or intersection of the islands is not permitted. Therefore destruction of the surfaces - resulting in ergodization - takes place when the islands approach each other. On the other hand, squeezing the surfaces to some extent at the inside of the torus reduces ergodization in the examples cited since the minimum distance of the islands is increased. However, too strong a compression at the inside again leads to island overlap and is the reason for ergodization of runaway trajectories at high energies.

In order to study the change of width of the islands, numerical calculations with regard to small helical perturbations (7 kA) were performed. A substantial decrease of the island width in the case of small compression at the inside of the torus is obtained. Conversely, compression at the outside increases the island widths and also leads to considerable deformation of the island shape (Fig.5).

6. Influence of Pressure on Ergodization

For current and pressure distribution functions of the type given in eq. 1 the equilibrium field in the large-aspect ratio approximation can relatively easily be calculated by calculating the displacement $\Delta_p = \Delta_p(\rho, \beta_{pol}, \mu, \nu, R_0/a)$ of the magnetic surfaces /2/. The surface coinciding with the plasma boundary is assumed to be fixed. When increasing

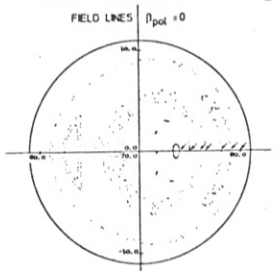

Fig.6

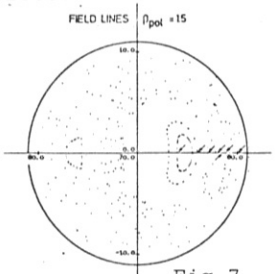

Fig.7

the plasma pressure, i.e. β_{pol}, the position of the magnetic axis $\Delta_p(\rho=0)$ moves towards the outside of the torus. With reference to the last section, this results in unfavourable compression of the magnetic surfaces. This negative prognosis is confirmed by the computational results presented in Figs.6 and 7 ($\mu = \nu = 3$, 50 toroidal revolutions). In the case of $\beta_{pol}=0$ the shift is rather small ($\Delta_p(0)=0.4$ cm) and the field line pattern is essentially the same as in Fig.1 ($\Delta_p \equiv 0$). For $\beta_{pol}=1.5$, which is the maximum value that was achieved in PULSATOR, the shift is 1.4 cm and a considerable increase of ergodization in the outer plasma region is to be noticed (Fig.7).

7. Conclusions

Our investigations refer in particular to a situation where phase locking of tearing modes with a coupling point at the outer side of the torus exists. Such coupling is usually observed in PULSATOR for the m=2/n=1, m=1/n=1 modes a few ms before the external disruption but no information on the coupling of other modes (e.g. m=2/n=1 with m=2/n=2) is available. For the case of coupling the compression of the magnetic and drift surfaces was found to be essential. From the outlined calculations we deduce a rather insensitive behaviour of medium energy runaways against ergodization. Ergodized trajectories occur in the case of high energy or at a rather high degree of field ergodization (possibly explaining runaway losses at internal and external disruptions). Furthermore, it was found that for a given tearing mode activity the degree of field ergodization increases with plasma pressure. Thus, the increase of pressure possibly explains the pronounced tendency toward disruption with rising density that is observed in the PULSATOR tokamak.

Acknowledgements

The support of W.Lotz in the numerical treatment is gratefully acknowledged. We are indebted to H.Wobig for pointing out the analogy of runaway trajectories and magnetic field lines.

References

/1/ G.Fußmann et al., 7th International Conference on Plasma Physics and Controlled Nuclear Fusion Research, Innsbruck 1978, IAEA-CN-37-T4

/2/ G.Fußmann, B.J.Green, H.P.Zehrfeld, IPP III/49 (to be published).

Very Low-q Discharges Free from Major Disruptions in DIVA

K. ODAJIMA, M. NAGAMI, S. YAMAMOTO, H. OHASA, S. SENGOKU,
H. KIMURA, T. YAMAUCHI, K. KUMAGAI, A. FUNAHASHI, H. MAEDA
and Y. SHIMOMURA

Japan Atomic Energy Research Institute, Tokai, Naka, Ibaraki, Japan

A very low-q discharge is one of the most attractive method to obtain high-β tokamaks. The plasma column in tokamaks, however, is disrupted by so called disruptive instability when the safety factor at limiter becomes low. This paper describes the experimental results carried out in DIVA for mhd activities including the disruptive instabilities in very low-q discharges ($1.3 \leq q_a \leq 2.5$).

DIVA is a tokamak having a teardrop-shaped shell inside a vacuum chamber and an axisymmetric divertor. The vacuum surfaces including a rail limiter and the inner surface of the shell are coated with titanium. Level of gas- and metal-impurities is very low and the radiation loss including charge exchange loss is 10 ~ 20 % of ohmic heating power and the $z_{eff} \approx 1$. The plasma has non circular cross section, and the effective radius is determined by $\bar{a} = l_p/2\pi$, where l_p is circuit length of the non-circular cross section. Determined effective radius of the shell $\bar{b}$ is 12 cm and that of the plasma in normal cases is 10 cm with distance between the limiter and the shell surface d_l = 1.5 cm. Generally defined q_a is employed, i.e. $q_a = (\bar{a}/R)(B_T/\bar{B}_P)$ where $\bar{B}_P = \mu_0 I_P/2\pi\bar{a}$. Therefore, the defined safety factor q_a is that for a straight column and a safety factor including toroidal effect is a few per cent larger than the defined value.[1)]

In order to observe the disruptive instability, neon gas is injected into a stable discharge with $q_a \leq 2.5$. The radiation loss increases and the disruptive instability is excited with good reproducibility. Various types of precursor oscillations of m=2/n=1 are observed, e.g. simply growing fluctuations or small fluctuations followed by sudden growth.

Figure 1 shows events immediately before and during the disruption. About 100 μs before the negative spike, mhd activity gradually increases, and X-ray signal from central chord decreases and from outer chord increases slowly. This means a spread of a current channel. The events in this phase are similar to those of minor and/or internal disruption. Then m=2/n=1 mode suddenly grows up to 5 ~ 8 % within 30 μs, and loop voltage drops steeply, i.e. the major disruption appears. The signal in outer chord rapidly increases, which means rapid spread of the hot column. The radiation loss including charge exchange loss is 40 kW before the neon injection and increases gradually up to 250 kW at the negative spike. These results suggest that the internal or minor disruption and impurity cooling enhance the m = 2 mode up to 4 ~ 6 % which triggers the negative spike. Therefore the observed behavior of the current disruption in this experiment with $q_a \sim 2$ is very similar to that in high-q discharge. It should be noted that the amount of neon injected to induce the disruption in the case with a divertor is 3 times larger than that without the divertor but the separatrix does not affect the major disruption as shown in a previous experiment.[2)]

In DIVA, a discharge in $q_a < 2$ region has been stably obtained by reducing a radiation loss. Examples of the discharge are shown in Fig.2. When the plasma current is crossing through $q_a = 2$, m=2/n=1 which may be surface mode grows up to $\tilde{B}_P/B_P = 4$ % and the loop voltage rises, but negative voltage spike is not usually observed. The characteristic feature of the mhd activity is not changed by changing the current rising time from 2.5 to 6 ms. When the plasma

has a separatrix in the shell, duration of voltage increase is shorter than the case without the separatrix, and the mhd activity is much smaller than that without the separatrix by a factor of 4. Therefore the separatrix stabilizes the surface mode. When the discharge fall into $q_a < 2$ region, fluctuations including m=3/n=2 are observed by magnetic probes but the level is very low, i.e. $\tilde{B}_P/B_P = 0.05$ %. Large sawtooth oscillations are observed in soft X-ray signal and loop voltage, and the energy confinement time τ_E is dominated by these internal disruptions. The average energy confinement time, however, follows Alcator scaling with a higher numerical factor in front of $\bar{a}^2 n_e q_a{}^{1/2}$.[3)]

When the limiter is inserted to $\bar{b}/\bar{a} = 1.35$, a stable $q_a < 2$ discharge can be obtained only during 3 ~ 6 ms without divertor, and the plasma column is slowly shifted outward because of no control field. This behavior is observed also in high-q discharge with $\bar{b}/\bar{a} = 1.35$. The mhd activity is weaker in a $q_a < 2$ discharge than in high-q discharge even with $\bar{b}/\bar{a} = 1.35$. The results suggest that the plasma with $\bar{b}/\bar{a} = 1.35$ can be obtained with a suitable control field. Operating the divertor with $\bar{b}/\bar{a} = 1.35$, the low-q discharge is more stable and reproducible. With the divertor, however, the volt-second is not enough and the duration with $q_a < 2$ is only 5 ms.

Examples of neon injection into the stable $q_a < 2$ discharge is shown in Fig.3. It should be noted that no major disruption occurs in $q_a < 2$ region which is contrast with disruption in $q_a > 2$ region. When neon gas is injected into a stable $q_a = 1.6$ discharge, the loop voltage increases as increasing radiation loss, and because of increasing resistivity the plasma current decreases. After the safety factor q_a becomes larger than two, the major disruption occurs. The number of observed disruptions at different q_a values is plotted in Fig.4. It can be clearly seen that the disruptive instability does not appear in $q_a < 2$ region. This result consistents with the conclusion that the origin of the disruption is m=2/n=1 internal mode.

Low-q discharges are investigated and following results are obtained:

1) Large m=2/n=1 fluctuations induced by impurity injection is the direct trigger of the major disruption near $q_a = 2$.

2) Separatrix does not affect the major disruption.

3) Reducing impurity level, the $q_a < 2$ discharges are stably obtained with $\bar{b}/\bar{a} = 1.2$ and probably with $\bar{b}/\bar{a} = 1.35$.

4) Increase of loop voltage and m=2/n=1 mode, probably surface mode, are observed when $q_a \simeq 2$ and stabilized by the separatrix magnetic surface.

5) The major disruption cannot be excited in $q_a < 2$ discharges.

These results encourage the attempt to achieve a high-β tokamak free from dangerous current disruptions by employing the very low-q discharge in a large device.

The authors are indebted to Dr. M. Wakatani and members of Theoretical group of JAERI for their stimulating and valuable discussions and members of DIVA operating group for their excellent assistance in the experiment. They would like to thank Drs. S. Mori, Y. Obata, M. Yoshikawa and Y. Tanaka for their support.

Reference

1) H. Ninomiya, private communication.
2) Y. Shimomura et al., Phys. Fluids 19 1635 (1976).
3) H. Maeda et al., 7th International Conference on Plasma Physics and Controlled Nuclear Fusion Research (Insbruck, 1978) paper T-3-1.

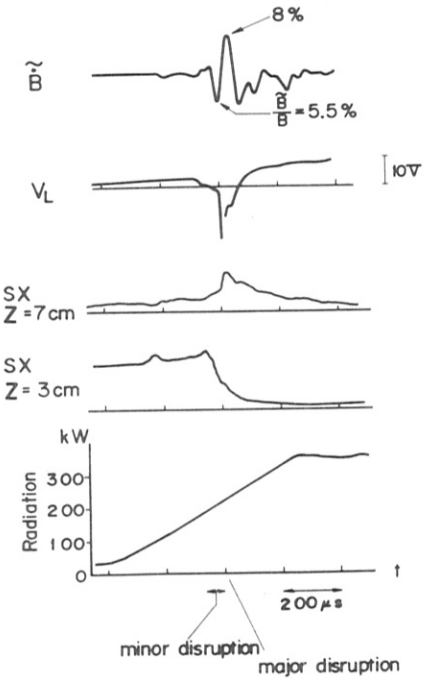

Fig.1 Typical example of major disruption. Neon is injected into stable q_a = 2.5 discharge at 1.5 ms before the negative spike. The disruption is separated into two steps, the first is slow decrease of V_L and the second is abrupt drop of V_L.

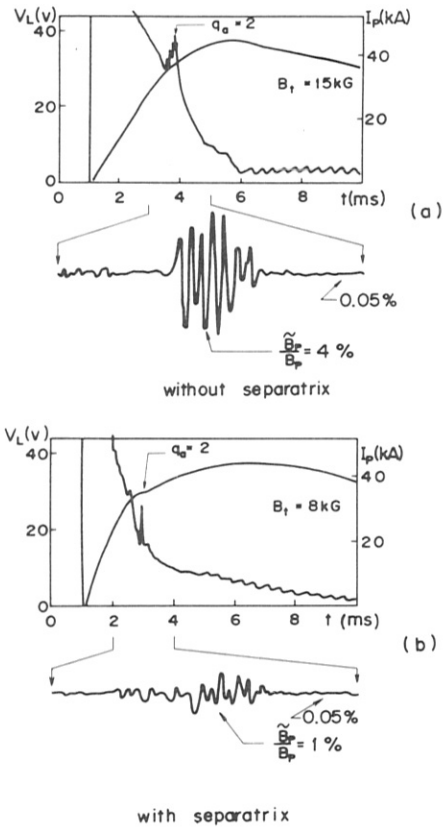

Fig.2 Examples of q_a < 2 discharge. (a); without separetrix (b); with separatrix. When the plasma current crossing through q_a = 2, m = 2 surface mode grows up to 1 % for the case with separetrix and 4 % without. In q_a < 2 region, sawtooth oscillations are seen in loop voltage, and magnetic fluctuations including m=3/n=2 is very weak typically 0.05 % in both cases.

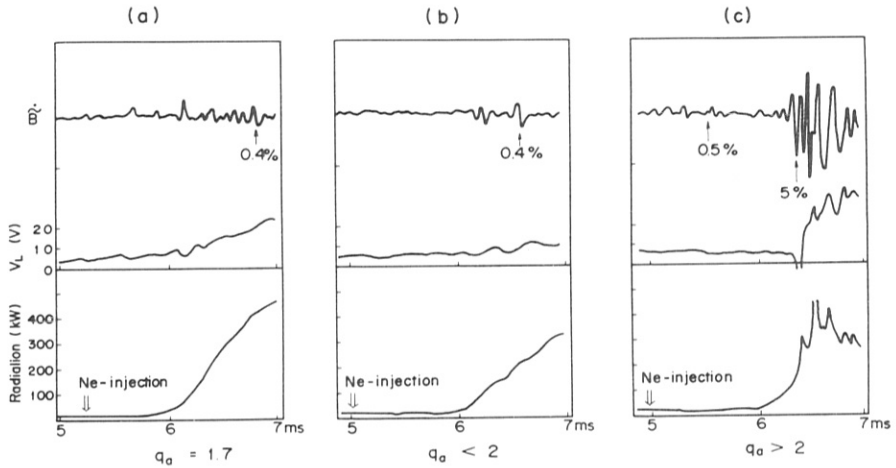

Fig.3 Neon injection into q_a = 1.7 (a), and q_a is around two discharges [(b) in case q_a < 2 and (c) in case q_a > 2]. Radiation loss in all cases increases in almost the same manner, but there is no major disruption in the former two cases in contrast to the last.

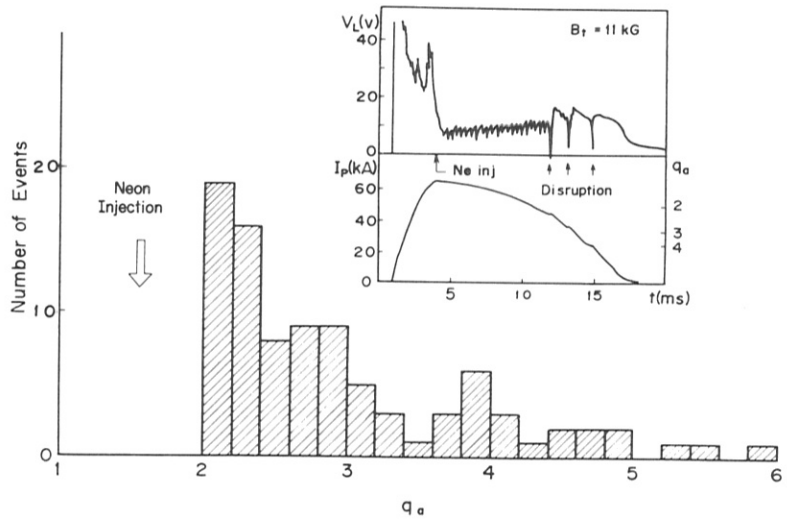

Fig.4 The number of observed disruptions at different q_a, when neon gas is injected into stable q_a = 1.6 discharge. It can be clearly seen that the disruptive instability does not occur in q_a < 2 region.

Experimental Study on Limit of the Safety Factor in JFT-2 Tokamak

M. MAENO, N. SUZUKI, S. KONOSHIMA,
T. YAMAMOTO, M. SHIMADA, and N. FUJISAWA

JAERI, Tokai, Naka, Japan

Introduction

Stable low-q discharges play an important role in realizing a low-cost tokamak reactor. The maximum discharge current in tokamak is limited by the current disruption. This paper describes the experimental results on limiting factors leading to the current disruption in the JFT-2 device.

Experimental Conditions

The JFT-2 device is a circular tokamak with a major radius of 90 cm, and shell radius b;36 cm. Rail type limiters were used in the experiment. Titanium was gettered to reduce light and heavy impurities.(1) Experiments were made in the following experimental conditions: toroidal magnetic field B_t;12—17 kG, plasma current I_p;110—140 kA, plasma minor radius a;15—20 cm, safety factor on the limiter surface q_a;1.7—3.3, and mean electron density $\bar{n}_e$;$(2—6.5)\times10^{13}$ cm^{-3}. Working gas is hydrogen.

Disruptions in Medium q_a($q_a \gtrsim 3$) Discharges

Stable discharges of $q_a \gtrsim 3$ were always obtained under the condition of low radiation loss power. The current disruptions were observed in the following cases; (a) dirty discharges, (b) discharges with increasing density,(1) and (c) neon injected discharges. In each case, m=2 oscillations and radiation grew up remarkably just before the current disruption(Fig.1).

MHD oscillations grew ~1 msec before the negative voltage spike (NVS) of the order of 100 V (does not include the small minor disruption here). Magnetic field fluctuations, and soft X-ray fluctuations had the same frequency, and had structures of m=2 and m=1 modes, respectively. The phases of these modes were locked to each other. Fluctuations $\tilde{B}_\theta$ of poloidal magnetic field B_θ rose up to 5 % of B_θ before the NVS. The radiation power was also enhanced during the growth of the oscillations. As shown in Fig.1(b), the radiation, cooling mainly the edge, increases 2.5 times as large as during the steady state (from 52 to 130 kW). In most cases, radiation power reached 60—80 % of the Joule input power. As the oscillations grew, the surface temperature of the limiter also rose abruptly by 140 degrees (from 350 to 490 °C). The observation was made in case (b). The heat flux to the limiter, as shown in Fig. 1(c), increases by 13 times to reach 80 kW, ~1 msec before the current disruption. This sudden change of the limiter heat load is tentatively interpreted as the enhancement of the radial heat transport caused by the MHD oscillations.

In the medium q_a discharges, the enhanced radiation loss changes the profile of the plasma current and induces the growth of the m=2 oscillations. The radial heat transport enhanced by the fluctuation, and resulting strong plasma-wall interaction again increase the radiation, and this process finally leads to the current disruption. The m=2 tearing mode seems to be the most plausible cause of the disruption. The edge radiation cooling by impurity plays an important role in this process, so that reduction of the impurity is essential in realizing the stable discharge of medium q_a. The attainable q_a of the stable discharges decreases with decreasing the radiation loss power, as shown in the region (A) of Fig.2.

Disruption in Low q_a Discharges

Possibility of obtaining low q_a discharge was tested by preparing the clean wall condition (titanium was flushed on the whole torus wall). However, the current disruptions are always observed at the value of q_a around 2.0, as shown in the region (B) in Fig.2.

Figure 3 shows the typical time behaviours of I_p, V_L and P_R for low q_a discharges. In this case, no radiation enhancement is observed until the current disruption, so that radiation loss and the above-mentioned (in medium q_a) process are not the cause of the disruptions in this case. Plasma current was increased to reach 140 kA to give q_a=1.9. A typical mode evolution is shown in Fig.3. The mode number decreased with plasma current increase. Minor spike late in the discharge was preceded by growing m=2, n=1 oscillations on $\tilde{B}_\theta$. The m=2 oscillations grew up to $\tilde{B}_\theta/B_\theta$=5—8 % in 50 μsec just before the disruption. Since the time constant of the liner is about 200 μsec, oscillations must have grown in shorter than 50 μsec, which is much shorter than the growing period of the oscillation in medium q_a discharge (~1 msec). Theoretical growth rates of m=2 tearing(2), and kink modes(3) are roughly estimated to be 3×10^3/sec, 2×10^5/sec, respectively. In this case, m=2 kink mode is the probable cause of the disruption. To check the effect of the shell stabilization, experiments were performed under the condition of different limiter radius. Attainable minimum q_a of 1.7 and 1.9 was obtained when b/a were 1.8 and 2.4, respectively. This result can be interpreted to suggest the possibility of the shell stabilization against the m=2 kink mode.

Conclusion

In medium q_a ($q_a \gtrsim 3$) discharges, the current disruption was avoidable by reducing the impurity radiation. The enhanced radiation loss plays an important role in the growth of the oscillations, which are considered as the m=2 tearing mode. The attainable q_a reduced with decrease of the radiation loss, and stable $q_a \gtrsim 2$ discharges could be obtained by preparing clean surface.

The current disruptions always occurred when $q_a \lesssim 2$, even under clean wall conditions. The radiation loss and resulting current channel shrinkage are not causes of the disruption in the $q_a \lesssim 2$ discharges. The m=2 kink mode is considered to induce the current disruption and hinder the discharge from going into the $q_a < 2$ region.

References

(1) S. Konoshima et al., J. Nuclear Materials, 76 & 77 (1978) 581.
(2) H. P. Furth et al., Phys. of Fluids, 6 (1963) 459.
(3) V. D. Shafranov, Zh. Tekh. Fiz., 40 (1970) 241 [Sov. Phys.-Tech. Phys., 15 (1970) 175].

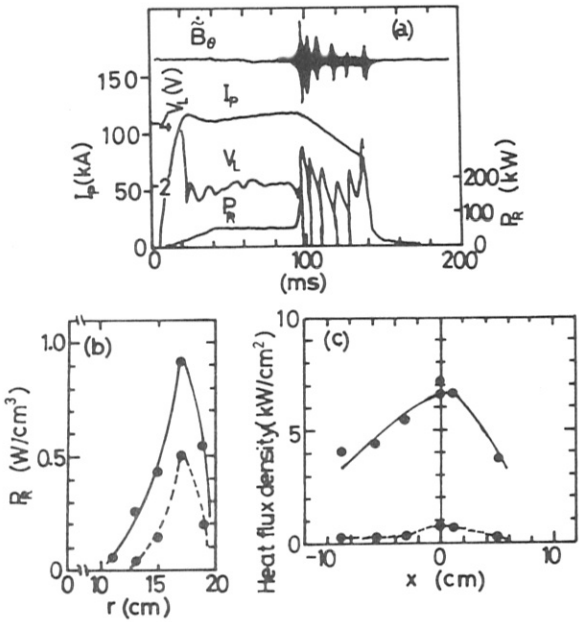

Fig.1. (a) Time variations of poloidal magnetic field fluctuations $\tilde{B}_\theta$, plasma current I_p, loop voltage V_L and radiation loss power P_R. Mean line-of-sight density $\bar{n}_e$ is about $(5\text{–}6.5)\times10^{13}$ cm^{-3}.
(b) Distribution in the X direction (along the rail limiter) of the enhanced heat flux to the limiter. Solid and dotted curves show the heat fluxes just before the disruption and during the steady state, respectively. The surface temperature of the limiter was measured with an infra-red camera.
(c) Radial profile of the enhanced radiation loss density. Solid and dotted curves represent the radiation loss just before the disruption and during the steady state, respectively.

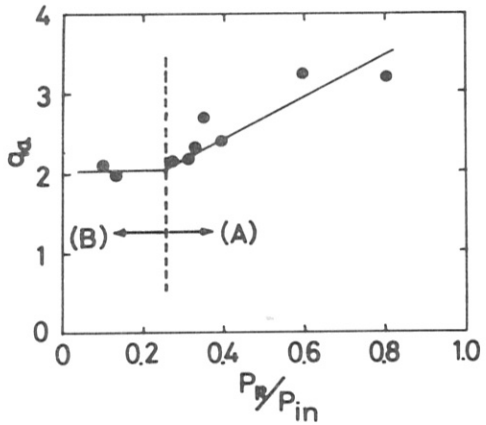

Fig.2. The dependence of the attainable q_a on radiation loss power. P_R is the radiation loss power and P_{in} is Joule input power. P_R/P_{in} is the value just before the disruption.

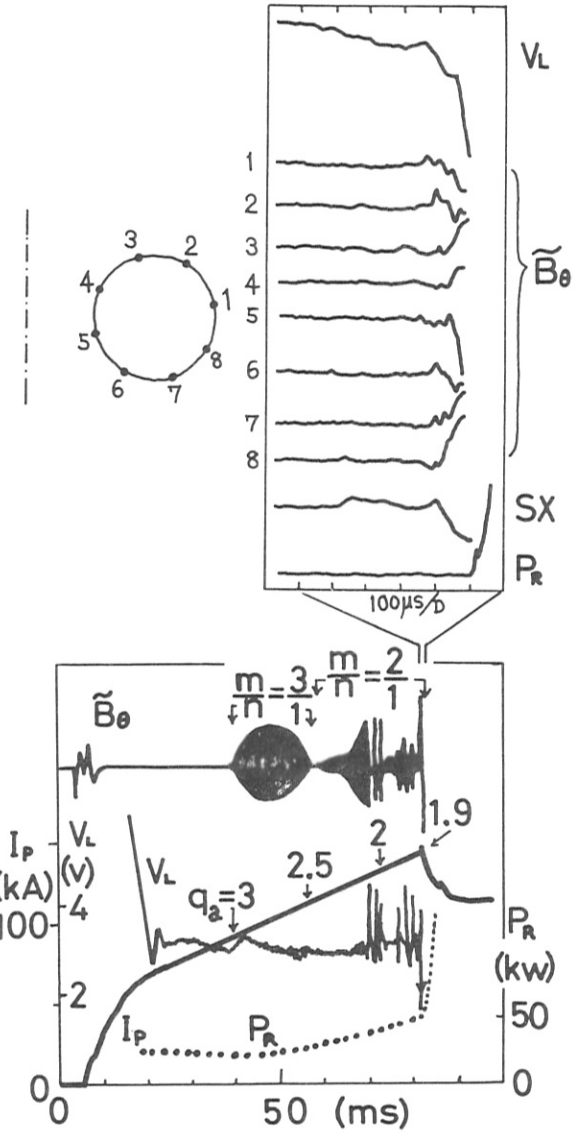

Fig.3. Typical time behaviours of poloidal magnetic field fluctuations $\tilde{B}_\theta$, plasma current I_p, loop voltage V_L and radiation loss power P_R in the case of clean wall condition. Magnetic field fluctuations (m=2), V_L, soft X-ray intensity (SX) and P_R are shown in the upper part of the figure. $n_e \simeq 1.5 \times 10^{13}$ cm^{-3}.

SURVEY OF MHD MODES AND THEIR EFFECTS IN ORMAK, ISX-A, AND ISX-B*

J. L. Dunlap, R. D. Burris, J. H. Harris,† A. P. Navarro,‡ and V. K. Paré

Oak Ridge National Laboratory, Oak Ridge, TN 37830, U. S. A.

Introduction: A comparison of some features of the three tokamaks is given as Table 1. The ORMAK and ISX-A have ceased operation. The ISX-B has completed a checkout phase with studies of circular, ohmically heated plasmas in which it performed much like ISX-A. Shaped and injection heated plasmas are being studied, but the data base for these is not sufficient to include details in this report.

Diagnostics for mode structures were the usual Mirnov loops for $\tilde{B}_\theta$ and collimated soft x-ray detectors for the internal fluctuations $\tilde{X}$. The $\tilde{X}$ measurements on ISX-A, and thus far on ISX-B, used only a single x-ray channel which viewed vertically across the center of a minor cross section. Multiple channels were used on ORMAK in a fashion which permitted m number determinations at several plasma radii. For detailed studies, analog signals were stored on magnetic tape and later digitized for fast Fourier transform analysis.

More complete descriptions of most of the observations are available elsewhere.[1]

Typical Mode Patterns: The "steady state" portion of the discharges usually shows one of two types of general mode behavior.[2] One, Type A, is characterized by strong m = 2 $\tilde{B}_\theta$ and $\tilde{X}$ and weak internal disruptions with short sawtoothing periods. The other, Type B, has weak $\tilde{B}_\theta$ but more pronounced internal disruptions with longer periods. Type A was favored by operation at high density and at low q_ℓ. Type B extended farther into those regions when neutral beam heating was added in ORMAK. In ISX-A, weak Type A early in the discharge could be converted into Type B by a programmed gas puff.[3]

Loop signals with Type B in ORMAK were m = 3 or 4; in ISX-A, the present evidence indicates simultaneous 2 and 3. We have only loop definitions of toroidal mode number, always n = 1.

Effects of Impurities: For most of its lifetime, ORMAK was characterized by $5 \leq Z_{eff} \leq 10$. The ISX plasmas have had $Z_{eff} \leq 2$. The lower impurity levels produced broader profiles and a significant extension of the operating

regime stable against disruption, as illustrated in Figure 1. Most of ORMAK's operation was with $q_\ell \approx 5$, and that of ISX-A with $q_\ell \approx 3.5$. Practical low q limits of operation for ORMAK were $q_\ell \approx 3.5$ (OH) and 2.6 (NBI). ISX-A operated well at 2.7; we did not attempt a thorough study at lower q. High density and low q limits of operation usually took the form of a series of soft disruptions with dominant m = 2 rather than hard disruptions. The enhanced stability of ISX-A against large m = 2 and the gas puff control resulted in its operation almost exclusively with Type B discharges. By way of contrast, much of the parameter space explored by ORMAK was marked by Type A behavior or by only marginal stability to large m = 2.

Mode Coupling: Studies of the Type A discharges in ORMAK showed m = 1 and 2 structures in $\tilde{X}$ while the $\tilde{B}_\theta$ showed m = 4, then 3, and finally 2 as the discharge developed. At any given time, the modes present had the same frequency and coincided in phase along an outward directed minor radius. Most of the Type B behavior in ORMAK was characterized by identical $\tilde{X}$ (m = 1) and $\tilde{B}_\theta$ frequencies. An interesting exception was that in some discharges with neutral beam injection, the frequency of $\tilde{X}$ just prior to internal disruption was significantly lower than that of $\tilde{B}_\theta$. This behavior is illustrated in Figure 2. A definite frequency relation between the two signals may not exist, but a ratio of approximately 2/3 was most often observed.

In ISX-A we noted the dominant frequency of the m = 1 $\tilde{X}$ changing from a value lower than that of the loop signal to synchronization with the loop as the plasma recovered from an internal disruption, as has been reported[4] for TFR. We have no evidence of this from ORMAK.

Disruptions that develop out of relatively quiet discharges, after a brief interval of growing m = 2 with the last few cycles showing distinctive distortion patterns associated with coupled m = 2 and m = 1 modes, have been reported in a number of tokamaks. The soft disruptions which terminate our Type B discharges develop out of briefly growing m = 2, and the last cycles usually show these characteristic distortions. In this connection it is interesting that ORMAK Type A discharges near the low q and high density limits could display these characteristic patterns, grossly distorted and with $\tilde{B}_2/B_\theta \approx 1\%$, for tens of milliseconds without disrupting.

Modes and Confinement: We found a correlation of gross energy confinement time, τ_E, and mode activity in ORMAK in the case of large m = 2 at low q. τ_E declined and the level of the m = 2 increased as q_ℓ was progressively

lowered. Degradation of τ_E by large m = 2 was also observed in ISX-A, but not systematically mapped. In both devices the m = 2 was accompanied by degradation of particle confinement as well.

Disruptions During Current Rundown: Plasmas that are well behaved with regulated I_p often disrupt during current rundown. A gradual approach of the singular surfaces may be involved, since in ORMAK we observed that r_1 remains relatively fixed but r_2 moves inward as I_p is reduced.

Arcing and Disruptions: An experiment in ISX-B by Mioduszewski, Clausing, and Heatherly[5] has revealed a relationship between unipolar arcs and soft disruptions. The arrangement monitored current flow from the wall of the vacuum vessel to a metal sample mounted near the edge of the plasma. In well behaved discharges, arcing was detected only at the initial breakdown and in the quenching phase during I_p rundown. In discharges with soft disruptions, the arcing sample showed current pulses up to 20 A coincident with the disruptions.

Acknowledgment: It is a pleasure to acknowledge the cooperation and assistance of our many colleagues in the Experimental Confinement, Plasma Technology, and Plasma Theory Sections during this work.

---

*Research sponsored by the Office of Fusion Energy (ETM), U. S. Department of Energy, under contract W-7405-eng-26 with Union Carbide Corporation.

†Present address, University of Wisconsin, Madison, WI 53706.

‡Visitor from J. E. N., Madrid, Spain.

1. Thermonuclear (Fusion Energy) Division Annual Progress Reports for 1975 (ORNL-5154), 1976 (ORNL-5275), and 1977 (ORNL-5405).

2. L. A. Berry et al., 5th IAEA Conf. on Plasma Physics and Controlled Nuclear Fusion Research (Tokyo, 1974) I, 101.

3. M. Murakami et al., 7th IAEA Conf. on Plasma Physics and Controlled Nuclear Fusion Research (Innsbruck, 1978), CN-37-N-4.

4. EQUIPE TFR, Nucl. Fusion 17, 1283 (1977).

5. P. Mioduszewski, R. E. Clausing, and L. Heatherly, to be published in J. Nucl. Mater.

Table 1. Comparisons of the Tokamaks

DEVICE	PLASMA SHAPE	SHELL	R(cm)	a_ℓ(cm)	I_p, B_T(kA,kG)
ORMAK	Circular	Yes	80	23	170,26
ISX-A	Circular	No	92	26	120,13
ISX-B	Circular	No	93	27	150,12
	Elliptical and D			27/50	

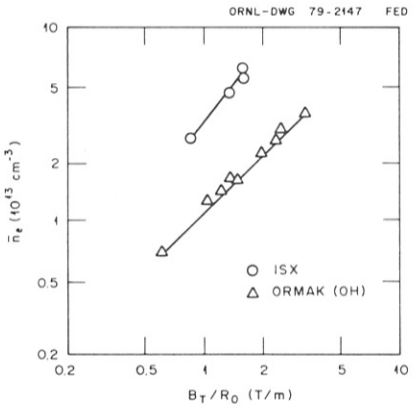

Figure 1. Comparison of stability against disruption (hydrogen plasma).

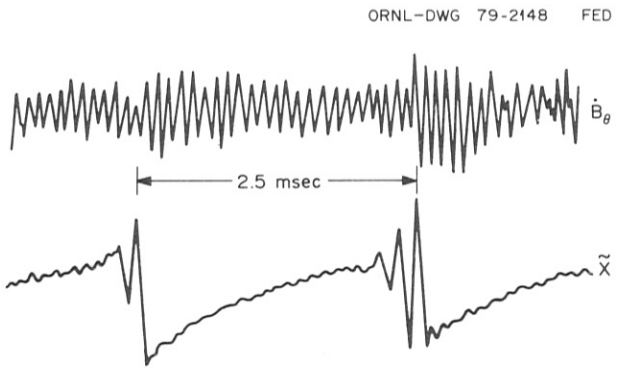

Figure 2. Internal disruptions in ORMAK with neutral beam heating. The $\tilde{X}$ channel includes a 100 Hz high pass filter.

LOW-q(a) DISCHARGE BY CURRENT-DENSITY-PROFILE CONTROL IN THE RESISTIVE-SHELL TOKAMAK, JIPP T-II

K. Toi, S. Itoh*, K. Kadota, K. Kawahata, N. Noda,
K. Sakurai, K. Sato, S. Tanahashi and S. Yasue
Institute of Plasma Physics, Nagoya University, Nagoya, JAPAN
*Research Institute for Applied Mechanics, Kyushu University, Fukuoka, JAPAN

ABSTRACT In JIPP T-II, the current-density-profile control is carried out by the careful pre-programming of both gas puffing and plasma current waveform. The major disruptions are completely suppressed by the method and a high density tokamak plasma with low-q(a) is obtained with better stability, where the line-average electron density $\bar{n}_e \leq 8.5\times10^{13}\,cm^{-3}$ and $q(a) \geq 2.2$.

INTRODUCTION Tokamak research has been devoted in obtaining a high density plasma with low-q(a) as the first step of attainment of high-β value. In a resistive shell tokamak such as JIPP T-II, the current-density-profile control is the most effective way to obtain a low-q(a) plasma[1].

EXPERIMENTAL ARRANGEMENTS The JIPP T-II plasma[2,3] is maintained in the equilibrium position by feedback-controlling the vertical and horizontal magnetic fields, and the plasma radius is always defined by half of a rail-type limiter distance, i.e., a_L=15 cm. The hydrogen gas is fed by the programmable piezo-electric valves. The plasma current waveform is varied by the charging voltage of three blocks of capacitor banks. Thomson scattering, VUV spectrometer, PIN diodes etc. are used in the experiment.

CURRENT-DENSITY-PROFILE CONTROL BY PRE-PROGRAMMING OF GAS PUFFING AND PLASMA CURRENT WAVEFORM The high density tokamak plasma can be obtained by gas puffing in the course of discharge. The strong gas puffing is apt to lead to the remarkable shrinkage of current channel and major disruption. The process is stopped by controlling the current density profile through heating the outer plasma region. The second current rise is effective for heating the region. We examine whether the current density profile can be controlled to the favourable one for MHD stability and what is the optimum condition for success in the current-density-profile control and obtaining a high density plasma with low-q(a). Figure 1 shows the time variations of plasma parameters in three cases, where case I:with a strong gas puffing without the second current rise, case II:with the second current rise in the constant density operation and case III:the optimum combination between the strong gas puffing and the second current rise. In Fig.2 time evolutions of profiles of electron temperature and density are shown for three cases. In case I, the remarkable cooling and shrinkage are observed. It is seen from case II that the second current rise is effective for heating the outer plasma region. The MHD oscillations m/n=4, 3 and 2 are successively observed during the second rising phase of plasma current. In case III, the second current rise is applied after 10 msec from the strong gas puffing. The relative amplitude of magnetic perturbation $\tilde{\delta B}_\theta/B_\theta$ is suppressed within 5×10^{-4}, though q(a) reaches 2.5. We derive the current density profile by solving the magnetic diffusion equation,where the classical conductivity with the usual trapped electron correction has been adopted(Fig.3). The $Z_{eff}(r)$ profile has been adjusted iteratively so that the calculated loop voltage and q(r)=1 surface should be best-fit for the experimentally obtained ones, respectively, where the q(r)=1 surface is approximately defined as the position where the sawteeth oscillations are inverted[4,5]. The favourable profile of current density against the MHD stability is produced by the electron heat balance between the heating effect of the outer region by the second current rise and the cooling one by the strong gas puffing.

We examine the control criterion that the current density profile can be successfully controlled, changing the increasing rate of electron density, the second increase of plasma current etc. Figure 4 shows the relative amplitude of magnetic perturbation as a function of the ratio of plasma

current to line-average electron density during the second rising phase of plasma current, where q(a)=2.2-4.5, $\bar{n}_e$=1.8-8.5x10^{13}cm^{-3} and the rise time of the second current increase τ_R=15-30 msec. The stability "window"($\tilde{\delta B}_\theta/B_\theta < 10^{-3}$) can be found in the range $20\times10^{-13} \lesssim I_p/\bar{n}_e \lesssim 30\times10^{-13}$ kA.cm^3. The upper limit is set by overheating of the outer plasma region by the second current rise and the lower one by intense cooling of the region by gas puffing. The above control criterion is also successfully applied to the initial current rising phase of tokamak discharge and the lowest q(a) discharge(q(a)=2.2) has been obtained in $\bar{n}_e$=5x10^{13}cm^{-3}.

The stability of low-m mode(m/n=2, 3/2 and 3) for the current density profiles of cases I, II and III is investigated theoretically. The time behaviours of delta prime related with tearing mode[6] and the perturbed potential energy for kink mode[7] are shown in Fig.5. Introduction of toroidal effect for tearing mode[8] does not change the stability evaluation by Fig.5 except for 74 msec(cases I, II and III) for m/n=3/2 and 94 msec(case I) for m/n=3/2. The results of the above analysis agree well with the experimental data after 90 msec.

It is concluded that the current-density-profile control has been successfully carried out by programming both gas puffing and plasma current waveform, and the growth of m/n=2 mode is reduced to the lower level and the m/n=3/2 is completely suppressed.

ACKNOWLEDGEMENTS We wish to express our appreciations to Prof. K. Matsuura, Prof. J. Fujita and Mr. Y. Kawasumi for their cooperations of plasma measurements.

REFERENCES

[1] Glasser, A. H. et al., Phys. Rev. Lett. 38(1977)234.
[2] Toi, K. et al., IPP Nagoya Research Report, IPPJ-322(1978).
[3] Fujita, J. et al., in Plasma Physics and Controlled Nuclear Fusion Research(Proc. 7th Intern. Conf. Innsbruck, 1978).
[4] Von Goeler, S. et al., Phys. Rev. Lett. 33(1974)1201.
[5] Equipe TFR, Nucl. Fusion 17(1977)1283.
[6] Furth, H. P. et al., Phys. Fluids 16(1973)1054.
[7] Shafranov, V. D., Soviet Phys. Tech. Phys. 15(1970)175.
[8] Glasser, A. H. et al., Phys. Fluids 19(1976)567.

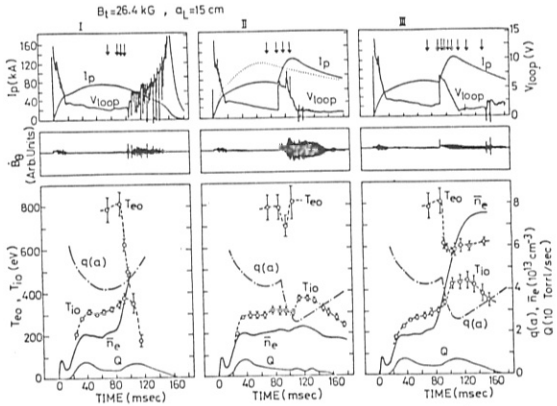

Fig.1 Time variation of plasma parameters in cases I, II and III.

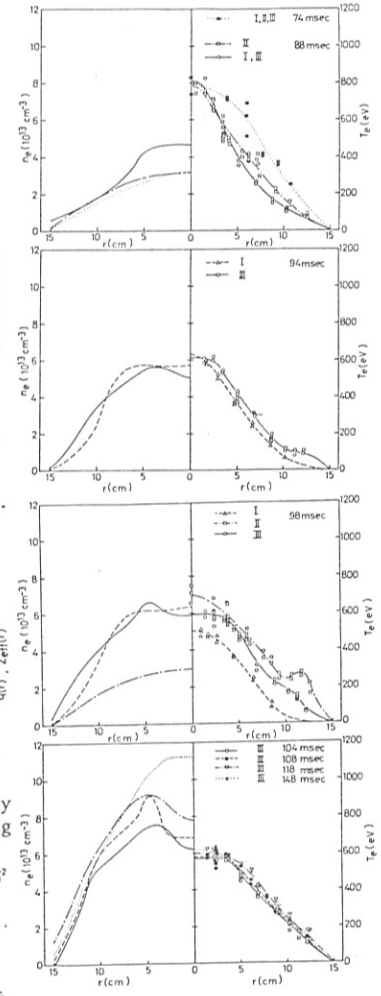

Fig.2 Time evolution of profiles of electron temperature and density for cases I, II and III.

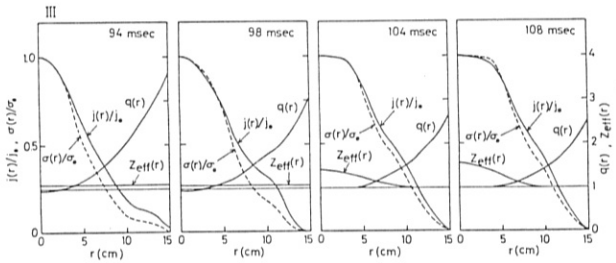

Fig.3 Time evolution of profiles of current density , safety factor etc. during the second rising phase of plasma current of case III.

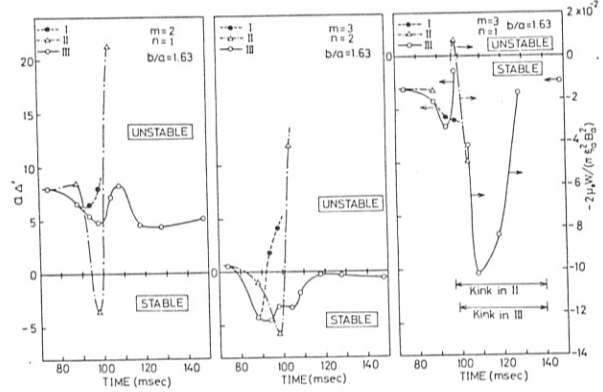

Fig.5 Time behaviour of delta prime for tearing mode and perturbed potential energy for kink mode.

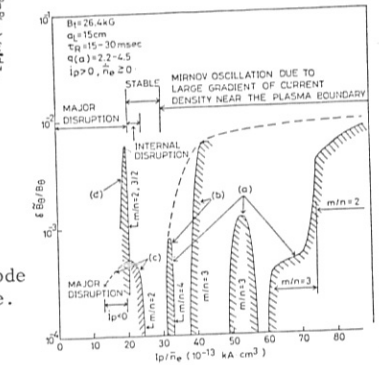

Fig.4 Relative amplitude of magnetic perturbation as a function of $I_p/\bar{n}_e$.

Poloidal Rotation as the Cause of the m=1 Mode in Tokamaks

A.A. Ware
University of Texas at Austin

Abstract. It is shown that the internal m=1 mode observed in the center of Tokamak discharges can be explained as an MHD interchange mode driven by the weak poloidal rotation which must be present for equilibrium.

Very few experimental measurements have been made of the safety factor q ($\equiv rB_\phi/RB_\theta$) near the magnetic axis in Tokamaks. Of these only the measurements of Makishima et. al.[1], using magnetic probes in a low current low temperature discharge, have had both good time resolution and reasonable accuracy. It was found that the m=1 mode commenced as soon as q reached unity at r=0 and that q never fell below unity. Instead a flat plateau region was generated with q=1. A similar conclusion is suggested by the ion beam measurements of q by Goldston on ATC[2], but because of the limited (±10%) accuracy it was possible to conclude only that q did not fall below 0.9 near the magnetic axis. The formation of a q=1 plateau suggest that the m=1 mode is an MHD interchange mode rather than a tearing mode, since one of the nonlinear effects of interchange convecting cells is to eject or annihilate any shear field which would make $\underset{\sim}{k}\cdot\underset{\sim}{B}$ nonzero, an effect which was observed in toroidal pinch discharges[3]. If the unstable condition which is driving the interchange mode is maintained by some other process, the convection will continue maintaining the $\underset{\sim}{k}\cdot\underset{\sim}{B}$=0 plateau.

In this paper a possible mechanism is suggested for driving an interchange mode, namely poloidal rotation combined with a negative gradient of the plasma mass density. Using the weak poloidal rotation required by neoclassical theory for poloidal equilibrium and a shear-free model, MHD theory leads to frequencies and growth rates in agreement with experiment and to the correct sign for the wave velocity. It should be noted however, that the recent work of Zhakarov[4] has shown from a more

accurate treatment of the m±1 harmonics that a weak pressure gradient is sufficient to make the m=1 mode MHD-unstable. The rotational destabilizing effect will add to the pressure gradient effect of Zhakarov; but here, for simplicity, the destabilizing effect of the pressure gradient is ignored.

A simple model is taken with q=1 for the range $0 \le r \le r_s$ where r_s is a small fraction of the tube radius a. Over this range the plasma is assumed to have a constant angular rotation speed $\Omega \equiv \bar{v}_\theta/r$ which is formally taken to be of order v_{T_i}/R_0, although the numerical value from neoclassical theory used below is somewhat smaller than this ($\sim v_{T_i}/5R_0$). A small perturbation of the plasma velocity is considered $\underset{\sim}{v} = \Sigma\, \underset{\sim}{v}_m(r) \exp i\,(\omega t + m\theta + \phi)$ with m = m-1, m, m+1. For simplicity the components $\underset{\sim}{v}_{m\pm1}$ are chosen to give $\delta\underset{\sim}{B}_{m\pm1} = 0$, where $\delta\underset{\sim}{B}$ is the perturbation to the magnetic field. This rules out any ballooning effect and, in particular, the destabilizing effect of the pressure gradient found by Zakharov. For the fundamental, $\underset{\sim}{k}\cdot\underset{\sim}{B} = 0$ and hence δB_r and $\delta B_\perp$ are zero, where the subscript $_\perp$ refers to the direction of $\underset{\sim}{B}\times\underset{\sim}{\nabla}p$. Assuming $\omega \lesssim \Omega$ the linearized equation of motion to order $(r/R)^2$ is then

$$i(\omega+\Omega)\rho\underset{\sim}{v}_m - 2\rho\Omega(\underset{\sim}{v}_m\times\underset{\sim}{i}_\phi) + \underset{\sim}{i}_r\Omega^2 r\delta\rho = -\underset{\sim}{\nabla}(B\delta B_\parallel + \delta p)_m \qquad (1)$$

with the perturbation in the plasma mass density ($\delta\rho$) given by

$$i(\omega+\Omega)\delta\rho = -v_{rm}\rho' - \rho\nabla\cdot\underset{\sim}{v}_m \qquad (2)$$

where the prime denotes $\partial/\partial r$. The curvature term in the Maxwell stress tensor $(\underset{\sim}{B}\cdot\underset{\sim}{\nabla}\underset{\sim}{B})$ is zero to this order for q=1. The usual MHD equations for $\delta B_\parallel$ and δp give $(B\delta B_\parallel + \delta p) = [(B^2+\gamma p)\underset{\sim}{\nabla}\cdot\underset{\sim}{v} - v_r\rho\Omega^2 r]/i(\omega+\Omega)$ and hence, from eq. (1)

$$\underset{\sim}{\nabla}\cdot\underset{\sim}{v}_m \sim r\Omega^2\rho v_m/(B^2+\gamma p) = 0 \qquad (3)$$

to high order in (r/R). By taking the ϕ-component of the curl of eq. (1) and substituting from eqs. (2) and (3), the equation for v_{rm} is

$$(\omega+\Omega)^2[r\rho(rv_r)']' - (rv_r)[(2\omega\Omega+\Omega^2)\rho' + (\omega+\Omega)^2(\rho/r)] = 0 \qquad (4)$$

where the subscript m has now been dropped. Assuming a parabolic form for the mass density $\rho = \rho_o[1-(r/a)^2]$, since $r\rho' \ll \rho$ over the range $0 \le r \le r_s$, an approximate form of eq. (4) is

$$(rv_r)'' + (rv_r)'/r + (k^2 - \frac{1}{r^2})(rv_r) = 0 \qquad (5)$$

where $k^2 = 2(\Omega^2 + 2\omega\Omega)/a^2(\omega + \Omega)^2$. This is now a Bessel equation and the solution is $(rv_r) \propto J_1(kr)$. Taking the boundary conditions to be $v_r = 0$ at $r = r_s$ requires $kr_s = 3.8$, giving the dispersion relation

$$\omega^2 + (2\omega\Omega + \Omega^2)(1 - \delta^2) = 0 \qquad (6)$$

with $\delta = \sqrt{2}\, r_s/3.8a$. Since δ^2 is small, to a good approximate eq. (6) gives

$$\omega = -\Omega \pm i\delta\Omega. \qquad (7)$$

For a more general radial dependence of ρ, eq. (6) can be obtained with

$$\delta^2 = -\int_0^{r_s} r^2 \rho' v_r dr \Big/ \int_0^{r_s} r\rho(v_\theta^2 + v_r^2)dr \qquad (8)$$

For the conditions corresponding to the slow rise part of a sawtooth, the neoclassical theory discussed in an accompanying paper[5] gives a typical value of $\bar{V}_\theta$ to be $\sim 0.4(B_\theta/B)(ZT_i/m_z)^{\frac{1}{2}}$. Taking Z=8, from eq. (7) the predicted wave velocity $(-\omega_r r/m)$ is $V_\theta = +0.8\, v_{T_z} r/R$, the predicted angular frequency is $\Omega = 0.8 v_{T_z}/R$ and the growth rate is $\delta\Omega = \sqrt{2} r_s \Omega/3.8a$, assuming the parabolic density variation. The sign of the wave velocity agrees with experiment, namely positive, the sign of the electron diamagnetic drfit. For ion temperatures from 300 to 500 eV and R=100cm, the predicted frequency range is 7 to 10 kH_z in close agreement with the observed frequency of 10kH_z in ST[6] and in TFR[7]. For ST, taking T_i = 350eV (S. von Goeler, private communication), $r_s/a = 2/13$ and R = 109cm, the predicted growth rate is $2.7 \times 10^3 sec^{-1}$ compared with the observed growth rate[6] of $3 \times 10^3 sec^{-1}$. For TFR taking T_i = 530eV (J. Tachon, private communication), $r_s/a = 5/20$, and R = 98cm, the predicted growth rate is $5.9 \times 10^3 sec^{-1}$ compared with an observed growth rate[7] of $3.3 \times 10^3 sec^{-1}$.

In the absence of any mechanism keeping ρ' negative, the interchange mode would be self stabilizing. However, mechanisms are present to maintain ρ' negative. In addition to the trapped particle pinch effect,

a stronger contribution will come from the inward impurity ion diffusion. In the presence of electrostatic trapping, this inward flow of the heavy impurity ions is not as strong as was originally predicted in neoclassical theory, but it is still inwards and is a stronger effect than the pinching of the plasma as a whole[8]. These effects will continue to drive the m=1 convection, which in turn will maintain the shearless region with q=1 as observed.

1. K. Makishima, T. Tominaga, H. Tohyama and S. Yoshikawa, Phys. Rev. Letters 36, 142(1976).
2. R.J. Goldston, Princeton Plasma Physics Laboratory Report PPPL-1432, April 1978.
3. A.A. Ware, Nuclear Fusion 1962 Supplement - Part 3, p. 869.
4. L.E. Zakharov, Nucl. Fus. 18, 335(1978).
5. A.A. Ware, R.D. Hazeltine and J.C. Wiley, paper presented at this Symposium.
6. S. von Goeler, W. Stodiek and N. Sauthoff, Phys. Rev. Letters 33, 1201(1974).
7. T.F.R. Group, Proc. 7th European Conf. on Controlled Fusion and Plasma Physics, Vol. II, p.1 (1975).
8. R.D. Hazeltine and A.A. Ware, Phys. Fluids 20, 1880(1977).

"Neoclassical Theory of the Sawtooth Oscillations: An m=0, n=0, Poloidal Rotation Instability"

A.A. Ware, R.D. Hazeltine, J.C. Wiley
University of Texas at Austin

Abstract For plasmas with a substantial impurity concentration ($n_z Z \sim n_i$) and near the magnetic axis where the m=1 mode is assumed to keep density and temperature gradients small, it is shown that an m=0, n=0 poloidal rotation instability occurs at a critical electron temperature in close agreement with observed temperatures.

As discussed in an accompanying paper,[1] the m=1 mode observed in the central region of Tokamak plasmas is interpreted as an interchange mode. Here this interchange mode is assumed to keep the density and temperature gradients of all particle species small so that the only force tending to cause poloidal rotation is the electron viscous force due to the current $j_\parallel$. A hydrogen plasma (n_i,n_e) is considered with a single high-Z impurity having concentration such that $n_z Z \sim n_i$. The electrons and hydrogen ions are taken to be in the plateau regime, the Z-ions in the Pfirsch-Schluter regime. Starting with the poloidal momentum balance equation for the whole plasma, accurate to first order in the Larmor radii (i.e., diagonal pressure tensor $\underline{\underline{P}}$), but keeping the convective inertia terms because of the large impurity ion mass, multiplying by $(R_0+r\cos\theta/R_0)^2$ and averaging over θ gives, for equilibrium

$$(\Sigma \bar{n}_j m_j)\frac{\partial \bar{V}_\theta}{\partial t} = -\frac{\overline{(P_\parallel + P_\perp)\sin\theta}}{R_0} - \frac{\bar{V}_\parallel^2}{R_0}\Sigma\,\overline{n_j m_j \sin\theta} = 0 \qquad (1)$$

where θ is the poloidal angle and the bar denotes a simple θ-average. Using the lowest order momentum balance equation parallel to $\underset{\sim}{B}$, namely

$$\frac{B_\theta}{B}\frac{\partial P_\parallel}{r\partial\theta} = -\underset{\sim}{i}_\parallel \cdot \Sigma n_j m_j \underset{\sim}{V}_j \cdot \nabla \underset{\sim}{V}_j$$

and the continuity equation for either ion species

$$n_j \frac{\partial V_{j\parallel}}{r\partial\theta} = \frac{V_{j\theta}}{\Theta r}\frac{\partial \tilde{n}_j}{\partial\theta} - \frac{2\bar{n}_j E_r \sin\theta}{R_o B_\theta} \qquad (2)$$

where $\Theta \equiv B_\theta/B$ and $V_\theta = \Theta V_\parallel - (E_r/B)$, the equilibrium condition reduces to

$$\overline{(P_\parallel - P_\perp)\sin\theta} - 2\Sigma\,\overline{\tilde{n}_j m_j \sin\theta}\left[\left(\frac{\bar{V}_\theta}{\Theta}\right)^2 + \left(\frac{E_r}{B_\theta}\right)^2\right] = 0 \qquad (3)$$

Using quasi-neutrality to eliminate $\tilde{n}_z$, the electron and hydrogen ion contributions to Eq. (3) are given by standard neoclassical theory[2]. Substituting from reference 2 and dividing by the factor $\pi^{1/2} n_i m_i v_{T_i} r/2R_0$, Eq. (3) becomes

$$\frac{\bar{V}_\theta}{\Theta}\left\{1 - \frac{X_c}{2} - \left(\frac{m_z}{Z} - \frac{m_i}{2}\right)\frac{(1-X_c)}{2T_i}\left[\left(\frac{\bar{V}_\theta}{\Theta}\right)^2 + \left(\frac{E_r}{B_\theta}\right)^2\right]\right\} = \left(\frac{m_e}{m_i}\right)^{1/2}\left(\frac{T_e}{T_i}\right)^{1/2}\frac{\sigma_\parallel E_\parallel}{n_i e}$$

$$\times\left\{1.2 + 0.4\,\frac{T_i X_c}{T_e} + \frac{m_z}{Z}\left(\frac{0.79 + 0.38\frac{T_i X_c}{T_e}}{2\,T_e}\right)\left[\left(\frac{\bar{V}_\theta}{\Theta}\right)^2 + \left(\frac{E_r}{B_\theta}\right)^2\right]\right\} \qquad (4)$$

where $X_c \equiv \mathrm{Re}\,\tilde{\Phi}_c/rT_i$, with $\tilde{\Phi}_c$ the $\cos\theta$ component of the poloidal electrostatic potential variation $\tilde{\Phi}(\theta)$ and $\sigma_\parallel$ is the parallel conductivity allowing for Z_{eff}.

With the large impurity concentration assumed, the Z-ion terms are dominant in generating the potential $\tilde{\Phi}$. We require the Z-ion continuity equation (Eq. 2), the parallel momentum balance for these ions, namely

$$-\frac{5T_i}{3}\frac{\partial n_z}{\partial\theta} - n_z Ze\frac{\partial\tilde{\Phi}}{\partial\theta} = n_z m_z\left[\frac{V_\theta}{\Theta}\frac{\partial V_\parallel}{\partial\theta} - \frac{V_\parallel V_\perp r\sin\theta}{\Theta R_0}\right] \qquad (5)$$

and charge neutrality

$$Zn_z = n_e - n_i = N_e\exp(e\tilde{\Phi}/T_e) - N_i\exp(-e\tilde{\Phi}/T_i) \quad . \qquad (6)$$

We first note that if the linear approximations to equations (2), (5) and (6) are taken, the solution for the potential is

$$\frac{e\tilde{\Phi}}{T_i} = \left(\frac{Z\bar{n}_z}{\bar{n}_i + \frac{T_i}{T_e}\bar{n}_e}\right)\frac{\left[\bar{V}_\theta^2 + \left(\frac{E_r}{B}\right)^2\right]}{\left[\Theta^2 C_{ss}^2 - \bar{V}_\theta^2\right]}\frac{r\cos\theta}{R} \qquad (7)$$

where $c_{ss} \equiv \left[\frac{5}{3} + \frac{Z^2\bar{n}_z}{\bar{n}_i + (T_i\bar{n}_e/T_e)}\right](T_i/m_z)^{1/2}$ is the slow sound speed associated with the impure hydrogen plasma with the assumed collisionalities and Θc_{ss} is the wave velocity of the corresponding slow compressional magnetosonic wave with wave vector in the θ-direction. A typical magnitude for Θc_{ss} is $v_{T_i}/50$ so that even weak

C 2

rotation will encounter the resonance involved in the denominator of Eq. (7). Clearly a more accurate treatment of Eq. (2), (5) and (7) is required. Provided $(\nu_{iz}/\omega_{bi}) << (r/R)^{\frac{1}{2}}$ the quadratic (non-linear) terms in these equations are more important than the collisional terms which have been neglected. Assuming this inequality, the non-linear equation for $\tilde{\Phi}$ is

$$A_2\left[\left(\frac{e\tilde{\Phi}}{T_i}\right)^2 - \overline{\left(\frac{e\tilde{\Phi}}{T_i}\right)^2}\right] - A_1\frac{e\tilde{\Phi}}{T_i} + \left[\bar{V}_\theta^2 + \left(\frac{E_r}{B}\right)^2\right]\frac{r\cos\theta}{R_0} = 0 \qquad (8)$$

where $A_1 = \left(\bar{n}_i + \frac{T_i}{T_e}\bar{n}_e/Z\bar{n}_z\right)\left(\Theta^2 c_{ss}^2 - \bar{V}_\theta^2\right)$ and

$$A_2 = \left\{\left(\frac{\bar{n}_i + \frac{T_i}{T_e}\bar{n}_e}{Z\bar{n}_z}\right)^2\left(\frac{5T_i}{6m_z} - \frac{3}{2}\bar{V}_\theta^2\right) - \frac{1}{2}\left[\frac{(\frac{T_i}{T_e})^2\bar{n}_e - \bar{n}_i}{Z\bar{n}_z}\right]\left(\frac{5T_i}{3m_z} - \bar{V}_\theta^2\right)\right\}.$$

The two Eq. (4) and (8) have been solved numerically and some example solutions for the $\cos\theta$ component of $\tilde{\Phi}$ are plotted in dimensionless form $(X_c \equiv Re\tilde{\Phi}_c/rT_i)$ against the parameter $Y = (T_e/T_i)^{\frac{1}{2}}\sigma_\parallel E_\parallel/n_i e v_{T_z}$ in Fig. 1. $\bar{V}_\theta$ follows similar s-shaped curves. The solutions have been stopped at the onset of a shock, namely when $V_\theta = \Theta c_{ss}$ at $\theta = \pi$.

It is clear that instability will occur at or just before the point where $\partial X_c/\partial Y = \infty$, since a small increase in X_c increases the electron trapping and hence increases $E_\parallel$ to maintain the current. Poloidal acceleration occurs towards a new equilibrium with much larger values of $\bar{V}_\theta$, X_c and with increased $E_\parallel$. The plasma can only stay for a small time in the new equilibrium (if it ever reaches it), because the electrons are being cooled via the terms $\bar{V}_\theta\left\{\left[\overline{(P_{e_\parallel} - P_{e\perp})\sin\theta/R_0}\right] + \overline{\tilde{n}_e e\tilde{E}_\theta}\right\}$, the energy going to the mass motion and viscous ion heating, and because increased $E_\parallel$ requires $\partial j_\parallel/\partial t < 0$. The plasma will revert to its original state via a second instability (the other part of the S-curve where $\partial X_c/\partial Y = \infty$). The electron temperature will be limited to that giving the critical value of Y; the table below compares this predicted value of T_e with various experimental measurements of T_e for those cases where the other relevant parameters are reported. A possible explanation of the

high predicted values for PLT with T_i = 5keV and for ISX is the fact that higher order ion Larmor effects will be significant in these cases.

1. A.A. Ware, paper presented at this Symposium "Poloidal Rotation as the Cause of the Internal m=1 Mode."

2. R.D. Hazeltine and A.A. Ware, Phys. Fluids 19, 1163(1976).

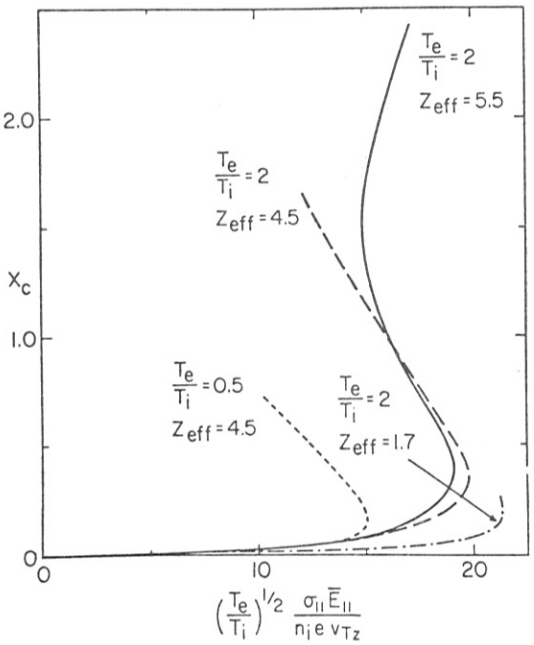

Fig. 1. Example solutions for X_c when Z=8 and m_z/m_i=16.

Experiment	EXPERIMENTAL DATA					Theory
	n_{e0} ($\times 10^{-13}$)	T_{i0} (eV)	$E_\parallel$ (10^3Vcm^{-1})	Z_{eff}	T_{e0} (eV)	T_{e_0}(eV)
TFR	4.5	530	4.4	5	1,150	1,100
PLT	3.3	800	1.6	3.5	2,300	2,200
	4.5	5,000	1.1	3.5	3,400	4,500
DITE	4.3	270	4.8	4.8	800	760
ISX	3.7	220	3.3	3.5	490	760
	6.1	480	2.9	3.1	990	1,490

VARIATIONNAL CALCULATION OF THE NON-LINEAR GROWTH OF THE Q = 1 ISLAND

André SAMAIN and Marc DUBOIS

ASSOCIATION EURATOM-CEA SUR LA FUSION
Département de Physique du Plasma et de la Fusion Contrôlée
Centre d'Etudes Nucléaires
Boite Postale n° 6. 92260 FONTENAY-AUX-ROSES (FRANCE)

An important problem related to disruptions is the growth rate of the magnetic islands which may develop on the magnetic surfaces q = 1, q = 2 ... When the island width becomes larger than the resistive layer of the tearing theory, the problem is non-linear. It has been studied numerically [1], [2], [3], [4] and analytically in the case of small q = 2 islands [5]. The authors of [5] assume that the plasma is in equilibrium, then they express that the electric current induced in the vicinity of the island, by the evolution of the magnetic configuration, is consistent with the discontinuity of the magnetic field imposed by the MHD solutions in the outer regions. A similar calculation has been done to study the possibility of magnetic islands due to thermal effects [6]. These calculations use the constant ψ approximation and therefore they do not apply as they are to the case of a q = 1 island. Here we will consider this case, using the hypothesis that at each time there exists a well defined separatrix or at least that the change of topology takes place within a layer, thin compared to the island width. Also we assume that the plasma is in equilibrium outside this layer and that the magnetic field is continuous across it. This situation and the generalized Ohm law impose the growth rate, which we obtain by variationnal methods.

VARIATIONNAL PRINCIPLE

We introduce the helical flux $\psi(r, \theta, t)$ (r, θ are the polar coordinates around the magnetic axis Oz) which in the absence of the island would be minimum at the radius $\bar{r}$ of the q = 1 surface :

$$\psi_{eq}(r) = \alpha \left(\frac{(r^2 - \bar{r}^2)^2}{\bar{r}^4} + \frac{2\eta c^2}{\pi \bar{r}^2} t \right) \qquad \text{for } r \neq \bar{r} \qquad (1)$$

At a time t, we have $\psi = G(\phi, t)$ where $\phi = \phi(r, \theta)$ is the area inside the magnetic line passing at (r, θ). Of course the value ϕ_s of ϕ at the separatrix and the function $G(\phi, t)$ have distinct specifications in the three regions R having different magnetic lines topologies, i.e. the island and the inner and outer regions. The magnetic lines are selected among a set of families of lines, each family of which exhibits a separatrix and is defined by a set of parameters α. The lines of the family defined by the parameters α embrass the areas $\phi = \phi(r, \theta, \alpha)$, $\phi_s = \phi_s(\alpha)$. The actual magnetic lines coincide at a time t with the surfaces of

the family $\alpha(t)$, but could be undefined near the separatrix.

In each region R the plasma equilibrium implies that the current density ($- c/4\pi \cdot \Delta\psi$) is a function of ψ (or of ϕ). Being given the function $G(\phi, t)$ this is equivalent to the statement that we have

$$\delta \iint_{D(\alpha)} |\nabla \psi'|^2 \, 2\pi r \, dr \, d\theta = - \oint_{\phi(r,\theta,\alpha) = \phi^*} (\delta\vec{\xi} \times \vec{ds})_z \, |\nabla \psi|^2 \qquad (2)$$

for all the variations $\delta\alpha$ of α near $\alpha(t)$. $D(\alpha)$ is any domain of R limited by the lines $\phi(r, \theta, \alpha) = \phi^* \equiv$ constant, $\psi' = G(\phi(r, \theta, \alpha), t)$; $\delta\vec{\xi}$ is the local displacement of the lines $\phi(r, \theta, \alpha) = \phi^*$ associated with $\delta\alpha$ and $\vec{ds}$ is the integral element on these lines. We choose in each region R a surface $\Sigma(\alpha)$ limited by a line $\phi(r, \theta, \alpha) = \phi_s^* \neq \phi_s(\alpha)$ near the separatrix, and in the inner and outer regions by lines $\phi(r, \theta, \alpha) = \phi_1^*$ and $\phi(r, \theta, \alpha) = \phi_2^*$ respectively. Adding Eqs. (2) taken for each R, and using the continuity of $|\nabla\psi|$ across the separatrix, we obtain

$$\delta \left[\left(\int_{\phi_1^*}^{\phi_s^*} + \int_0^{\phi_s^*} + \int_{\phi_s^*}^{\phi_2^*} \right) \left(\frac{\partial G(\phi,t)}{\partial \phi} \right)^2 \mathcal{P}(\phi,\alpha) \, d\phi \right] + \delta \mathcal{M}_{ext} = 0 \qquad (3)$$

Where the ϕ_s^* in each region R and ϕ_1^*, ϕ_2^* are kept constant, and where

$$\mathcal{P}(\phi,\alpha) = \frac{1}{d\phi} \left(\iint_{\phi(r,\theta,\alpha) = \phi, \phi + d\phi} |\nabla \phi(r,\theta,\alpha)|^2 \, r \, dr \, d\theta \right)$$

$$\delta \mathcal{M}_{ext} = \left(\oint_{\phi(r,\theta,\alpha) = \phi_2^*} - \oint_{\phi(r,\theta,\alpha) = \phi_1^*} \right) (\delta\vec{\xi} \times \vec{ds})_z \, |\nabla \psi|^2 \Big)$$

The quantity $\delta \mathcal{M}_{ext}$ is the work to be spent on the plasma in the domains $\phi(r, \theta, \alpha) \leqslant \phi_1^*$ and $\phi(r, \theta, \alpha) \geqslant \phi_2^*$, assumed to be held by superconducting sheets at the two surfaces $\phi(r, \theta, \alpha) = \phi_{1,2}^*$, to achieve the deformation $\delta\alpha$ of these surfaces.

For $\alpha = \alpha(t)$, the quantity $\mathcal{P}(\phi, \alpha) \cdot \partial G(\phi, t)/\partial\phi$ is equal to the integral $\oint_\phi \vec{\nabla\psi} \times \vec{ds}$ over a magnetic line ϕ. The continuity of $\nabla\psi$ across the separatrix and the Ohm law $-\left(\frac{\partial \psi}{\partial t} + \vec{v} \nabla \psi\right)/c = -c\eta \, \Delta\psi / 4\pi$, where $\operatorname{div} \vec{v} = 0$, impose that

$$\delta \left(\int_{\phi_1^*}^{\phi_s^*} + \int_0^{\phi_s^*} + \int_{\phi_s}^{\phi_2^*} \right) \left(\frac{\partial G(\phi,t)}{\partial t} \, G'(\phi) + \frac{\eta c^2}{8\pi} \mathcal{P}(\phi,\alpha) \left(\frac{\partial G'(\phi)}{\partial \phi} \right)^2 \right) d\phi = 0 \qquad (4)$$

for any variation $\delta G'$ of the function $G'(\phi)$ near $G(\phi,t)$, exhibiting the same $G'(\phi_s)$ in the three regions and such that $G'(\phi_{1,2}^*) = G(\phi_{1,2}^*, t)$.

It is convenient to introduce a parameter x labelling the lines of each family α, such that to the separatrix corresponds a fixed value x_s of x. Then $\phi = \phi(x, \alpha)$, $\mathcal{P}(\phi,\alpha) = \prod(x, \alpha)$ and $G(\phi, t) = g(x, t)$. If x_0, x_1, x_2 correspond to the island axis and to the lines $\phi = \phi_1^*$, $\phi = \phi_2^*$, $\left(\phi(x_{0,1,2}, \alpha) = 0, \phi_1^*, \phi_2^*\right)$,

the principle (3) gives , for any $\delta\alpha$

$$\left(\int_{x_1}^{x_s}+\int_{x_0}^{x_s}+\int_{x_2}^{x_s}\right)\left(\frac{\partial\Pi}{\partial\alpha}-\frac{\partial\Pi}{\partial x}\cdot\frac{\partial\phi/\partial\alpha}{\partial\phi/\partial x}\right)\frac{1}{\partial\phi/\partial x}\left(\frac{\partial g}{\partial x}\right)^2 dx\,\delta\alpha+\delta\mathcal{M}_{ext}=0 \qquad (5)$$

and determines $\alpha = \alpha(t)$ at time t when the function g(x, t) is known. The time evolution of g(x, t) is given by (4) which becomes

$$\delta\left[\left(\int_{x_1}^{x_s}+\int_{x_0}^{x_s}+\int_{x_2}^{x_s}\right)\left(\left(\frac{\partial g}{\partial t}-\frac{\partial g}{\partial x}\cdot\frac{\partial\phi/\partial\alpha}{\partial\phi/\partial x}\cdot\frac{d\alpha}{dt}\right)\frac{\partial\phi}{\partial x}\,g'\,dx+\frac{\eta c^2}{8\pi}\,\Pi\,\frac{(\partial g'/\partial x)^2}{\partial\phi/\partial x}\,dx\right)\right]=0 \qquad (6)$$

for all variations of g'(x) near g(x, t), preserving the unicity at $x = x_s$ and the value of $g(x_{1,2}, t)$ at $x = x_{1,2}$.

APPLICATION TO THE CASE OF q = 1

We choose a test family of lines near the surface $r = \bar{r}$, the lines of which have the equation $(r^2 - \bar{r}^2)^2 - s.\cos\theta = u$, where, for $r < \bar{r}$, $s = s_1$, $u = s_1.x$, and for $r > \bar{r}$, $s = s_2$, $u = s_2 x$. Here the parameters α are s_1 and s_2, and x is the label corresponding to each line of the family. If $\mathcal{J}(x) \equiv \int (x+\cos\theta)^{1/2}\frac{d\theta}{2\pi}$, we have in the island : $-1 < x < 1$, $\phi(x,\alpha) = (\sqrt{s_1}+\sqrt{s_2})\,\pi\,\mathcal{J}(x)$,

and $\Pi(x,\alpha) = 8\pi^2\bar{r}^2\,(\sqrt{s_1}+\sqrt{s_2})^2/\sqrt{s_1 s_2}\cdot\mathcal{J}(x)\cdot\mathcal{J}'(x)$

in the inner (1) and outer (2) regions : $1 < x < x_{1,2}$, $\phi(x,\alpha) = \pi\left(\bar{r}^2 + (-1)^{1,2}\sqrt{s_{1,2}}\,\mathcal{J}(x)\right)$,

and $\Pi(x,\alpha) = 8\pi^2\,\bar{r}^2\left(\mathcal{J}(x)\cdot\mathcal{J}'(x)\right)$

For large enough $x_{1,2}$ we may calculate $\delta\mathcal{M}_{ext}$ from the linear MHD perturbation in the two domains $\phi < \phi_1^*$ and $\phi > \phi_2^*$. For q = 1, only the outer domain contributes :

$$\delta\mathcal{M}_{ext} = \pi^2\,B\,\frac{4a^2}{\bar{r}^6}\,\frac{s_2\cdot\delta s_2}{(\phi_2^*-\pi\bar{r}^2)} \qquad (7)$$

The value of $g(x_{1,2}, t) = G(\phi^*_{1,2}, t)$ is the equilibrium value (1)

$$g(x_{1,2}, t) = a\,\frac{(\phi^*_{1,2}/\pi - \bar{r}^2)^2}{\bar{r}^4} + \frac{8a\eta c^2}{\pi\,\bar{r}^2}\cdot t \qquad (8)$$

Eqs. (7), (8) may be safely used for $x_{1,2} \sim 3$. We may then approximate g(x, t) in each region R by a linear function of x, varying inside the island from g_o for $x = -1$ (axis) to g_s for $x = +1$ (separatrix) and outside from g_s to $g(x_{1,2}, t)$. The variationnal principles (6) and (7) give equations for the evolutions of the parameters $\alpha = (s_1, s_2)$ and (g_o, g_s). These equations have a solution

$$\begin{cases} s_1 = \sigma_1^2\,\tau\,\bar{r}^4 \quad , \quad s_2 = \sigma_2^2\,\tau\,\bar{r}^4 \\ g_o = \gamma_o\,a\,\tau \quad , \quad g_s = \gamma_s\,a\,\tau \quad , \quad \tau = \dfrac{\eta c^2 t}{4\pi\bar{r}^2} \end{cases} \qquad (9)$$

The width δ of the island is then given by $\delta^2 = (\sigma_2+\sigma_1)^2\cdot\frac{\eta c^2 t}{4\pi\sqrt{2}}$

we find $\sigma_1 = 1.2$, $\sigma_2 = 1.1$ and $\delta^2 = 3\,\frac{\eta c^2 t}{4\pi}$, in agrement with the computations [4].

Of course such a solution (9) would not exist for q = 2 where $\delta.r$ and not δ^2 varies as $\frac{\eta c^2}{4\pi}\cdot t$.

The time τ which is necessary for the island to invade the volume inside the surface q = 1 may be estimated by taking $\delta \sim r$. This gives

$$\tau \sim \frac{1}{3}\left(\frac{\eta c^2}{4\pi}\right)^{-1}\cdot\bar{r}^2 \qquad (10)$$

CONCLUSION

If the internal disruption consists in the growth of a q = 1 island conserving its topology, the inertial forces in the plasma would be of the order of $\rho\bar{r}/\tau_d^2$, where τ_d is the duration of the disruption. For measured values of τ_d , these inertial forces are negligible compared to the magnetic force $(-c/4\pi.\Delta\psi)_x.\nabla\psi$. Hence, the plasma is in equilibrium and $\nabla\psi$ is continuous across the separatrix : therefore τ is given by (10). It appears that the time calculated in this way is much longer than the observed duration of internal disruptions : for this reason we believe the internal disruption is not explained by the usual schema of a growing m = 1 island.

[1] WHITE et al., Plasma Phys. and Cont. Nucl. Fus. Res. 1976, Vol. 1 p. 569 (1977)

[2] BISKAMP, D., WELTER, H., " " " " p. 579

[3] DANILOV et al., " " " " p. 591

[4] SYKES, A., WESSON, J.A., Phys. Rev. Lett., 37, (1976), 140

[5] RUTHERFORD, P.H. Phys. Fluids, 16, (1973), 1903

[6] REBUT, P.H., SAMAIN, A., Proc. 5th Eur. Conf. on Controlled Fusion and Plasma Physics Grenoble Vol. I p. 29, II p. 232

Quasi MHD Nonlinear Dissipation and the Major Disruption

E. Minardi
UKAEA - EURATOM Association[+)]
Culham Laboratory, Abingdon, Oxon

In a cylindrical Tokamak with helical symmetry one can consider an intermediate quasi MHD regime which is described by solutions of the diffusion equation for the magnetic field such that the helical magnetic flux and the integral $K = \int_V \vec{A}\cdot\vec{B}\,dV$ are approximately conserved during a time which is not very small with respect to the electric dissipation time (more precisely, a time such that first order terms in the Coulomb collisions are taken into account /1/). In this regime, the time behaviour of the helical flux is described by the equation /2/

$$\frac{1}{4\pi m}\left(\Delta\chi_1 + \frac{2\pi}{Rz}\frac{\partial}{\partial z}\nabla^2 A_{1\theta}\right) = j_0(\chi_0+\chi_1) - j_0(\chi_0) + \frac{j_0(\chi_0+\chi_1)}{E_0}\frac{d\chi}{dt} \qquad (1)$$

where

$$\frac{d\chi}{dt} = \frac{\partial\chi_1}{\partial t} + \vec{v}\cdot\nabla(\chi_0+\chi_1)$$

and $A_{1\theta}$ is so chosen as to satisfy at every time the constraint K = const.

Here I would like to present, on one hand, some example of solutions of Eq. (1) which indeed describe an intermediate MHD semicollisionless regime in the sense defined above. On the other hand, I will point out the connection of these solutions with the latest phase of the major disruption observed in Tokamaks.

[+)] Presently on leave at Max-Planck-Institut für Plasmaphysik, Garching, Germany.

I specifically consider an initial situation such that an originally unstable kink-like mode has reached saturation as a consequence of nonlinear effects. This helical deformation is superimposed to a given purely radial Tokamak equilibrium created by an axial current, whose central core, with parabolic profile, has a radius r = a. Thus Eq. (1) predicts a dissipative instability provided that the ratio a/b of the current edge to the radius b of the conductive vessel is sufficiently small. This instability is essentially purely radial (m = o, n = o) but is initially triggered nonlinearly by the helical deformation with $m \neq 0$, $n \neq o$. Indeed, the time evolution of the radial part of the helical flux $\chi_{10}(r)$, in an expansion in which the helical deformation is assumed to be small (order $\lambda \ll 1$), is described by the equation

$$\frac{1}{4\pi}\Delta\frac{\chi_{10}}{m - n q(r)} = j_0(\chi_0+\chi_{10}) - j_0(\chi_0) + \frac{j_0(\chi_0+\chi_{10})}{E_0 m}\left(\frac{\partial\chi_{10}}{\partial t} + v\frac{d}{dz}(\chi_0+\chi_{10})\right) \qquad (2)$$

where the initial value of χ_{10} is determined in the order λ^2 /2/ by the helical deformation. In this connection it is worthwhile to note that one cannot take a thermal fluctuation as initial value of χ_{10} because in this case many dissipation times would be needed in order to produce a sizeable effect and this will strongly contradict the K and χ invariance on which Eq. (2) is based.
Thus the effect of the helical deformation just consists in producing a large initial perturbation of χ_{10} which then can reach the region where the nonlinear effects described by Eq. (2) are important in a time sufficiently short to preserve the K and χ invariance. A striking consequence of these nonlinear effects is that the time behaviour of the process assumes an explosive character.

At this point, I must stress the fact that the helical deformation alone is not sufficient for driving a radial instability such that the K and χ invariance is consistently preserved. For this purpose, one needs the existence of a velocity field related to some kind of anomalous diffusion process. Indeed, the striking fact described by Eq. (2) is that, in the presence of a given radial velocity field v(r), the magnetic system adjusts itself in order to conserve as much as possible the helical flux, notwithstanding the dissipation, at least in the volume average, provided the diffusion is rapid enough. So an anomalous diffusion process (related, e.g. to the local ergodization of the lines of force) induces a quasi MHD unstable behaviour

of the helical plasma. The various aspects of this behaviour are illustrated in the figures (calculated by D.B. Albert /3/) where we have considered two physical cases:

1. The shrinking case. In this case the current is parabolic for $r < a$ and constant for $a < r < b$. It is assumed that as a consequence of some complicated diffusive process at $r \gtrsim a$, an inward radial plasma velocity exists implying the shrinking of the current channel. The resonant surface is situated at $r > a$.

2. The expanding case. The current is parabolic for $r < c$, constant for $c < r < a$ and zero for $a < r < b$. The unperturbed resonant surface is situated outside the current channel and near the edge $r = a$. An outward radial velocity field is assumed as a consequence of some complicated diffusive process in the region of the resonant surface.

References

/1/ E. Minardi, Nucl.Fusion 16, 427 (1976); 17, 614 (1977); Proceedings of the Workshop on Theory of Magnetically Confined Plasmas, Varenna, Italy (Pergamon Press, Oxford, 1978)

/2/ E. Minardi, Nucl. Fusion 18, 215 (1977)

/3/ E. Minardi and D.B. Albert - To be published in Nucl. Fusion.

Figure Captions

Fig. 1: Case of shrinking current. Time evolution of the following quantities:
(a) Moving boundary of the current channel $u_r = 2\frac{a(t)}{a}\left(\frac{r}{1-nq(a)/m}\right)^{1/2}$ with $a(0) = a$
(b) Ratio of the axial electric field to the applied field $\hat{E}_z = E_z(a,\tau)/E_0$ given by Eq. (6.6) of Ref. /2/.
(c) Index of helical flux conservation in the current shift $R(b) = \left|\eta' d\chi/dt \Big/ \left(j_0(\chi) - j_0(\chi_0)\right)\right|_{u=0}$

Fig. 2: Evolution of the current profile in the case B of Fig.2, starting from the initial profile $j_0 = j_0^0\left(1 - \Gamma r^2/a^2\right)$.

Fig. 3: Case of expanding current. Time evolution of the following quantities, up to $\tau = 2\cdot 10^{-4}\,\tau_D$
(a) Current density
(b) $\hat{E}_z = E_z(a,\tau)/E_0$
(c) Dissipative part of the current density $Q = (d\chi/dt)/m\,\eta\, j_0^0$.
(d) Index of helical flux conservation $P = (d\chi/dt)/V\,d\chi/dr$.

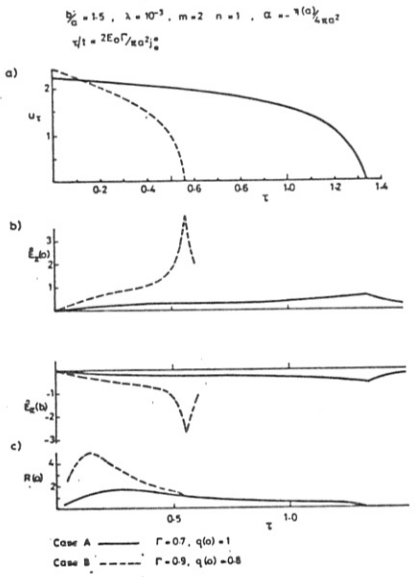

Fig. 1

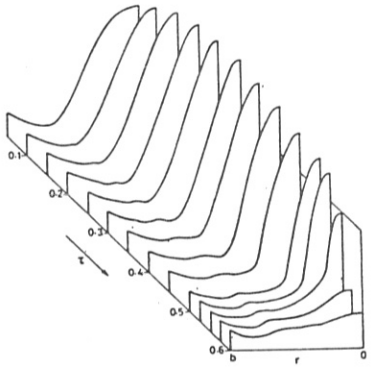

Fig. 2

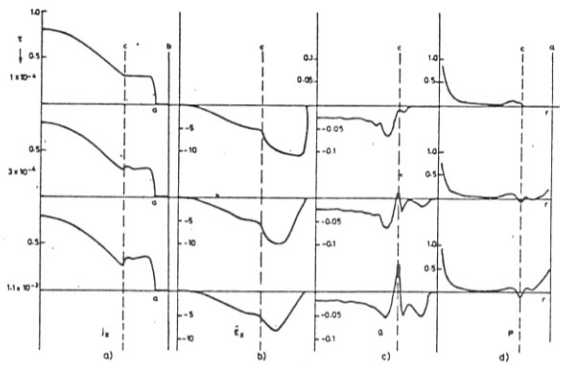

Fig. 4

Internal and External Disruptive Instabilities in the PLT Tokamak

N. R. Sauthoff, S. von Goeler*, D. R. Eames, and W. Stodiek
Princeton University, Plasma Physics Laboratory
Princeton, NJ 08540 U.S.A.

I. Introduction

Disruptions in PLT have been analyzed using a 20-channel X-ray imaging system, and more recently a 93-channel upgrade consisting of 75 detectors viewing horizontally and 2 arrays of 9 detectors each looking vertically. In this report, previous results are summarized and evolutions of the central core during some m=1 bursts are described.

II. Review of PLT Disruptions

Disruptions observed on PLT can be calssified according to (a) their severity (minor/major), (b) the precursor oscillations (m=1,2,3,none,or mixtures), and (c) the location of the disruption [1,2]. In some cases, the minor disruption occurred near the resonant surface of the dominate precursor. In other cases, it was located significantly inside the resonant surface of the dominant mode; in several such cases, accompanying faster oscillations near the point of disruption suggested involvement of modes of different [3-6] rather than the same [7] helicity. The minor disruption of discharges with hollow temperature profiles [8,9] was also described in Ref. 1. Major disruptions with m=2 and asymmetric components occurred in some cases with abnormally large radius of q=2 and the associated steep gradients (probably due to edge shrinkage and the constraint of $q \geq 1$ at the center); this behavior agrees with the linear destabilizing tendency of gradients on tearing modes (neglecting diffusive and kinetic effects)[10], larger saturation amplitude [7], and nonlinear coupling of modes of adjacent helicity by both quasilinear profile modification and mode coupling [3-6]. However, interpretations in terms of other processes such as rippling modes, bifurcated equilibria, and neoclassical effects have not been excluded.

III. Internal Modes

Attempts have been made to explain "sawtooth" oscillations of the central electron temperature [11] on the basis of resistive internal kink modes [8,12,13]. This model has invoked the growth of an m=1 island and the motion of the hot center toward the X-point where the energy is transported toward the outer half of the island created by the reconnection of a hot inner and a cold outer flux surface. In the conventional simulation without diamagnetic effects [8] complete reconnection annihilates the hot central peak and the heat diffuses over an annular region near the q=1 surface. Previous experimental confirmation has been based on the growth rate of the emissivity fluctuation and the repetition time of the sawtooth (which is presumed to be related to the onset of an explosive growth phase due to the evolution of the shear at the singular surface).

In PLT with neutral beam injection, the agreement between theory and experiment is not as simple as that in ORMAK [12,13]; the repetition time expands from ~5-10 ms without injection to ~20-40 ms with 400 kW injection. In ORMAK, the extension of the period was related to a fourfold increase in the radius where q=1, whereas in PLT the resonant surface does not move more than ~20% (remaining at 8-10 cm). The greater breadth of the heat deposition profile or modified ordering of time scales might afford explanations for the slower increase of growth rate within the tearing mode model.

In the remainder of this section we present information on the evolution of m=1 modes, bursts of which can either be correlated with internal disruptions or seemingly merely decay without disruption.

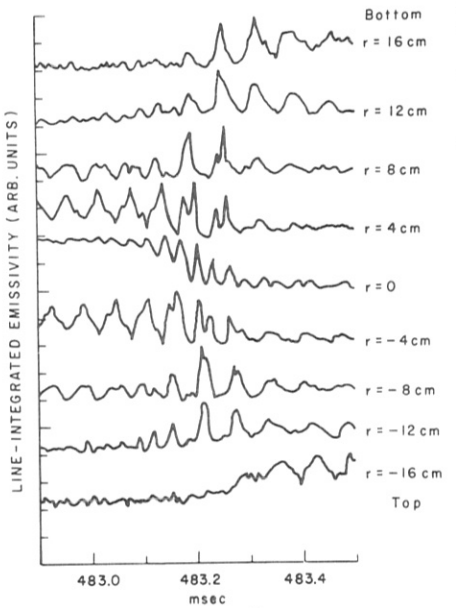

Fig. 1
793108

Figure 1 shows signals of line-integrated emissivities on detectors viewing horizontally at the listed tangent radii near the time of a sawtooth drop at 483.20 ms. The m=1 oscillations at fundamental rotation frequency ω are visible on the ±8 cm traces until 483.10 ms after which a more complicated double-peaked structure is evident; a slightly phase-shifted 3ω perturbation complicates the interpretation but is likely unimportant as it is absent in other cases. The central trace exhibits purely 2ω behavior since the "hot spot" passes within view twice per revolution. The central oscillation also exhibits a constant maximum prior to disruption, corresponding to the repetitive view of the displaced hot center; the progressive decrease of the minimum of the oscillation is due to an increase of the displacement and a resultant excursion to regions of lower emissivity. Away from the center but within the range of the central displacement, the hot center is also seen twice per cycle, but the peaks are not equally spaced; the magnitude of the central displacement can be determined directly by assuming a rotation of the peak such that the projected radii of the peak at the intensity maxima equal the tangent radii of the detectors. Using this technique, a displacement less than 4 cm is found at 483.13 ms, near 8 cm from 483.15 to 483.20 ms, and 9-10 cm from 483.21 to 483.27 ms. The commencement of the reduction of the peak emissivity as seen at the center (where the effects of the 3ω component should be less prominent) coincides with the approach of the peak emissivity region to the outer radius of the normal mode (near 10 cm) and presumably the radius of q=1.

The inward spiral trajectory of the peak after disruption is better displayed in the relatively small sawtooth of Fig. 2. The displacement rises from ~2 cm at 502.8 ms to ~5 cm at 503.35 ms and 6 cm at 503.8 ms; the peak emissivity region then spirals inward from 5 cm at 505.0 ms to ~4 cm at 505.6 ms and ~3 cm at 505.9 ms. The disturbance of the outer radii beyond the limit of the initial mode at ~8 cm indicates that near the time of disruption the peak region creates a localized protrusion into the previously concentric circular surfaces. The flatness of the traces between peaks following the disruption indicates the absence of the peaked emissivity region along that line of sight; using the double-peaked structures to determine the position of the center and the commencement of the flatness to indicate the edge of the peak, the radial dimension of the peaked emitting region can be found to be ~4 cm. The onset of disruption at ~503.4 ms concides with the near interception of the innermost previously undisturbed surface by the center of the peak.

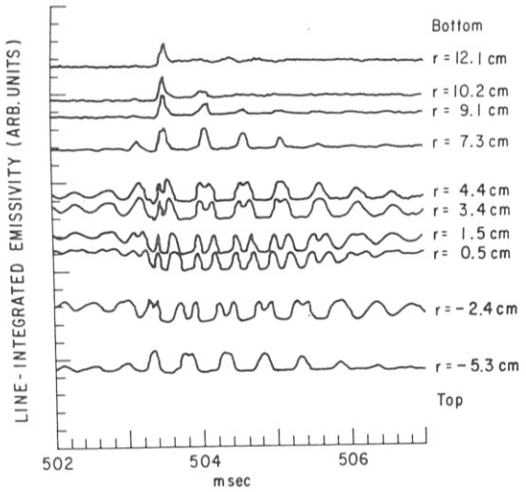

Fig. 2
793109

Figure 3 shows a burst of m=1 activity of roughly 7 ms duration which allows the equilibrium to return to nearly its initial state; the maximum excursion was ~3 cm, which was considerably less than the extent of the mode.

The dichotomy of the outcomes of bursts of m=1 activity may be related to the extent of the radial excursion of the magnetic axis. If the axis approaches the radius of q=1, energy is lost from the center, whereas if the mode decays prior to interaction at q=1, considerably less central transport results.

IV. Discussion

The multiplicity of the precursors of external disruptions, ranging from a seemingly single mode with disruption at its resonant surface to apparently independent modes with disruption at an intermediate location, suggests either a variety of causes for the onset of disruption (e.g., limiter interaction and stochasticity) or a diversity of components which undergo a common progress (e.g., onset of a turbulent state by mutual destabilization of modes [14]).

The persistence of the central region of peaked emissivity through the internal disruption and the subsequent inward spiral of the pared filament illustrates the inadequacy of the traditional model [8] in explaining the final stages of the sawtooth in some circumstances. A mechanism which limits the extent of reconnection seems to be capable of arresting the outward motion of the magnetic axis toward the X-point and restoring the surfaces to their original topology, rather than permitting the annihilation of the primal axis.

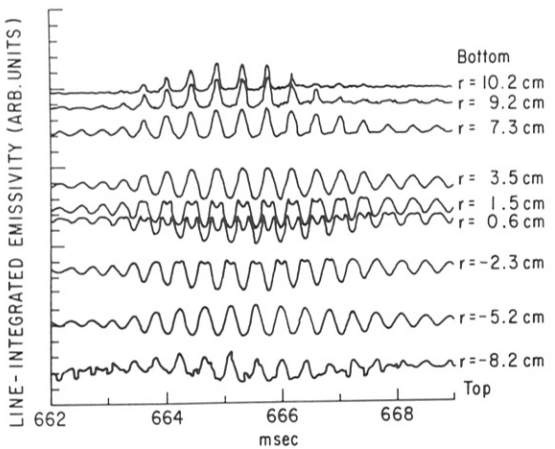

Fig. 3
793110

V. Acknowledgements

The authors express their indebtedness to Drs. D. Monticello and R. White for trenchant discussions, and especially to the late Dr. Bruce Waddell, two of whose last efforts were considerations of the partial reconnection and the changes of the sawtooth repetition rate mentioned in this paper.

---

*Present address: Max Planck Institut fur Plasmaphysik, Garching, Germany.

References

[1] SAUTHOFF. N.R., VON GOELER, S., and STODIEK, W., Nucl. Fus. 18, 1445 (1978).
[2] BOL, K., et al., Innsbruck, IAEA Conference, Paper CN-37-A-1 (1978).
[3] WADDELL, B.V., CARRERAS, B., HICKS, H R., HOLMES, J.A., and LEE, D.K., Phys. Rev. Lett. 41 1386 (1978).
[4] HICKS, H.R., CARRERAS, B., HOLMES, J.A., and WADDELL, B.V., ORNL/TM-6096 (December 1977).
[5] CARRERAS, B., WADDELL, B V., and HICKS, H.R., ORNL/TM-6175 (March 1978).
[6] CALLEN, J.D., WADDELL. B.V., CARRERAS, B., et al., Innsbruck, IAEA Conference, Paper CN-F-1-1 (1978).
[7] WHITE, R.B., MONTICELLO, D.A., and ROSENBLUTH, M.N., Phys. Rev. Lett. 39, 1618 (1977)
[8] WHITE, R.B., MONTICELLO, D.A., ROSENBLUTH, M.N., and WADDELL, B.V., Berchtesgaden IAEA Conference, Paper I, 569 (1976).
[9] CARRERAS, B., HICKES, H.R., and WADDELL, B.V., ORNL/TM-6570 (October 1978).
[10] GLASSER, A., VON GOELER, S., SAUTHOFF, N.R., and SELBERG, H., PLT Review Meeting, Princeton Plasma Physics Laboratory (May 1978).
[11] VON GOELER, S., STODIEK, W., and SAUTHOFF, N., Phys. Rev. Lett. 33, 1201 (1974).
[12] WADDELL, B.V., JAHNS, G.L., CALLEN, J.D., and HICKS, H.R., Nucl. Fus. 18, 735 (1978).
[13] JAHNS, G.L., SOLER, M., WADDELL, B.V., CALLEN, J.D., and HICKS, H.R., Nucl. Fus. 18, 609 (1978).
[14] FURTH, H.P., "Economic Theory of the Disruptive Instability" (this conference).

Some Aspects of Disruptive Instabilities in Alcator A

I.H. Hutchinson and D.O. Overskei

Massachusetts Institute of Technology
Cambridge, Massachusetts, U.S.A.

The tokamak Alcator A experiences, from time to time, a variety of 'disruptions' i.e., violent alterations of the current profile on a time scale faster than that of normal resistive current diffusion. The character of these events may be categorized according to both the stage of the discharge at which they occur and also their immediate effect on the plasma parameters. Here we discuss disruptive instabilites under three headings. First we discuss those that are associated with rising current. These have a different signature from the more familiar instabilities and we present evidence to show that they are related to the formation of hollow current profiles. Secondly, some observations are made concerning what may be considered the 'classic disruptive instability', characterized by a large negative voltage spike related to rapid current-channel expansion and occurring typically close to the time of maximum current. Finally, we consider those disruptions which lead directly to total termination of the plasma current.

Current-Rise Disruptions[1]

Sequences of perturbations of the loop voltage during the rise of plasma current have been observed on many tokamaks and have been correlated with MHD activity of decreasing poloidal periodicity (m).

On Alcator A such series of disruptions are often observed. Statistically, the disruptions are found to occur predominantly not at limiter safety factor (q_ℓ) values that are integral but at $q_\ell \simeq 1.6$ m, where m is integral, equal to the poloidal periodicity of the related helical magnetic perturbation. These facts indicate that the site of the disruptions' initiation is not near the plasma edge but well inside the column. Observations of second-harmonic electron cyclotron emission show an abrupt decrease in electron temperature throughout the plasma at the time of each disruption This decrease is sometimes as much as 50% in the most severe disruptions, particularly at the lower m numbers (2-4). More typically, however, it is less than about 20%.

The cyclotron radiation measurements show also that the electron temperature profile remains peaked at the centre throughout the current rise phase. However, an analysis of the current diffusion equation indicates that for the experimental T_e profiles and the timescales in Alcator A, a hollow current profile should form due to the skin effect. Moreover the ratio of q_ℓ to the minimum q value inside the plasma is typically found to be ~ 1.6 for the calculated current profiles. Thus, it seems, it is the minimum q value in the plasma which determines the MHD mode instability not the limiter q. This is quite consistent with the theoretical model of the double tearing mode.

We find that these disruptions appear to have a regulating effect on the electron temperature during the current rise such that the plasma never evolves far from a state of marginally hollow current. However their overall effect is strongly deleterious to the plasma parameters throughout the ensuing discharge. Severe disruptions in the early phases greatly increase the tendency to disrupt later in the discharge. This effect appears to be related to impurities.

These early disruptions can be avoided or at least reduced in intensity by two means: increasing the electron density and reducing the rate of current rise. These measures reduce the ratio of ohmic power to the rate of plasma energy increase and thus reduce the temperature, the conductivity, and hence the tendency to form hollow current profiles.

Classic Disruptive Instabilities

Disruptions which occur at times when the current is no longer rapidly changing can have severity widely varying, from those which perturb the plasma temperature by as little as 10% to those which lead to total termination of the discharge. This latter extreme is discussed later.

The timescales in which the rapid evolution, characteristic of the disruptions, occurs in Alcator are such that the penetration (L/R) time for poloidal flux through the vacuum chamber ($\sim$80 μs) must be considered. This time sets the timescale over which the loop voltage and total measured current (plasma plus bellows current) can vary in response to plasma perturbations. The typical duration of the observed negative voltage spike is generally of this order; though, somewhat surprisingly, as Fig. 1 illustrates it often appears rather shorter than this. In any case, a measurement of the central temperature from cyclotron radiation (confirmed by soft x-ray diodes) which has $\sim$10 kHz bandwidth ($\sim$15 μs) shows the fall in temperature to take $\sim$ 60-100 μs. Moreover the fall begins, to within our resolution, simultaneously with the leading edge of the voltage spike.

FIG. 1

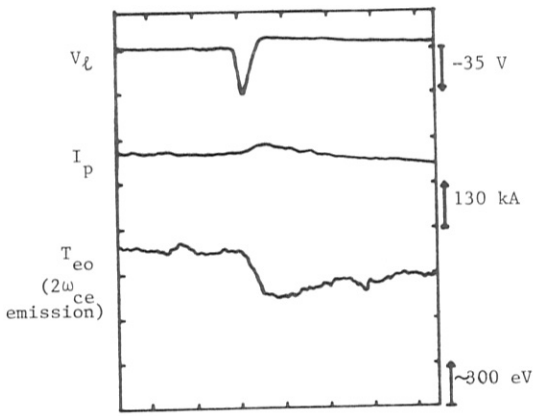

A notable feature of the m=2, n=1 mode, which is generally closely related to disruptions, has been observed. This consists in a 'locking' effect whereby the rotation of the mode is stopped. Fig. 2 illustrates the effect. The m=2 mode

grows in amplitude until gradually a distortion appears and the cos 2 θ magnetic coil eventually shows a non-sinusoidal signal with increasing period. Such a distortion is indicative of nonuniform rotation of the mode presumably due to incipient mode locking occurring periodically as the mode passes the locking point. Eventually the mode locks completely and all oscillation on the coil signal ceases. In Fig. 2, four milliseconds later a disruption occurs and then ~1 ms afterwards the m=2 signal reappears but at much higher frequency, characteristic of more benign modes. Thereafter more normal plasma behaviour ensues and sawteeth (absent before) appear in the plasma centre.

FIG. 2

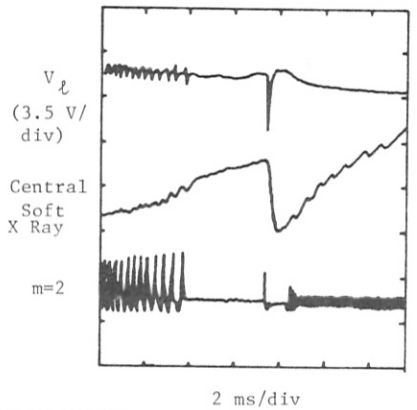

It is not unusual for the m=2 mode to be locked for perhaps 100 ms which may constitute most of the discharge, before a disruption occurs. Sometimes, towards the end of the discharge, the mode simply begins to rotate again without a disruption. In the presence of this large saturated mode, no sawteeth are observed and the plasma density generally is significantly depressed relative to discharges with comparable parameters and no such MHD problems. We find that strong gas puffing helps to avoid these large m=2 modes.

FIG. 3

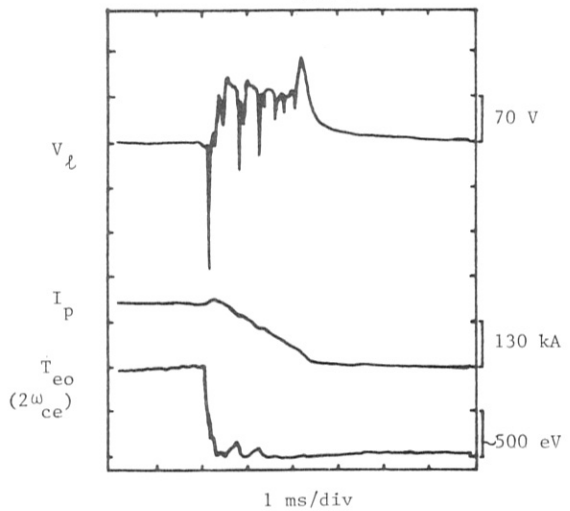

Current Termination

Sometimes a severe disruption will lead to a complete termination of the plasma current. An example is shown in Fig. 3. As can be seen the time taken for the current to reach zero is typically 2 ms. During this period a number of negative voltage spikes occur (6 in this case), indicating that the current terminates through several distinct disruptions. The timescale for each of these is typically ~ 100 μs, as before. The central

FIG. 4

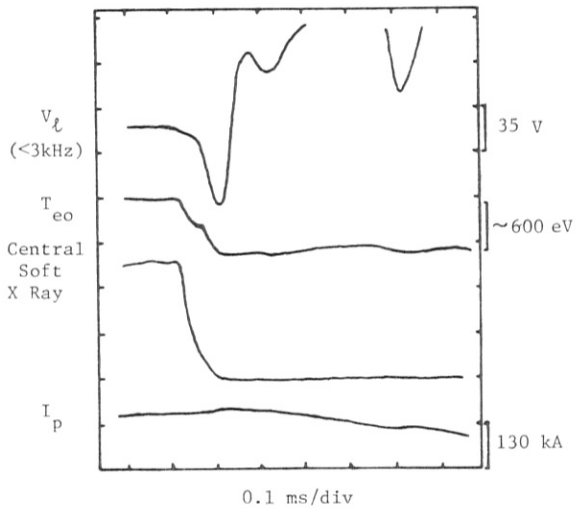

temperature during the current decay remains very low. After the first disruption, which typically lowers the temperature to perhaps 10% of its previous value in ~100 μ s, it often recovers somewhat until the next disruption in the series occurs, causing it to fall again, typically to < 50 eV at each disruption. Soft x-ray measurements indicate that throughout the current decay the plasma is shifted inwards. A detector viewing at 4 cm inside sometimes shows significant signal during the recovery while that at 4 cm outside shows no signal. However the position loop would indicate a shift of only ⩽ 2 cm consistent with the equilibrium expectations for a tokamak with copper shell when virtually all plasma energy is lost.

Figure 4 shows the first disruption in a current termination sequence. It should be noted that the main drop in voltage occurs about 40 μs after the temperature begins to fall. This is similar to an effect noticed on Pulsator[2]. However, close inspection reveals that there is a preliminary fall in voltage simultaneous with the temperature fall. Moreover, the cyclotron emission reveals that the temperature actually drops in two stages, one associated with the preliminary voltage drop and a second associated with the major spike. This two-stage process is apparent in many of the more severe disruptions including some which do not lead to total current termination.

Acknowledgements

We are greatly indebted to all the Alcator group for their support and encouragement.

References

1. A detailed account of this work is submitted to Nuclear Fusion.
2. F. Karger et al. in Plasma Physics and Controlled Nuclear Fusion Research (Proc. 6th Int. Conf., Berchtesgaden) 1, IAEA, Vienna (1977) 267. See also S.V. Mirnov and I.B. Semenov, ibid 291.

ON THE STABLE REGIONS IN CURRENT V DENSITY PARAMETER SPACE WITH OHMIC AND ADDITIONAL HEATING

J. Hugill and A.J. Wootton

Culham Laboratory, Abingdon, Oxon, OX14 3DB, UK
(UKAEA/Euratom Association)

THE STABILITY DIAGRAM

The region is described in plasma current v electron density parameter space where stable operation is obtained in the DITE tokamak. It has been found possible to plot the data for different values of toroidal field, B_T on the same diagram by normalising the axes to $1/q_L$ and $\bar{n}_e R/B_T$, where $\bar{n}_e$ is the line averaged electron density, R = 1.17 m is the major radius and q_L the safety factor at the limiter. The upper density limit is set by disruption and is sensitive to the condition of the vacuum walls. The stable region expands as the level of impurity in the plasma is decreased, for example by gettering the walls with titanium [1].

Data collected from a large range of experiments [2] shows the same general behaviour. These experiments suggest that impurity radiation is an important indirect cause of disruption at high density, especially radiation from low-Z impurities such as oxygen and carbon which are significantly reduced by gettering. The usual explanation is that low-Z impurities, radiating mainly from the edge of the discharge, produce a contraction of the current channel resulting in a destabilisation of tearing modes, especially that with poloidal mode number, m = 2 and toroidal mode number, n = 1 which is the usual precursor to a disruption.

With these ideas as a background, we discuss the MHD stability of the discharge during recent experiments in DITE with a) neutral injection heating and b) low-q operation with ohmic heating.

DIAGNOSTICS

The main diagnostics available are a multi-channel 2 mm microwave interferometer, which can detect density perturbations due to tearing mode and sawtooth oscillation and a set of 16 small coils at one major azimuth, equally spaced around the plasma at a radius of 0.29 m, which measure the amplitude and poloidal mode number, m of magnetic perturbations in the poloidal field, The mode structure was confirmed by specially wound coils with sensitivity $\sim \cos m\theta$. The limiter radius is 0.26 m.

NEUTRAL INJECTION EXPERIMENTS

These experiments were done at a plasma current, I = 150 kA, $B_T = 1.8 \rightarrow 2.2$ T and $\bar{n}_e \sim 1.6 \rightarrow 2.6 \times 10^{19}$ m^{-3}. Tangential co-injection power up to 600 kW at an extraction voltage of 25 kV was used.

In an ungettered torus the discharge stability is improved. The density rise during injection and, at the end of a 40 ms pulse, exceeds the stability limit without injection by ~ 30%. The amplitude of sawtooth oscillations increases and their period decreases during the pulse. If they are present initially, m = 2 oscillations tend to disappear. There is no substantial change in the loop voltage or in the profile of electron temperature measured by Thomson scattering, so there is no reason to expect a large change in the current distribution. However, the electron energy balance in the discharge centre is considerably modified by large changes in total radiation, electron-ion equipartion and power transfer from fast ions, which may explain the changes in sawtooth behaviour.

In a gettered torus the situation is quite different. Instead of sawtooth oscillation, the amplitude of m = 2 instabilities tends to increase and a disruption follows. In this case the increase in total radiation is much less and there is a noticable reduction in loop voltage. These changes could be consistent with a contraction of the current channel produced by a heating of the discharge centre, observed in similar discharges at lower power [3], although the absence of sawtooth oscillation is a puzzling feature.

LOW-Q OPERATION

Recently, we have obtained discharges with $q_L \sim 2.3$ with the following parameters: $B_T = 1.35$ T, $I_p = 170$ kA, $\bar{n}_e = 1.2 \rightarrow 2.8 \times 10^{19}$ m^{-3}, loop voltage ~ 2 V. Sawtooth oscillations indicate q = 1 at r = 0.06 m and there is a low level m = 2 mode with $\Delta B_\theta / B_\theta \sim 0.3\%$. These discharges are at a lower density than has been quoted for similar q_L values in other devices and they are maintained at nearly constant plasma current for ~ 90 ms at $q_L < 2.6$ and ~ 30 ms at $q_L \sim 2.2$. The density can be steady (with gas feed) or rising at up to 3×10^{20} m^{-3} s^{-1}. Factors which have been found important for stability are

a) The use of at least two titanium getters operating continuously between discharges (10 minutes), estimated to cover 2/3 of the vacuum wall.

b) Careful control of the gas flow rate. Too high a feed rate leads to a rapidly growing m = 2 mode and disruption. A density increase is only possible when the m = 2 mode is absent.

c) Avoidance of a 'hard' disruption which extinguishes the plasma current. These appear to decondition the vacuum wall and/or limiters.

d) Insertion of a 0.095 m diameter carbon rod to a radius of 0.22 m ($q \sim 1.6$) did not produce a large change in the discharge behaviour, suggesting that the outer layer of plasma, including the $q = 2$ surface, is relatively cold. Disruption was still preceded by oscillations on the coils with $m = 2$.

DISCUSSION

From the above mentioned experiments and others a picture emerges of the relatively stable discharge which precedes the development of precursor oscillations and disruption itself. This has a fairly well compressed current channel with sawtooth activity in the centre. The $q = 2$ surface is on the edge of the main current channel, which is cooled by radiation or thermal conduction to the walls and limiter. The $q = 2$ surface typically contains > 90% of the total current. $m = 2$ oscillations are at a low level ($\Delta B_\theta / B_\theta < 1\%$) or absent. Disruption is preceded by a growing oscillation with $m = 2$ and sometimes a reduction in sawtooth activity. These changes are precipitated by an influx of cold fuel or impurities.

If we assume that cooling of the edge region occurs then it is clear that the current gradient near the $q = 2$ surface is unlikely to be increased and the current density in the centre will not decrease. Thus, the reasons for the destabilisation of the $m = 2$ mode and the reduction of sawtooth oscillations is not immediately evident.

References

[1] S.J. Fielding, et al., Nuclear Fusion 17 (1977) 1382.

[2] W. Pfeiffer and R.E. Waltz, Nuclear Fusion 19 (1979) 51.

[3] K.B. Axon, et al., Nuclear Fusion 18 (1978) 981.

MHD Model of Current Disruptions in Tokamak Discharges

G. Lisitano
Max-Planck-Institut f. Plasmaphaysik
EURATOM-Association
8046 Garching, Fed. Rep. of Germany

Schlieren techniques at millimetre wavelengths have added a few more complementary features to those already known on the current disruptions of the Pulsator tokamak. As shown in the following, the behaviour of the schlieren signals suggests that the current disruptions may be excited by a layer of enhanced plasma resistivity at the plasma edges owing to plasma-wall interaction or gas feed effects. In order to link the interaction processes at the plasma edges with the observed MHD activity in the plasma interior, an MHD model of current disruptions is proposed. The model, which complements the standard picture of MHD helical instabilities, emphasizes that the MHD activity in the plasma interior is dominated by runaway, superthermals and/or the most energetic electrons.

The schlieren technique is shown schematically in Fig. 1. Transverse electron density gradients deflect the seven λ = 2 mm wave beams which explore the Pulsator tokamak plasma along vertical chords. The distance between two neighbouring beams in Fig. 1 is 2,8 cm. Figure 2 shows the typical behaviour of the internal (up to 94 ms) and major disruption phases. Note the similarity of the sawtoothing in both disruption phases. The hard X-ray radiation from the limiter outside is more than one order of magnitude larger than that from the limiter inside. Figure 3 shows the schlieren signals of the symmetric channels 3 and 5 (see Fig. 1) and the time correspondence of i)the current position signal OUT-IN as delivered by magnetic pick-up coils, ii) the loop voltage U and iii) the discharge current I. Note in Fig. 3 the dramatic increase of the schlieren signal of channel 3 (at the onset of a major current disruption at t_s = 80 ms), which indicates that the core of the plasma density has been displaced inwards. Enlarged time scale measurements have shown that this plasma, and hence current displacement, takes place within a very few microseconds. This inward displacement of the core of the discharge current is characteristic of almost all current disruptions. Note in Fig. 4 the step-like increase of the schlieren signal amplitude of the inner channel 3 (at r = - 2.8 cm in Fig. 7) at each negative spike of a phase of minor disruptions (lasting from t = 80 ms to t = 90 ms), indicating a step-like displacement of the discharge current core inwards. This behaviour is in agreement with the step-like variation of the current position signal (upper trace). Figure 5 shows the precursor oscillations of a major current disruption at t = 99.6 ms. The upper trace of Fig. 5 shows the B oscillations of an m = 2 mode picked up with magnetic coils at the plasma edge. The lower traces of Fig. 5 show the corresponding density oscillations along the central λ = 2 mm wave radiating chord. Both precursor oscillations may be interpreted as being due to the cooling of the plasma edge owing to plasma-wall interaction occurring with increasing strength a few milliseconds before the onset of a major disruption. The sawtoothing (of an internal disruption phase) of the electron density along three vertical chords is shown in Fig. 5 up to the onset of a major disruption at t = 100 ms. In going from the outer channel 5 to the inner channel 3, an inversion of the sawtoothing (like that of the soft X-radiation in Fig. 2) of the internal disruption phase is observed. The rapid increase of the density of the outmost channel, preceding the onset of an internal disruption, suggests that a precursor plasma-wall interaction takes

place. The precursor plasma-wall interaction of an internal disruption seems to be similar, but of much smaller strength, to that of a minor or major disruption. It should be noted here that the observed indication of precursor plasma-wall interactions preceding each instability (internal, minor and external or major) is supported by the measurement of the radial density distribution (not shown here) after gas puffing at t = 40 ms in Fig. 5. In fact, the density increment after gas puffing, is in general for the lateral channels almost equal to or larger than for the central one, thus giving an inverted bell-shaped radial distribution of the density, which is obviously conducive to plasma-wall interaction effects.

The proposed linking mechanism between plasma-edge and the observed MHD activity in the plasma interior is described in the following by means of a general layout of a few elementary processes which are combined to explain the variety of experimentally observed phenomena. According to the model, the evolution of the current disruption is described as:

1) Plasma-wall interactions. One may distinguish the cases: a) symmetric or equilibrium discharge conditions and b)non symmetric or slightly off-centered discharges. As the plasma pressure increases, a point is reached where the plasma-edge interacts with the limiter wall, thus delivering impurities.

2)Impurities or gas feed may produce in case a) a sheet of cooling neutral gas surrounding the discharge current ring and in case b) asymmetric cooling of the discharge current ring.

3) Resistive constriction of the discharge current. The layer of high resistivity neutral gas tends to constrain the discharge current, i.e. would tend to pinch in or to displace the current.

4) MHD current redistribution. We indicate with $W_m = (1/2)L_i I^2$ the stored poloidal field energy, where $L_i/nH = 4\pi(R/cm)[\ln(8R/a) - 1.75]$ is the self-inductance of the discharge current ring; a is the plasma radius and R the radius of the discharge current ring. From $dW_m/dt = 0$ we obtain $dI/I = -(1/2)dL_i/L_i$. The tendency to pinch the discharge, i.e. to increase L_i and I cannot occur if the time variation of the resistive current constriction is too small. In fact, W_m would increase and this should be supported by an energy source which is not available for the short time variation being considered. It follows that a rapid resistive current constraint can only destabilize the plasma and this happens by lowering L_i, i.e. the self-inductance of the discharge current ring. As seen from the expression for the self-inductance L_i, the most immediate way to lower L_i is to increase a, the plasma radius, thus producing the observed flattening of the current profile. Lowering the self-inductance from L_i to $L_i - \Delta L_i$ means that an excess of stored magnetic field energy $\Delta W_m = (1/2)\Delta L_i I^2$ is now available. As will be shown in next elementary process 5), this excess of stored magnetic field energy, which must be immediately dissipated, is the energy source for the destabilization of the current, i.e. for its flattening profile.

5) Sifting and spreading of runaways. Because of the smaller value of the Coulomb collision cross-section of the most energetic electrons in comparison with the Coulomb cross-section of the bulk electrons, the layer of high resistivity neutral gas can only constrain the bulk electrons. As an example for case b), i.e. an off-centered growing plasma pressure, the rapid resistive gas constraint may tend to displace the core of the bulk electron current inwards. Of course, before displacing the bulk electron current, the layer of cooling neutral gas provides a steepening of the density profile at the plasma edge and this, in turn, is conducive of the various m precursor oscillations observed before each instability. The inward resistive constraint causes, however, destabilization of the discharge current ring owing to the immediate release of the stored magnetic field energy which is associated with the inward displacement of the discharge current. As will

be seen, the release of this excess of stored field energy determines the flattening of the current profile by increasing the plasma radius, a, of the radial distribution of the most energetic electrons. In fact, assuming infinite conductivity for the current density of the most energetic electrons $J = \sigma E$ (i.e. by neglecting resistive dissipative effects) and by neglecting dissipative radiation effects, the excess of magnetic field energy dW_m can be associated with the behaviour of the most energetic electrons by the fundamental MHD equation $dW_m/dt + \int v(JxB)dV = 0$, where the first term represents the rate of decrease of the stored magnetic field energy, whilst the second term represents the rate of doing work against the magnetic force JxB. The excess of magnetic field energy to be depleted is therefore that associated with the largest value of the conductivity, which is obviously that related to the most energetic electrons. In other words, the above energy equation represents a "sifting" effect of the MHD instability which spreads the most energetic electrons outwards from the bulk electrons of the plasma. This partly replaces the inward displacement of the bulk electrons until all runaway or most energetic particles are depleted. The resistive current constraint at the outer plasma edge is therefore partly compensated by the replacement of the bulk electrons with the hot electron current carriers which have been displaced outwardly, from the plasma interior, at the onset of the instability. In short, by means of the proposed mechanism the current destabilization in the plasma interior can be excited from the plasma edge by several processes such as i) interaction of the growing plasma pressure with the outer wall, ii) gas feed, iii) impurity drift waves, etc..

6) Recovery of runaway and/or most energetic electrons. The energy source for the recovery of the high energy particle losses is that supplied, as an example, by the O.H. induced energy.

----------Repeat of processes 1 to 6 ----------

This applies for the internal disruption phase.

7) Unbalanced depletion of energy (runaway or most energetic electrons). Owing to a strengthening of processes 1 to 5, process 6 is inadeguate to balance the plasma losses within an instability period (sawtooth duration). The equilibrium of the discharge current is strongly impaired and the bulk of the discharge current is displaced step-like inwards as shown by the schlieren signals of Fig. 4.

------Repeat processes 1 to 7 for the predisruption phase containing from 1 to several tens of minor disruptions. It also applies for the internal disruption phase with large sawtoothing preceding a minor or major disruption.----------

8) Current disruption. The total plasma collapse is reached by progressive destabilization of the discharge current ring owing to a further strengthening of processes 1 to 7. A single serie (of lager strength) of such processes may be, however, sufficent to determine a plasma collapse. The bursts of hard X-rays preceding a major disruption are those generated by the runaway electrons which are spreaded outwardly by process 5). The energy for the rapid loss transport of the energetic particles is given by the rapid inward displacement of the discharge current core, as shown by the schlieren signals of Fig. 3 and 4. The interaction of the collapsing current with the inner wall produces a sudden reduction of the external poloidal magnetic field, giving rise, as shown in Fig. 3, to a positive fast rise of the resistive loop-voltage drop, immediately following each negative voltage spike. In comparison with the last predisruption pulse, the much larger decrement of the self-inductance of the inward collapsing discharge current ring, generates a current pulse which is noticeably larger than those corresponding to the step current displacements of the predistruption phase shown in Fig. 4. The current pulses shown in Fig. 4 may be expressed by $dI/I = -(1/2)dL_i/L_i$, derived from $dW_m/dt = 0$. The large decrement dL_i of L_i and hence the large current pulses dI of the disruption phase are due to the impact of the cool plasma with the inner wall.

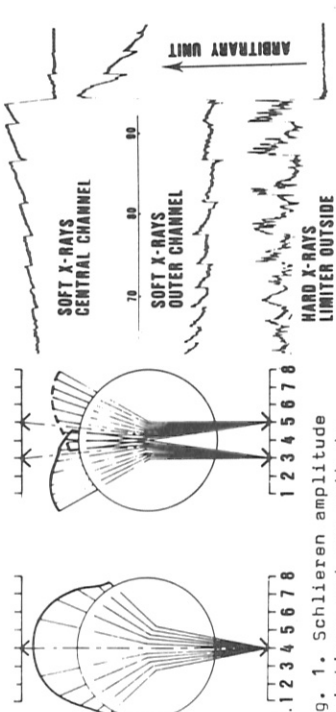

Fig. 1. Schlieren amplitude variations and ray path deflections of the λ= 2mm wave radiating lobes for $N_e = 10^{14} cm^{-3}$.

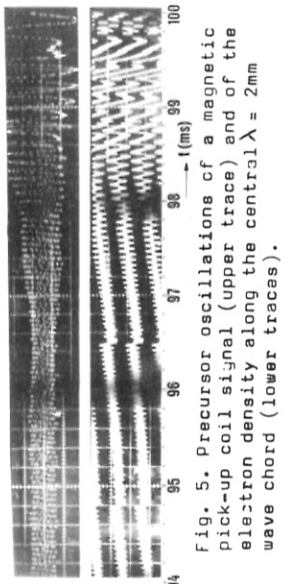

Fig. 5. Precursor oscillations of a magnetic pick-up coil signal (upper trace) and of the electron density along the central λ = 2mm wave chord (lower traces).

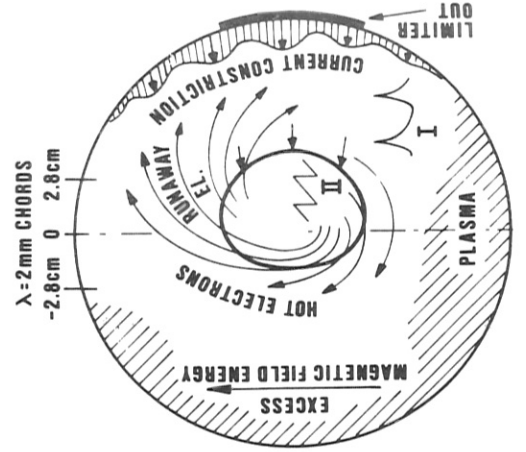

Fig. 7. Sketch of the current disruption model.

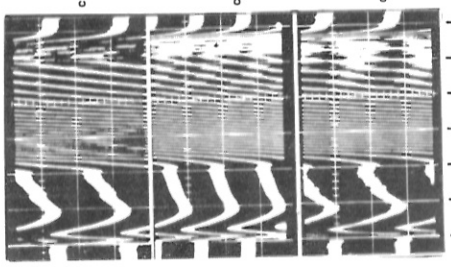

Fig. 6. Sawtooth relaxations of λ = 2mm wave phase-shift.

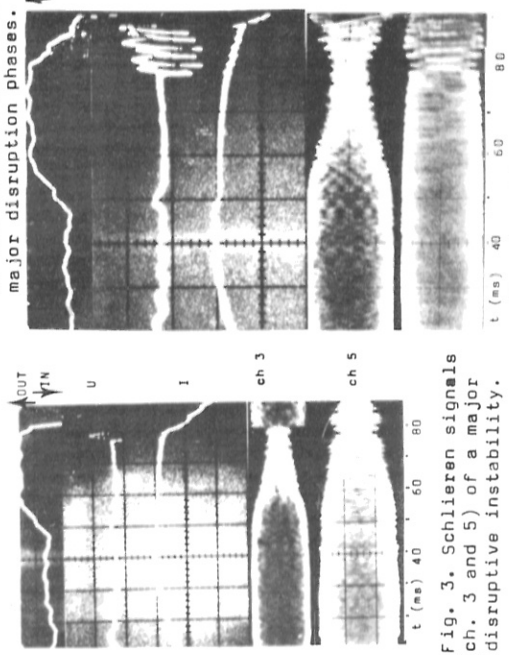

Fig. 4. Schlieren signals (ch. 3 and 4) of a predisruption phase.

Fig. 3. Schlieren signals (ch. 3 and 5) of a major disruptive instability.

Fig.2. Sawtoothing behavior of the internal and of the major disruption phases.

SIMULATION OF TOKAMAK DISRUPTIONS

R Pollard, M Turner, A Sykes and J A Wesson

INTRODUCTION

It appears that an explanation of tokamak disruptions must satisfy three requirements. Firstly it must involve interaction with the region outside the plasma to account for the observed loss of plasma energy and current. Secondly it must show how increasing the plasma current and the particle density both lead to disruptions and thirdly it must be based on the $m = 2$ instability whose growth is observed to precede the disruption.

A numerical simulation which includes these features and reproduces a disruption will be described shortly but first let us look at the saturation sizes of magnetic islands to be expected in tokamaks with typical current profiles.

MAGNETIC ISLANDS

The method of White et al[1] has been followed to calculate the full width, w, of magnetic islands for current profiles of the type

$$j = j_o \left(1 - \frac{r^2}{a^2}\right)^{\nu} \quad .$$

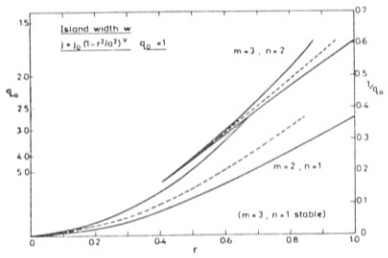

Figure 1

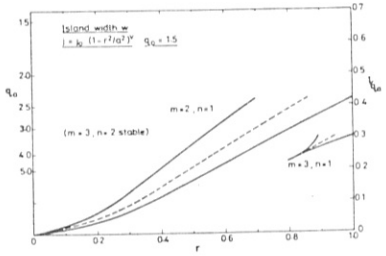

Figure 2

Figure 1 shows the island width of the unstable island against q_a, the value of q at the plasma surface, for $q_o = 1$. It is seen that the $m = 2$ mode produces the dominant island and that this touches the edge of the plasma at $q_a \simeq 2.7$. The only other unstable mode is the $m = 3$, $m = 2$ mode which is comparatively small.

Figure 2 gives the corresponding results for $q_o = 1.5$. The $m = 2$ island touches the wall at $q_a \simeq 2.4$. The $m = 3$, $n = 2$ mode is now stable

but an $m = 3$, $n = 1$ island appears outside the $m = 2$ island, touching the plasma edge at $q_a \simeq 3.3$.

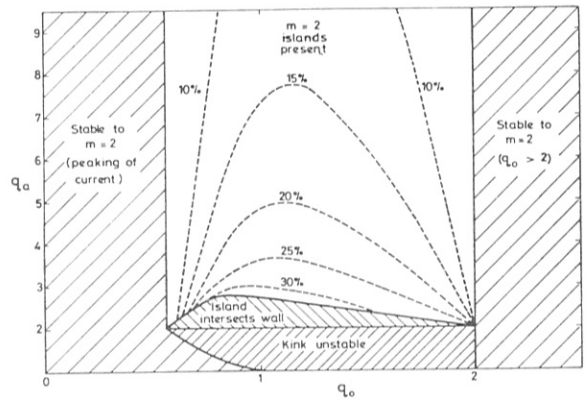

Figure 3

Figure 3 gives the complete results for the $m = 2$ mode for all values of q_o and q_a in the range of interest. If the current is gradually increased with q_o around unity the resonant surface moves outwards and the island grows until it touches the edge of the plasma. Alternatively, if the outer region of the plasma is cooled, the effective edge of the plasma moves inwards and contact of cold plasma with the island again results.

SIMULATION MODEL

We now return to the simulation. The three basic requirements for the model are (i) it must describe the growth of the $m = 2$ tearing mode, (ii) it must allow fast thermal transport parallel to the magnetic field to reproduce the connection around the island and (iii) it must include the limiter or other energy sink at the edge of the plasma.

The numerical code solves the equations of resistive mhd in $m = 2$ helical geometry on a 20×20 square mesh using an explicit, modified Lax-Wendroff scheme. The density is made constant and is enhanced to reduce the computation time. The central value of the resulting ratio of resistive to Alfven transit time is 5×10^3. The circuit conditions can be controlled. The electrical conductivity is proportional to $T^{3/2}$ and the ohmic heating is included. The temperature is zero at the limiter and is maintained constant along each field line by averaging. A small perpendicular thermal conductivity is allowed. The effect of the $m = 1$ relaxation oscillation is included by redistributing the pressure when q_o falls below unity.

SIMULATION OF DISRUPTION

Although arbitrarily large islands can be produced using profiles with smaller shear it is found that, for typical current profiles and no interaction with the "limiter", the $m = 2$ island saturates at widths between 0 and 30% of the plasma radius. However, when the limiter is included a dramatic increase is observed when the island touches the limiter.

Figure 4 shows results of a calculation in which the total current is increased in time. The timescale is given in milliseconds for a tokamak of 20 cm radius having an electrical conductivity corresponding to a central temperature of 1 keV. The island grows until at a width of about 25% it touches the limiter. The rapid growth then ensues and the island grows to fill the plasma region.

During the growth, the plasma around the axis is compressed by the two islands and q_o is driven below unity. Within the model this results in an $m = 1$ instability and removes plasma pressure from the neighbourhood of the axis.

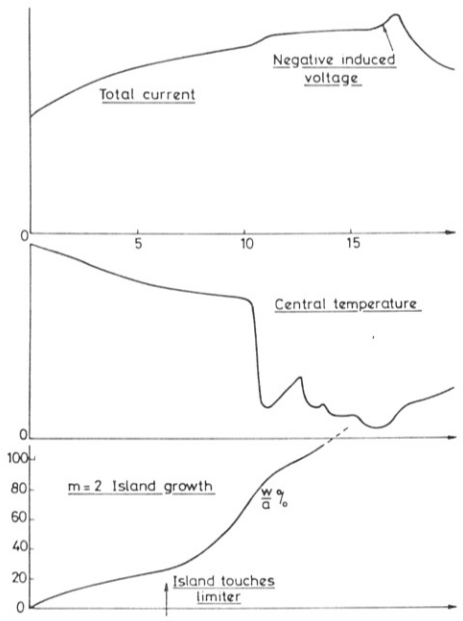

Figure 4

The island contact with the limiter cools a large part of the plasma but, in the simulation, this is only the first phase of the disruption. The second phase occurs when the central region of the plasma is expelled to the wall, bringing about a large negative induced voltage and a fall in the total current. This is seen in the last of the sequence of flux plots shown in Figure 5.

INTERPRETATION

It is believed that the explanation of the rapid island growth can be understood in terms of the time development of the current profiles as shown in Figure 6. At $t = 4.4$ the island is isolated from the limiter. At $t = 8.8$ contact with the limiter has been made. The temperature across the islands has fallen to a low level removing the current gradient on the outer side of the island and increasing it considerably on the inner (smaller r) side.

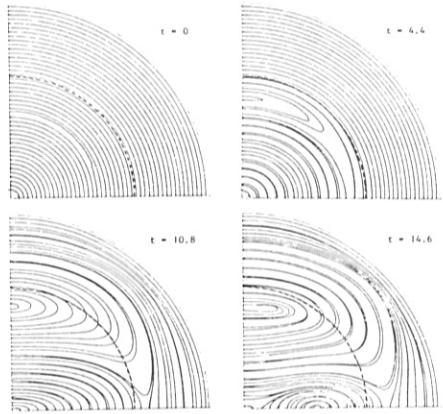

Figure 5. Time development of flux surfaces. Dotted line shows limiter.

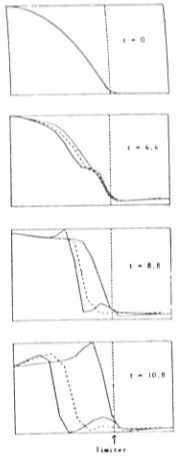

Figure 6. Time development of current distribution (at 0^o, 45^o and 90^o).

The potential energy available for disruption outside the island is

$$\delta W = \frac{\pi^2 R}{2} \int \frac{dj/dr}{(2-q)} \cdot \frac{(rB_r)^2}{B_\theta} \, rdr \quad .$$

It is seen that on the inner side, where $q < 2$, the current gradient is destabilising whereas on the outer side where $q > 2$ the current gradient is stabilising. Thus the contact with the limiter is seen to strongly enhance the destabilising current gradient and to virtually remove the stabilising current gradient. It seems likely therefore that this is the explanation of the first phase of the disruption. The cause of the disruptions which occur when the plasma density is increased may now be seen as being due to the increased cooling at the plasma edge and the movement inwards of an effective heat sink playing the role of the limiter. In the second phase the central plasma is expelled and the induced negative voltage is due to the resulting change in the plasma inductance. The fall in the total current occurs as a result of the loss of conducting plasma to the limiter.

CONCLUSIONS

In summary, a disruption has been simulated which shows many of the experimentally observed features. The disruption is basically due to the $m = 2$ mode and is caused by connection to the limiter (or cold plasma) producing a destabilising change in the current gradients outside the island. The loss of plasma current ultimately occurs as a result of the expulsion of conducting plasma.

1. White R.B., Monticello, D.A., Rosenbluth, M.N. and Waddell, B.V., Phys. Fluids, 20, 800 (1977).

D 1

STABILIZATION OF TEARING MODES: FEEDBACK STABILIZATION AND PROFILE TAILORING*

H. R. Hicks, B. Carreras†, J. A. Holmes, and B. V. Waddell‡

Oak Ridge National Laboratory
Oak Ridge, Tennessee 37830

ABSTRACT

Two possible methods of avoiding the nonlinear interaction of tearing modes are presented. In both cases it is only necessary to limit the saturated island widths below a critical level. It is not required that any modes be stabilized.

For q-profiles measured prior to some major disruptions[1], both the m/n=2/1 and 3/2 resistive tearing modes are linearly unstable. Low β, nonlinear, three-dimensional cylindrical calculations[2] have shown that the 2/1 mode destabilizes the 3/2 and other modes. On the time scale corresponding to the 2/1 linear growth rate γ_{21}, the plasma undergoes a sudden transition to a state with many overlapping islands, resulting in a large region filled with an ergodic field line. The Figures illustrate this for the PLT predisruption profile at $S=10^6$.

The desired elimination of this nonlinear mode coupling can be achieved by modifying either the initial conditions (profile tailoring) or the boundary conditions (feedback stabilization). These results are obtained with the computer program, RSF, which uses a discretization in r (minor radius) and a trigonometric series expansion in θ and ζ (the poloidal and toroidal angles).

It is not difficult to turn off the nonlinear coupling by modifying the equilibrium q-profile.[3] This can be accomplished by making either local modifications (e.g., flattening the current density near r_{21}, the 2/1 singular surface) or global modifications (systematic variation of the parameters defining the q-profile). The necessary and sufficient condition[4] to avoid mode coupling is that the single-helicity saturated island widths satisfy

$$\frac{1}{2}(W_{21} + W_{32}) < r_{21} - r_{32} \quad . \tag{1}$$

This is a less restrictive criterion than requiring that all modes be linearly stable.[3] The ability to achieve (1) experimentally, for example, by heating the plasma outside the 2/1 resonant surface, will in addition depend on transport effects not addressed here.

A feedback circuit has been used with some success to control disruptions on the TO-1 tokamak.[5] Moreover, single helicity calculations[6] have shown that it is possible to reduce the saturated width of the 2/1 mode by the use of an external feedback circuit. In our three dimensional calculation we find that by proper optimization of the circuit, (1) can be satisfied and the disruption avoided.

The feedback signal gain is characterized in terms of the ratio of the 2/1 flux to be imposed at the wall to the 2/1 flux at the resonant surface

$$\beta_o \equiv \psi_{21}(r=r_w)/\psi_{21}(r=r_s) \quad .$$

An estimate of the optimal value of β_o can be obtained[7] from linear tearing mode analysis by requiring $\Delta'_{21}=0$ where $\psi_{21}\Delta'_{21}$ is the discontinuity in the radial derivative of ψ_{21} at r_{21}. For the PLT profile this gives $\beta_o = -7$. The optimal value obtained by a nonlinear computation is $\beta_o = -12$ which, for PLT parameters, would correspond to an $\ell=2$ coil inside the vacuum vessel carrying about 2kA. It is necessary to keep the feedback signal locked in phase with the mode being stabilized.[6] The time delay of the feedback circuit, t_D, should be less than γ_{21}^{-1}. To prevent the 2/1 mode from flipping

sign it is necessary to periodically turn off the feedback coil. A good choice for the on and off periods and time delay is

$$t_{on} = t_{off} = t_D = 200\ \tau_{H\rho} \approx .9\ \gamma_{21}^{-1} \quad ,$$

where $\tau_{H\rho}$ is the poloidal Alfvén time. Thus the magnitude of the 2/1 amplitude is used as input only when feedback is not being applied. Figure 1 shows that this optimized feedback circuit is capable of keeping $w_{21} \lesssim .04a$. This satisfies (1) and avoids the destabilization of the 3/2 and other modes. As a result (Fig. 2b) the flux surfaces are largely intact and the ergodic regions remain rather small. Our analyses of other profiles, including T-4, show the generality of the results presented here for PLT.

---

*Research sponsored by the Office of Fusion Energy (ETM), U. S. Department of Energy under contract W-7405-eng-26 with the Union Carbide Corporation.

†Visitor from Junta de Energia Nuclear, Madrid, Spain.

‡Deceased.

[1]N. R. Sauthoff et al., "A Study of Disruptive Instabilities in the PLT Tokamak Using X-ray Techniques," PPPL-1379 (January 1978); S. V. Mirnov and I. B. Semenov in "Plasma Physics and Controlled Nuclear Fusion Research" (Proc. 6th Int. Conf., Berchtesgaden, 1976) 1, 291 (1977).

[2]B. V. Waddell et al., Phys. Rev. Letters 41, 1386 (1978); B. V. Waddell et al., Phys. Fluids (to be published); J. D. Callen et al., "Plasma Physics and Controlled Nuclear Fusion Research" (Proc. 7th Int. Conf., Innsbruck, 1978), to be published; B. Carreras et al., "Multiple Helicity Tearing Mode Calculations: Major Disruptions," this conference.

[3]A. H. Glasser et al., Phys. Rev. Letters 38, 234 (1977).

[4]J. A. Holmes et al., "Stabilization of Tearing Modes to Suppress Major Disruptions in Tokamaks," ORNL/TM-6707 (Dec. 1978).

[5]V. V. Arsenin et al., in "Plasma Physics and Controlled Nuclear Fusion Research" (Proc. 7th Int. Conf., Innsbruck, 1978), to be published.

[6]D. A. Monticello, et al., "Feedback Stabilization of Magnetic Islands in Tokamaks," PPPL-1477, September 1978.

[7]V. V. Arsenin and V. A. Chuyanov, Uspekhi Fizi. Nauk 123, 6 (1977); V. V. Arsenin, Sov. J. Plasma Physics 3, 524 (1977).

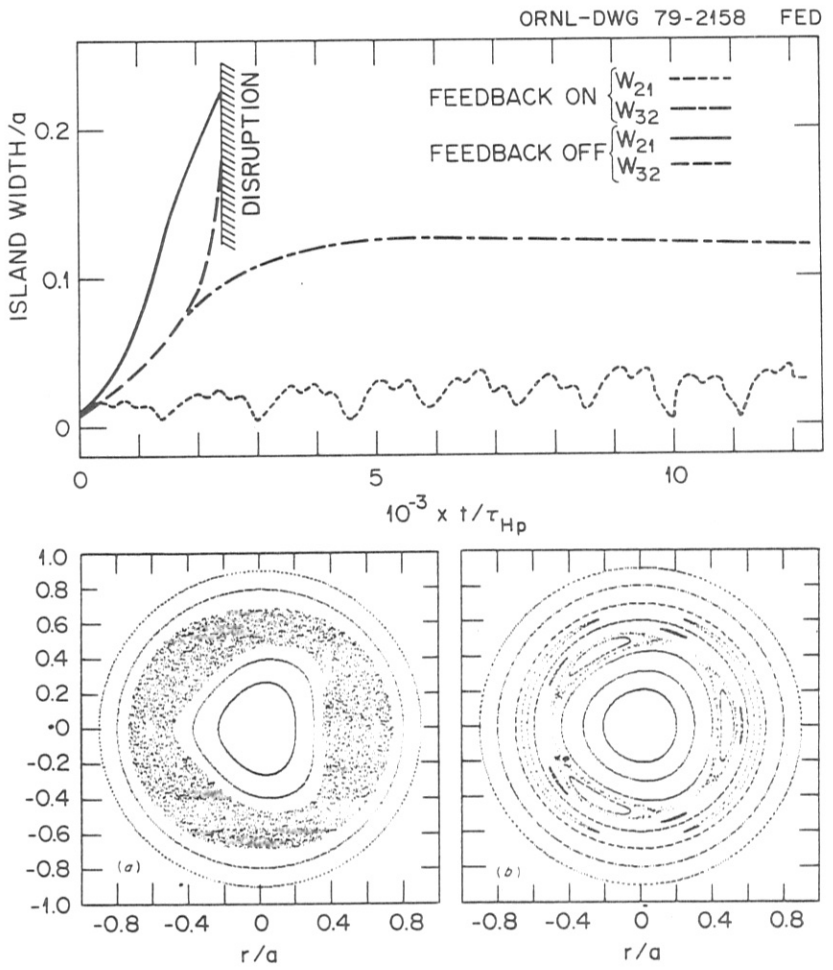

Figure 1 (Top): For the PLT profile, magnetic island widths of the 2/1 and 3/2 modes are plotted as functions of time for cases with and without feedback.

Figure 2 (Bottom): Without feedback (a) there is a large ergodic region filled with one field line. With feedback (b) most flux surfaces remain intact.

SINGLE HELICITY TEARING MODE EVOLUTION: MIRNOV OSCILLATIONS, SOFT AND INTERNAL DISRUPTIONS*

B. Carreras,† J. D. Callen, H. R. Hicks, and B. V. Waddell††
Oak Ridge National Laboratory, Oak Ridge, Tennessee 37830

Tearing modes seem to be responsible for most of the experimentally observed macroscopic behavior of tokamak discharges.[1] We study here their nonlinear evolution in the single helicity approximation to interpret Mirnov oscillations, internal disruptions, and some minor disruptions. We use the reduced set of resistive MHD equations[2] valid in cylindrical geometry in low β limit.

Mirnov Oscillations (m/n = 2): An elementary nonlinear tearing mode theory gives accurately the amplitude of the m = 2 poloidal magnetic field fluctuations (Mirnov oscillations) at the tokamak limiter.[3] The input required is the electron temperature profile from which the safety factor profile can be inferred. The saturation amplitude is obtained from a semianalytic nonlinear Δ' analysis.[4] The mode is assumed to saturate when the discontinuity in the radial derivative of the flux function ψ, as measured across the associated magnetic island, vanishes, i.e., when

$$\Delta'(w) \equiv \left[\left.\frac{d\psi_{21}}{dr}\right|_{r_+} - \left.\frac{d\psi_{21}}{dr}\right|_{r_-} \right] \Big/ \psi_{21}(r_{21}) = 0$$

where $r_\pm = r_{21} \pm w/2$, w being the magnetic island width. In linear theory, the δW energy is proportional to the linear Δ',[5] thus, this assumption appears equivalent to assuming that the mode saturates when the nonlinear δW vanishes. This analysis gives an absolute result for the amplitude of the magnetic field everywhere and in particular, at the limiter. A study of ORMAK (Fig. 1) and T-4 profiles gives results in agreement with experimental data. An understanding of Mirnov oscillations is important because their amplitude has been correlated experimentally (Fig. 1), with the confinement time.[6]

Internal Disruptions (m/n = 1): The m = 1 tearing mode is the dynamic mechanism which causes the abrupt drop phase in internal disruptions or sawtooth oscillations.[7] The mode begins to grow whenever q drops below unity at the plasma center, thereby inducing shear at the q = 1 surface r_s. Single helicity numerical calculations[8] have shown that the mode continues to grow until the magnetic axis of the island moves toward the geometric center of the plasma and thereby transforms the magnetic topology of the central core from the original one centered about the central magnetic axis to one centered about the magnetic island center.

Since the m = 1 tearing mode growth rate is much faster than the ohmic heating rate, the electron temperature is equilibrated along all of the reconnecting magnetic field lines and hence is flattened within the induced m/n = 1 magnetic island. It can be seen from flux conservation considerations,[9] that the region over which the electron temperature flattens ultimately extends out to $r_o \sim \sqrt{2} r_s$. Thus, immediately after the internal disruption, the temperature profile is flat within the radius r_o. Thereafter, on a much slower time scale, the combination of ohimc heating and radial electron heat transport reheats the plasma center back toward the centrally peaked electron temperature and current density profiles. An analytic model of internal disruptions,[10] which is based on the cyclic process in which the plasma core resistively overheats and drives q below unity, causing the m = 1 tearing mode to become unstable with an accelerating growth rate and ultimately to flatten the electron temperature profile as magnetic reconnection occurs, has been developed. It has been extensively and quite favorably compared with ORMAK data on the space-time evolution of internal disruptions and their m = 1 precursors.[10]

Recent results on the m/n = 1 nonlinear evolution for lower values of resistivity ($S = 10^6$) have extended the results presented in Ref. 8 to more realistic tokamak plasma parameters (Fig. 2).

Minor Disruptions Associated With Hollow Current Profiles (m/n = 2, 3,...): Hollow electron temperature profiles have sometimes been observed[6,11] during tokamak discharges and, in particular, at the beginning of some discharges.[12] The presence of such profiles is often accompanied by MHD activity which, in some cases, leads to disruptions. The nonlinear evolution of tearing modes for equilibrium current profiles which have a local minimum, could generate two sets of magnetic islands. This leads either to saturation of the tearing mode or to a redistribution of the flux and field line reconnection (Fig. 3). The latter case is not always accessible, since the condition for reconnection[13] is $\psi_*(0) \approx \max[\psi_*(r)]$, where ψ_* is the helical flux function for the mode we are considering (see Fig. 4). When the time evolution leads to reconnection of magnetic field lines, the time scale for the process is compatible with the time scale observed experimentally in some minor disruptions accompaning hollow temperature profiles. For a wide set of equilibrium q profiles, associated with hollow temperature profiles, we have studied the stability properties of tearing modes with m = 2, 3, 5, and 7. The results stated above are completely general for all these cases.

*Research sponsored by the Office of Fusion Energy (ETM), U. S. Department of Energy under contract W-7405-eng-26 with the Union Carbide Corporation.

†Visitor from Junta de Energia Nuclear, Madrid, Spain.

††Deceased September 14, 1978.

REFERENCES

1. J. D. Callen, et al., ORNL/TM-6564, September 1978 (to be published in the Proc. 7th Int. Conf. Innsbruck, 1978).
2. H. R. Hicks, et al., ORNL/TM-6096, December 1977 (to be published).
3. B. Carreras, et al., ORNL/TM-6403, July 1978 (to be published).
4. R. B. White, et al., Phys. Fluids 20 (1977) 800.
5. H. P. Furth, Propagations and Instabilities in Plasmas (Futterman, W. I., ed.) Stanford University Press (1973) p. 87.
6. L. A. Berry, et al., in Plasma Physics and Controlled Nuclear Fusion Research, (Proc. 6th Conf. Berchtesgaden, 1976) 1 (1977) 49; S. V. Mirnov, in Plasma Physics and Controlled Nuclear Fusion Research, (Proc. 7th Conf. Innsbruck, 1978) to be published.
7. S. Von Goeler, et al., Phys. Rev. Lett. 33 (1974) 1201.
8. B. V. Waddell, et al., Nucl. Fusion 16 (1976) 528.
9. B. B. Kadomtsev, Sov. J. Plasma Phys. I (1976) 389.
10. B. V. Waddell, et al., Nucl. Fusion 18 (1978) 735; G. L. Jahns, et al., Nucl. Fusion 18 (1978) 609.
11. N. R. Sauthoff, et al., Nucl. Fusion 18 (1978) 1445.
12. D.L. Dimock, et al., Nucl. Fusion 13 (1973); S. V. Mirnov, et al., Fiz. Plazmy 4 (1978) 50.
13. B. Carreras, et al., ORNL/TM-6570, October 1978 (to be published).

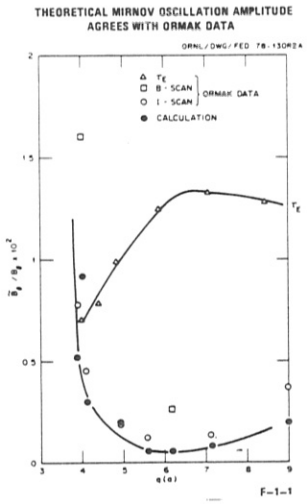

Fig. 1. Theoretical Mirnov oscillation amplitude compared with ORMAK data.

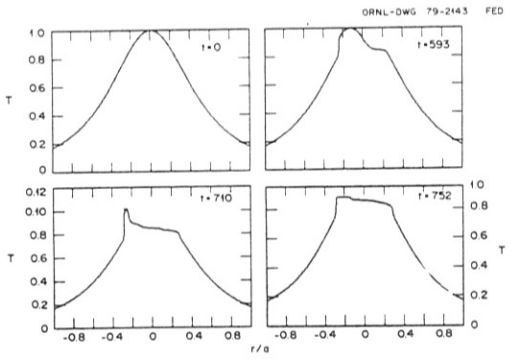

Fig. 2. Nonlinear evolution of the electron temperature profile due to m=1/n=1 tearing mode. ($S = 10^6$ and $\hat{\chi}_{\parallel} = 10^7$).

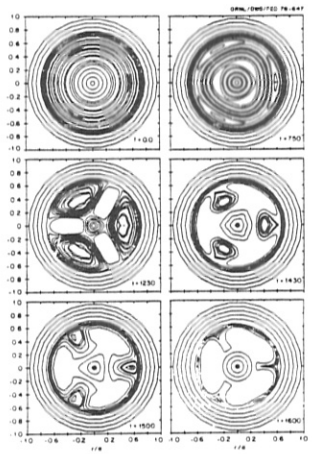

Fig. 3. Poloidal flux contours for m=3/n=1 showing the reconnection process.

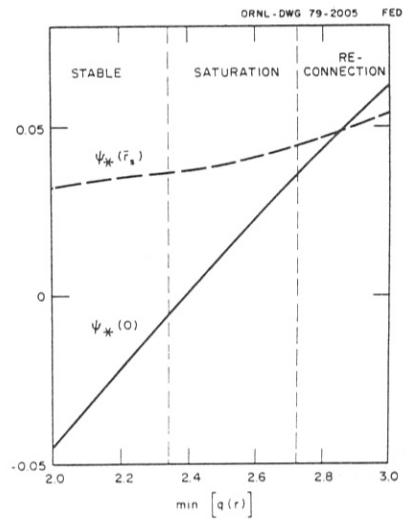

Fig. 4. The values of $\psi_*(0)$ and $\psi_*(\bar{r}_s)$ vs. q_m showing when reconnection is accessible.

High Beta Tearing and Ballooning Modes in Tokamaks

R. B. White, W. Park, and D. A. Monticello
Plasma Physics Laboratory, Princeton University
Princeton, New Jersey 08544 U.S.A.

and

H. Strauss
Fusion Research Center, University of Texas
Austin, Texas U.S.A.

I. Introduction

A three-dimensional numerical code (HIB) has been developed to examine the full nonlinear evolution of tearing and ballooning modes in a high beta tokamak. The code employs a reduced set of equations [1,2] obtained by using a lowest order expansion in the inverse aspect ratio $\varepsilon = a/R$. Problems related to the tokamak disruption, such as large $m = 2$ magnetic island development [3], the interaction of different helicities [4], ergodic field development [5], and divertor interaction [6] will be examined in low and high beta configurations. In addition, the nonlinear development of ideal and resistive ballooning modes will be examined.

Results thus far include good agreement of equilibria and linear growth rates of the ballooning mode with the Princeton Equilibrium and Stability code (PEST). In addition, the ballooning mode is found to have a second marginal stable point for large beta. Preliminary nonlinear results indicate that there is no effective nonlinear stabilization of the low n ballooning mode at small amplitudes. The resistive tearing mode is found to have the usual scaling $\gamma \sim \eta^{3/5}$ in both high and low beta ballooning-stable regimes.

II. The Reduced Equations

Using the tokamak ordering $B_\perp \sim \varepsilon B_\phi$, $q \sim 1$, and $\beta \sim \varepsilon$, where B_ϕ is the toroidal field, q the inverse rotational transform, $\varepsilon = a/R$ the inverse aspect ratio, and β the ratio of plasma pressure to magnetic field pressure, the fluid equations of motion, and Maxwell's equations are expanded to lowest order in ε. To lowest order the fluid velocity is found to be divergence free, corresponding to an incompressible toroidal field, and thus we write

$$\vec{v} = \vec{\nabla} u \times \hat{\phi} \quad . \tag{1}$$

We express the magnetic field in terms of the vector potential A,

$$\vec{B} = \vec{\nabla} A \times \hat{\phi} + B_\phi \hat{\phi} \tag{2}$$

with $J_\phi = -\nabla_\perp^2 A$. The toroidal field $B_\phi = I/R$, to this order can be written as $B_\phi = B_o + B_o R_o/R + I_1/R_o$, where the two corrections to the zero order constant toroidal field are due respectively to toroidal curvature and plasma current. To lowest order in ε we find $\vec{\nabla} P = \vec{J} \times \vec{B}$ and thus $\vec{\nabla}(P + B^2/2) = (\vec{B}\cdot\vec{\nabla})\vec{B}$, which implies

$$\vec{\nabla}(P + I^2/2R_o^2) = 0 \quad . \tag{3}$$

Applying $\hat{\phi}\cdot\nabla\times$ to the equation of motion then gives

$$\frac{d}{dt}(\nabla_\perp^2 u) = \hat{\phi}\cdot\vec{\nabla} A \times \vec{\nabla} J_\phi + \frac{\partial}{\partial \phi}\nabla_\perp^2 A + 2\left(\frac{\partial P}{\partial r}\sin\theta + \frac{1}{r}\frac{\partial P}{\partial \theta}\cos\theta\right) . \tag{4}$$

To advance the potential A, begin with $\nabla_\perp \cdot B_\perp = 0$, or $\partial B_\perp/\partial t = \nabla \times \vec{k}$, which gives $\partial A/\partial t = \vec{k}\cdot\hat{\phi}$. But $\partial B_\perp/\partial t = \vec{B}\cdot\vec{\nabla} V_\perp - \vec{V}\cdot\vec{\nabla} B_\perp =$ $\nabla \times [\vec{V}_\perp \times \vec{B}_\perp + (B_o/r)(\partial u/\partial\phi)\hat{\phi}]$, and thus $\partial A/\partial t = B\cdot\nabla u$, or

$$dA/dt = \partial u/\partial \phi \quad . \tag{5}$$

Finally for the pressure, we have

$$dP/dt = 0 \quad . \tag{6}$$

III. The Numerical Code

The reduced equations (4, 5, 6) are advanced by the code HIB. It is a three-dimensional code employing Fourier decompositions in θ and ϕ, and a radial grid in r. Typically, 50 radial grid points, 20 θ harmonics, and for nonlinear runs several ϕ harmonics, are used. A second order accurate explicit difference scheme similar to the two-step Lax-Wendroff method is used. The convolution of the Fourier modes, which is the most time-consuming part of the computation, is fully vectorized for the efficient use of the computer (CRAY - 1).

IV. Equilibria

Tokamak equilibria are obtained by the use of the flux conserving tokamak [7] concept. A cylindrical pressure and current profile is allowed to relax (flow velocity periodically set equal to zero) to an equilibrium. During this process, the pressure and rotational transform are flux conserved. Typically, the initial current profile is chosen to be parabolic, $J_\phi = (2/q_o)(1 - r^2)$ and the pressure profile $P = P_o(1 - r^2)^4$. Solving $\nabla^2 A = J_\phi$ to find A(r), we can then express the pressure and inverse rotational transform in terms of A

$$q(A) = 2q_o/(1 - 8Aq_o)^{1/2} \tag{7}$$

$$P(A) = \beta[(1 - 8Aq_o)^{1/2} - 1]^4 .$$

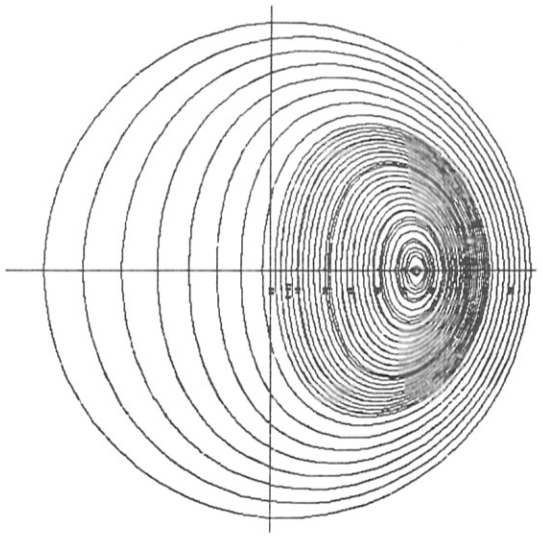

Fig. 1

Flux surfaces for a typical high β equilibria are shown in Fig. 1. Equilibria obtained were also checked

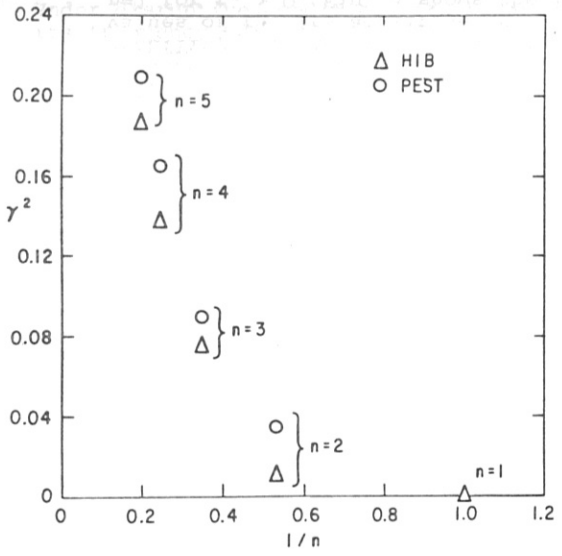

Fig. 2

by comparison with PEST, excellent agreement was obtained for R/a = 10.

V. Results of Numerical Calculations

In Fig. 2 is shown the obtained linear ballooning mode growth rates for PEST and HIB for several n values. The PEST equilibrium, which was used for both codes, had an inverse aspect ratio at $\varepsilon = 1/10$, so that agreement between the two codes should not be expected to be better than 10%. In Fig. 3 is shown the obtained growth rates for n = 1, 2 as a function of β, for the equilibrium discussed in Section IV with q(0) = 1. Here β refers to the peak (magnetic axis) value.

Note that we observe the high beta stabilization predicted previously [8 - 12] on the basis of model calculations.

The linear growth rate of the resistive mode has been examined in both high and low beta ballooning stable regimes. In the high beta regime ($\beta/\varepsilon \sim 2$ in Fig. 3) the growth rate is found to be given by

$$\gamma = 23\eta^{3/5}, \qquad (8)$$

which corresponds to a rather large equivalent Δ', on the order of $\Delta' = 200$. (Δ' is not well

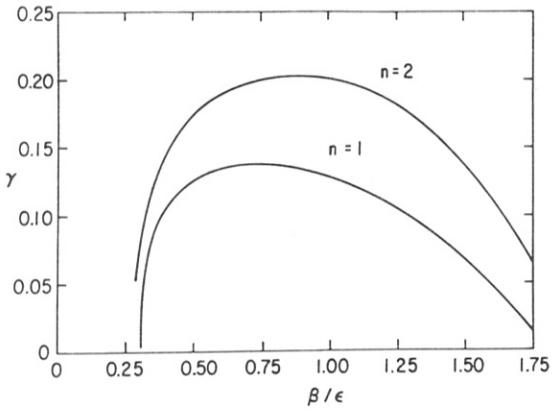

Fig. 3

defined in a high β equilibrium, this is only an approximate value for comparison with tearing mode growth rates found in low beta plasmas.)

Nonlinear ballooning mode results indicate that there is no effective nonlinear stabilization, at least for low n and moderate amplitudes. The mode continues at essentially the linear growth rate, developing very sharp current spikes, which in the presence of resistivity would undoubtedly lead to rapid tearing and consequent changes in topology. Nonlinear resistive ballooning modes will be investigated in the near future.

Acknowledgments

This work was supported by United States Department of Energy Contract No. EY-76-C-02-3073.

References

[1] ROSENBLUTH, M. N., MONTICELLO, D. A., STRAUSS, H., AND WHITE, R. B. Phys. Fluids 19, 1987 (1976).

[2] STRAUSS, H. R. Phys. Fluids 20, 1354 (1977).

[3] WHITE, R. B., MONTICELLO, D. A., AND ROSENBLUTH, M. N., Phys. Rev. Lett. 39, 1618 (1977).

[4] CARRERAS et al., Proc. Seventh International Conference on Plasma Physics and Controlled Nuclear Fusion, Innsbruck, 1978.

[5] STIX, T. H., Phys. Rev. Lett. 30, 833 (1973).

[6] WESSON, J. A., this conference.

[7] CLARKE, J. F. and SIGMAR, D. J., Phys. Rev. Lett. 38, 70 (1977).

[8] COPPI, B., FERREIRA, A., MARK, J. W-K., and RAMOS, J. J., Massachusetts Institute of Technology Report PPR-78/24 Submitted to Nucl. Fusion.

[9] MERCIER, C., Proceedings of the Seventh International Conference on Plasma Physics and Controlled Nuclear Fusion Research, Innsbruck, 1978.

[10] FIELDING, P. J. and HASS, F. A., ibid, and also Phys. Rev. Lett. 41, 801 (1978).

[11] LORTZ, D. AND NUHRENBERG, J., Phys. Lett. A68, 49 (1978).

[12] COPPI, B., FERREIRA, A., MARK, J. W-K., and RAMOS, J. J., to be published in Comments on Plasma Physics and Controlled Fusion.

MHD-INSTABILITY OF OHMICALLY HEATED PLASMAS IN URAGAN II

Ju.K . Kuznetsov and U.M. Tonkoprjad

Physico-Technical Institute of the Ukrainian Academy
of Sciences, Kharkov, USSR

I. Experiments with ohmic heating of plasmas in the stellarator URAGAN II show that similar to tokamaks the current and the plasma parameters are limited as a result of MHD-instabilities.

According to theory [1], the rotational transform ι_h of the stellarator field is one of the main parameters defining the character of the instability.

Experimental data on MHD-instabilities allow the determination of optimal regions for ohmic heating experiments. In this paper, experimental results are presented on MHD-instabilities and their influence on plasma behaviour observed in the l=3 "URAGAN II" [3] stellarator. ($a = 6.5 \div 8$ cm, $\iota_h(a) \leq 0.9$, $B\varphi \leq 22$ kG, $\bar{n}_e \leq 2 \times 10^{13}$ cm^{-3}, $kT_e \leq 300$ eV). The early experiments on this subject [4,5] were performed mainly with $\iota_h = 0.75$. Specific diagnostics are magnetic probes ($m \leq 6$, $n \leq 4$) and resonant windings inductively coupled with m = 1,2, n = 0,1 modes measuring perturbations of the magnetic field outside of the plasma column.

II. Characteristics of the Instability

We observe magnetic perturbations (M.P.) with frequencies up to 50 kHz in a wide range of parameters. The level of these oscillations appears to be a few orders of magnitude above thermal noise. At small currents $\tilde{B} \ll \tilde{E}$, $\tilde{n}$, $\tilde{T}$, and no resonant structure as predicted by theory is observed. We conclude that in this case the B fluctuations are secondary effects of some potential instabilities ($\tilde{E}$, $\tilde{n} \sim 10^{-2}$) in a plasma with high resistivity (drift type) which were not investigated in detail. With increasing current the MHD-instabilities become dominant. Fig. 1 shows the dependence of the level of MHD activity measured by one probe as a function of the plasma current. We see that the level of the instabilities sharply increases for certain current values, which depend on the magnetic fields of the stellarator $B\varphi$ and on ι_h. The space time structure of the m.p. is rather complicated and changes strongly during the pulse time and also with changing discharge conditions. Predominating modes are those with low m, n numbers. We only find qualitative agreement of our experimental data with theory. In the region $\iota_h(a) \geq 0.5$ the modes m=1, n=1 (current transform $\iota_c > 0$) and m=1, n=0 ("opposite" current direction $\iota_c < 0$) are dominant. Fig. 2 shows that for higher current the mode m=1, n=1 is increasing. Similar results are obtained if ι increases by changing ι_h for constant plasma current. The instability m=1, n=0 in the case $\iota_c < 0$ is dominant for all values of ι_h. Its amplitude is essentially higher than m=1, n=1 for $\iota_c > 0$. Fig. 3 shows the level of these modes as a function of I_p for both current directions. For $\iota_h < 0.5$ the modes with m=2,3,4 are dominant if $\iota_c > 0$.

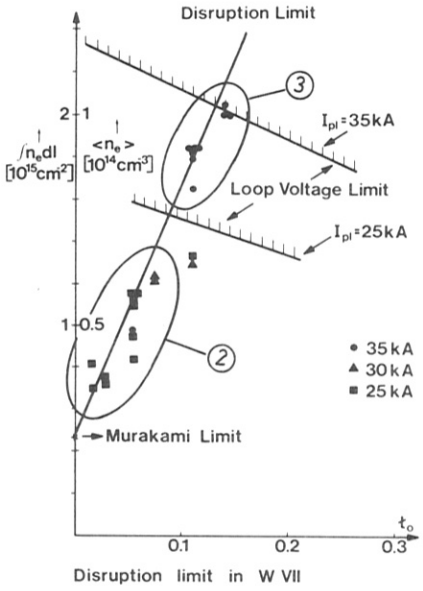

Fig. 1

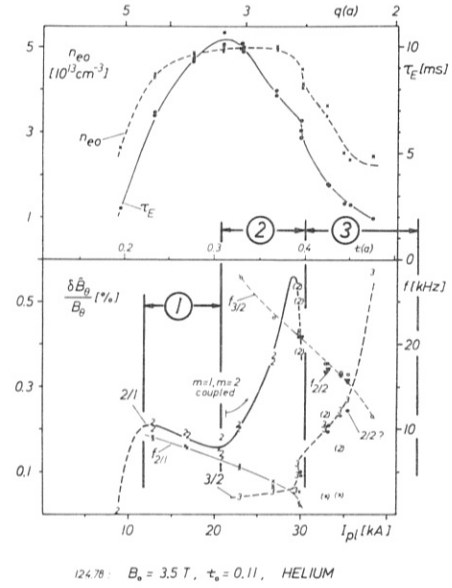

Fig. 2

Under disruptive conditions the 2,1 mode is coupled to the 1,1 mode (as seen from the soft-x-ray signals [5]) its relative amplitude $\delta\hat{B}_\theta/B_\theta$ being $\gtrsim 1$ % (B_θ is the poloidal field of the plasma current alone). With increasing amplitude the rotation of the 2,1 islands is progressively impeded by an interaction with the limiter. This is concluded from the signals becoming more and more non-sinusoidal and irregular [2]. Finally, the islands seem to be locked to the limiter, and the 2,1 frequency goes to zero. Disruptions seem to occur preferentially under conditions where the 2,1 amplitude is still increasing (corresponding to $I_{pl} \approx 28$ kA), i.e. where the 2,1 islands are not yet completely locked to the limiter.

Sometimes for $\iota_o \lesssim 0.055$ the amplitude and the frequency of the 2,1 mode are modulated by more than a factor of 2 in correlation with the sawteeth. Predisruptions are seen on the soft X-ray signals close to the q=2 surface with trigger sawteeth at q=1 [5]. It could not be found that these discharges are more favourable for disruptive instabilities than others. In addition to the 2,1 mode a small 3,2 mode is observed. Its frequency is 5 to 10 times that of the 2,1 mode. If coupling between two modes means that their frequencies are identical, a coupling between the 2,1 and 3,2 mode has never been observed.

For the disruptions observed in regime (3) in Fig. 1, ι_o and the electron density have to be increased, and $q(a) \approx 2$. The mode behaviour can generally be compared with that of regime (3) of

Fig. 2. The 3,2 mode is the only one which can easily be identified. Under disruptive conditions its relative amplitude is around 0.4 %, its frequency being approximately 5 kHz. The 2,1 tearing mode is no longer visible. However, it cannot be concluded from the measurements whether the 2,1 islands have disappeared, or whether only the rotation has stopped. Therefore, stationary islands could exist.

In addition to the 3,2 mode, modes with an m=2 symmetry are usually observed. They consist of a high frequency component which sometimes can be proved to be a 2,2 mode. Quite often its frequency is identical to that of the 3,2 mode. Sometimes a low frequency component can also be observed (shown in brackets). This could be a 2,1 kink mode. Its frequency corresponds roughly to twice the diamagnetic drift frequency at the q=2 surface which is very close to the limiter. No temporal evolution of any modes present could be clearly seen before a disruptive instability up to the leading edge of the positive spike in the plasma current. However, a very rapid evolution within a time short compared to the relevant oscillation times cannot be excluded.

The density limit due to current disruption increases strongly with t_o (Fig. 1). This is difficult to explain since the mechanism responsible for the disruptive instability is not very well known. Supposing the 2,1 tearing mode to be the relevant one in regime (2) in Fig. 1, a possible explanation may be the following: An increasing field has the tendency to stabilize the 2,1 mode [2]. This can be explained by the q=2 surfaces being shifted outward with respect to the current density profiles by the stellarator field [6]. A direct stabilizing effect of the stellarator field on MHD modes has not yet been observed. On the other hand, an increasing density modifies the j(r) profiles in such a way that the 2,1 mode can be destabilized [2,6]. Thus, an increasing density can compensate the stabilizing effect of the stellarator field on the 2,1 mode.

For regime (3) in Fig. 1 an explanation is even more difficult. The 2,1 tearing mode seems to be no longer relevant. Presumably it is replaced by another mode which needs a still higher density to become sufficiently unstable or to couple sufficiently strongly to a second mode. With reference to the current density profiles, a similar situation as in regime (2) can be found if the q=2 surface is replaced by the q=1.5 surface. Thus the 3,2 mode is expected to be unstable, as indeed is observed. However, a similar sharp increase of the 3,2 amplitude with increasing density as seen for the 2,1 mode [2] could not be found (similar to the increase between 20 and 30 kA in Fig. 2).

Another effect of the stellarator field on the discharge may be important with respect to current disruptions, i.e. the stabilization of the position of the discharge inside the vacuum vessel, since in a tokamak current disruptions are connected with a loss of plasma equilibrium. This stabilization is most clearly demonstrated by the fact that at t_o = 0.23 an ordinary discharge can be maintained without any vertical field.

In a tokamak discharge the stability of the plasma position is given by the curvature of the field lines of the vertical field (B_V const. in time). The stellarator field improves this stability,

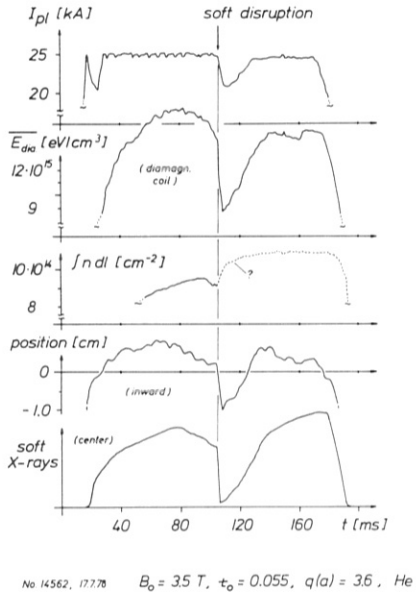

No 14562, 17.7.78 B_o = 3.5 T, t_o = 0.055, q(a) = 3.6, He

Fig. 3

and an equivalent t_o can be defined which has the same positional stability as the curved vertical field [7]. For W VII-A it can be estimated to be

$$t_{o,equ.} \approx 0.003 \ldots 0.004.$$

Since normal operating values for t_o are between 0.025 and 0.23, in the stellarator W VII-A the plasma position is theoretically 1 to 2 orders of magnitude better stabilized than in a tokamak with the geometry of W VII-A. However, since $t_{o,equ.} \sim (a/R_o)^2$, the equivalent t_o is much larger in tokamaks with small aspect ratio.

The consequence of the improved positional stability is that the plasma equilibrium is less sensitive to perturbations of the temperature profile (or internal inductance) and the energy density (or β_p). This is demonstrated by the example of Fig. 3. A helium discharge at t_o = 0.055 is shown with the 2,1 tearing mode dominating. The sudden breakdown of the central soft-X-ray intensity indicates a disruptive instability. However, the plasma reaches a new equilibrium, and the inward shift is limited to about 1 cm. A rough estimate of the new plasma position (B_V = const.) allows a shift of 1.7 cm which agrees approximately to the observed value. The calculation also shows that for a W VII-A tokamak a new equilibrium inside the vacuum vessel would not have been possible (for further discussion see [8]).

REFERENCES

[1] W VII-A Team, Proc. 6th Int.Conf. Berchtesgaden (1976), 2, IAEA, Vienna (1977) 81.

[2] W VII-A Team, Proc. 7th Int.Conf. Innsbruck (1978), paper H3.

[3] Murakami, M., et al., Nucl. Fusion 16 (1976) 347.

[4] W VII-A Team, Proc. 7th Int.Conf. Innsbruck (1978), paper H2.

[5] W VII-A Team, Proc. 8th Europ.Conf. Prague (1977), 1 (1977) 127 and 2 (1977) 236.

[6] W VII-A Team, to be published

[7] Yoshikawa, S., private communication.

[8] W VII-A Team, "Disruptions in the W VII-A Stellarator", this symposium.

EFFECTS OF THE STELLARATOR FIELD ON THE MHD MODE BEHAVIOUR CLOSE TO THE DISRUPTION LIMIT IN W VII-A

W VII-A Team, presented by R. Jaenicke

Max-Planck-Institut für Plasmaphysik
Association EURATOM-IPP
D-8046 Garching, F.R. Germany

ABSTRACT

In the stellarator Wendelstein VII-A the high density limit due to current disruption increases strongly with the stellarator field or external rotational transform ι_o. For $\iota_o \gtrsim 0.14$ current disruptions have not been observed. Also the MHD mode behaviour changes significantly with increasing ι_o. Nevertheless, disruptive and non-disruptive discharges do not belong to different mode behaviour regimes. Different modes can be unstable in disruptive discharges depending on the discharge conditions. Coupling of two modes is frequently observed, but never between the 2,1 and 3,2 modes. Finally the stabilization of the plasma position by the stellarator field is discussed.

In the Garching stellarator W VII-A the l=2, m=5 helical windings produce an external rotational transform ι_o with negligible shear [1]. To first order the total rotational transform $\iota = 1/q$ is the sum of ι_o and the rotational transform produced by the plasma current. Experimental results obtained in W VII-A are especially well suited for comparison with tokamak results since the q(r) profiles are similar to those of tokamaks. The results on MHD modes presented in this paper rely mainly on the measurements with poloidal magnetic field probes [2].

In W VII-A the disruption phenomenon has been investigated for a very limited number of shots only. In Fig. 1 the electron density of disruptive helium discharges is shown as a function of ι_o. The high density limit due to current disruption ("Murakami-limit" in tokamaks [3]) increases strongly with ι_o. At large ι_o, depending on the plasma current, the maximum attainable density is limited by the maximum available loop voltage, and disruptions are no longer observed [4]. Two regimes of mode behaviour can be distinguished.

At low ι_o (regime (2) in Fig. 1) the m=2, n=1 (2,1) tearing mode is dominant. The mode behaviour is similar to that of regime (2) in Fig. 2. Here the amplitudes and frequencies of different modes with increasing plasma current are shown in the lower half for a medium $\iota_o = 0.11$. The discharges were carried out with identical amounts of helium introduced during current buildup. The microwave line density was not constant due to the varying confinement time (see upper half of Fig. 2, $n_{eo} = 1.5\langle n_e \rangle \approx 5 \cdot 10^{-2} \int n dl$).

III. Influence of the Instability on Plasma Parameters

For more interesting regimes with $\iota_h > 0.5$ phenomena like disruptions in tokamaks are observed only at low magnetic fields ($B\varphi \lesssim 5$ kG) [4]: Excitation of MHD-instabilities leads to a sharp drop of the plasma current. For magnetic fields $B\varphi \gtrsim 5$ kG a quasistationary level of MHD-instabilities is set up, leading to increasing plasma losses. A further increase of the MHD-level results in a limitation of I_p (Fig. 4) and nT [4]. There are two components of m.p.: a low frequency one, which is highly reproducible, and a high frequency component. This situation is shown in Fig. 5. (The first component is indicated by dashed lines). The low frequency component is quasistationary at low current. With increasing current we observe a complicated change of amplitude and spatial phase. We explain this effect as a result of changing plasma equilibrium. Similar effects were observed in the regime of R.F. heated plasmas [6]. The second component is an MHD instability. We have observed that plasma losses are connected mainly with that component which shows a strong development for large plasma currents.

In Fig. 6 we show a picture summarizing the regimes of ohmically heated discharges. The maximum ι_c value (abscisses, see Fig. 4) is plotted as a function of ι_h. The horizontal lines correspond to a change of parameters like $B\varphi$, n and T. We see that the parameter ι_h determines the maximum value of ι_c.

IV. Conclusions

1) The best regime of OH is a high value of $\iota_h = 0.7 - 0.9$. Moving into the region of the m=1, n=1 mode at low currents ($\iota_h = 0.9$) is not connected with strong instabilities at $\iota = 1$.

2) The maximum current which can be used for efficient ohmic heating is given by $\iota_c \approx 0.4 - 0.5$. This value of ι_c is limited by MHD instabilities, the main mode being m=1, n=1. The regions $\iota_c < 0$ and $0 < \iota_h < 0.7$ are worse due to decreasing $\iota = \iota_c + \iota_h$ and an increase of the level of the MHD instability.

3) It is important to note that tokamak type hard disruptions are absent if the magnetic field is strong enough.

V. References

[1] R.M. Sinclair, S.Yoshikawa, W.Z. Harris, K.M. Yong, K.E. Weimer, J.Z. Johnson. Phys.Fl., 8, 118, 1965

[2] V.Z. Amelin et al.. "Ukrainian Physical Journal" (in Russian) 44, 1796, 1974.

[3] V.M. Zalkind, et al.. "Journal Technical Physics"(in Russian) 44, 1796, 1974.

[4] A.G. Diky et al., preprint 75-36 (Kharkov Physical Technical Institute), 1974

[5] J.K. Kuznetsov et al., preprint 75-34 (the same), 1975.

[6] A.G.Diky et al. "Plasma Physics" (in Russian), 3, 6, 1977.

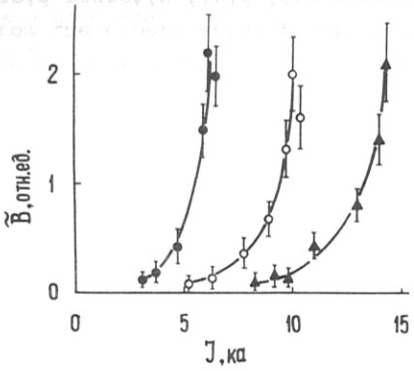

Fig. 1

$B\varphi$ = 7.2 kG (●)

12.0 kG (O)

18.8 kG (▲)

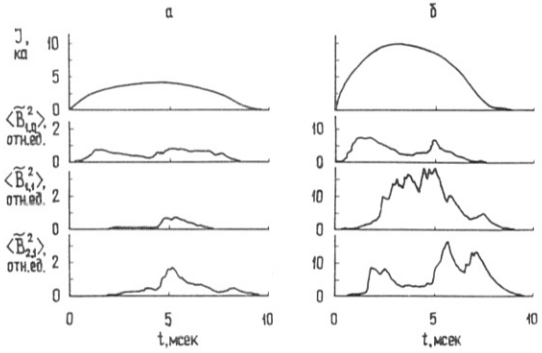

Fig. 2

$B\varphi$ = 16.8 kG

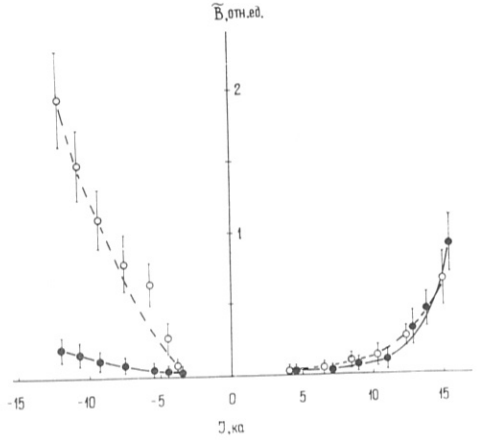

Fig. 3

● m=1, n=1

O m=1, n=0

$B\varphi$ = 16.8 kG

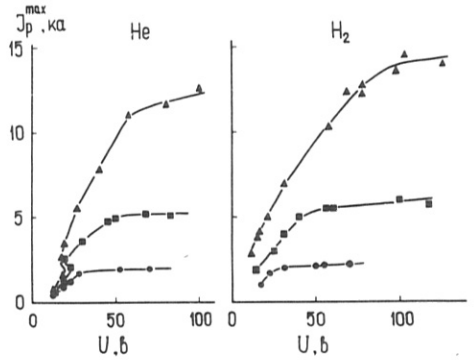

Fig. 4

$B\varphi$ = 2.4 kG (●)

7.2 kG (■)

16.8 kG (▲)

Fig. 5

m=1, n=1

$B\varphi$ = 7.2 kG

$t_h(a)$ = 0.75

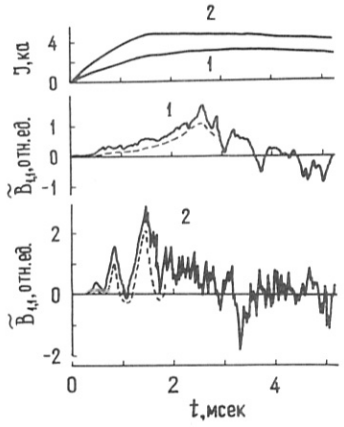

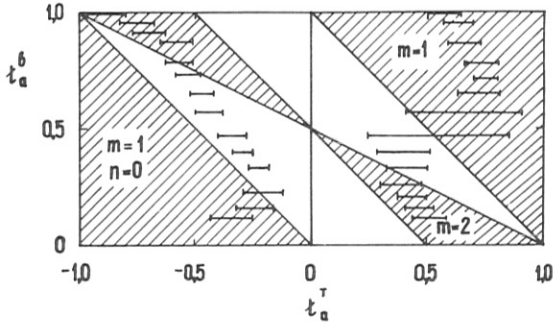

Fig. 6

$B\varphi$ = 2 kG - 20 kG

H_2, He

$\bar{n}_e = 0.2 - 2 \cdot 10^{13} cm^{-3}$

$\bar{T}_e$ = 50 eV - 300 eV

D 6

DISRUPTIONS IN THE STELLARATOR W VII-A

- Part I -

W VII-A Team
presented by P.Smeulders

Above an external rotational transform of $\iota_o = 0.14$ no current disruptions have been observed in the W VII-A stellarator. The l=2, m=5 field windings apparently increase the plasma stability. This is clearly seen from Fig. 1. The maximum achieveable density is a rapidly increasing function of ι_o. The apparent disruption limit is indicated by the solid line. At higher ι_o the maximum achieveable density is no longer limited by the disruptions, but by a collapsing confinement as reported previously [1], indicated by shaded lines. The observed disruptive discharges are marked in the figure. Because of the forthcoming neutral injection, the emphasis of the experimental programme has been laid on the high density regime and the collapse of the energy confinement. Therefore, a full systematic study of the current disruptions has not been made and we will base our analysis on a relatively low number of discharge types, in which hard or soft current disruptions happened to occur. Mostly they tend to occur at high electron densities when the energy confinement already starts to decline with increasing electron density.

Why disruptions suddenly occur is still not fully understood. They appear on one discharge in the middle of a series of identical shots for no obvious reason. In W VII-A they appear usually at that time in the discharges when a normal internal disruption should occur or just after.

The current disruptions have to be separated into two stages. The first or early stage is similar to the previous less harmful internal disruptions. The second stage is related to the plasma current decay. We will treat the first stage first and come to the second stage later on.

The first fast stage of the current disruption

The difference between an internal and external or current disruption from the experimental point of view is the extent of the assumed rapid magnetic field line connection (or ergodisation) over the plasma cross-section. In the case of an external disruption, the ergodisation reaches practically up to the plasma

wall. Because of the random appearance of the current disruption in time, statistical effects are very likely to play a role (for instance, the overlapping of several ergodizing islands stochastically in time). The left half of Fig. 2 shows the X-ray intensity radial profiles before a disruption (solid line) and after an external disruption (broken line). The steep X-ray intensity profile before the disruption is caused by the strong dependence on the electron temperature of the soft X-ray emission. Hence, the X-ray radial profile during the external disruption being rather flat clearly indicates that the plasma must have a more or less homogeneous electron temperature and density. In other words, ergodisation over the whole plasma cross-section has taken place in contrast to internal disruptions which only can have limited ergodisation in space (right half of Fig. 2).

This ergodisation is of course a feature common to all current disruptions. However, the circumstances that seem to lead to or are associated with the disruptions are not always the same. At lower $\iota(a)$, the disruptions are always associated with large (1,1) and (2,1) modes. A faster mode (supposed to be a (3,2) mode) is usually superposed on the X-ray signals. At high $\iota(a) \sim 0.5$ the (2,1) mode is usually not visible. A relatively large (3,2) mode and an irregular (1,1) mode are dominant. By allocating a radial position at which the disruption appears to start to each type of disruption, an attempt to classify the disruption has been made. This radial position is defined by the initial inversion point of the disruption as seen by the X-ray diode aray.

At low $\iota_o = 0.017$; $I_p = 25$ kA; $\iota(a) = 0.25$ the disruption appears to start from the q=1 surface. A strong (2,1) is coupled to the (1,1) mode. During these disruptions there is evidence of a faster supposed (3,2) mode.
At higher $\iota_o = 0.055$; $I_p = 25$ kA; $\iota(a) = 0.29$ (Fig. 3), it is not very clear at which rational q position the disruption starts. In this series of shots, the internal disruptions have occasionally the appearance of predisruptions usually observed at lower electron densities [2]. Such a disruption is just visible on the left side of the figure. At other times it seems the q=1 radius has moved outwards followed by a sawtooth disruption initiated at the q=1 surface. Again at other times it looks more like a m=2 sawtooth disruption. Shortly before the current disruption,

the supposed (3,2) mode is growing in amplitude. This series of shots is perhaps a good example that it is not so important which mode triggers off the disruption. At still higher ι_o = 0.11 and 0.14 and higher plasma currents I_p = 35 kA (ι(a) = 0.5), the m=2, n=1 mode is no longer visible. The disruption appears to be a large internal disruption (Fig. 4) starting from the q=1.0 surface at r = 5.5 cm. (However, in certain cases the disruption seems to start further outwards close to the q = 1.5 radius.) The m=3, n=2 is clearly visible and modulated during each disruption.

A further feature of Fig. 4 is the irregular mode and sawteeth behaviour.

This irregular behaviour has mostly disappeared at lower densities, but in this case also occasionally a quasi stationary m=1 asymmetry becomes visible on the X-ray signals. During the internal disruption (Fig. 7) the island rotation is apparently no longer impeded and oscillations over roughly one period occur.

Such an impeded rotation of the m=1 however has only occurred at lower ι(a) values together with the coupled (2,1) island, which was locked on the outer limiter segment.

At even lower densities a distorted slow turning (2,1) mode appears on the Mirnov coils as well as on the X-ray diodes. A further evidence of a stationary m=2 island structure comes indirectly from the observation of increased plasma losses around q(a) = 2 when the plasma current is varied during the discharge. Precisely then the m=2 is no longer visible.

So even for the current disruptions with q(a) ~ 2.0, the m=2 may take part in the field line connection.

References

[1] W VII-A Team: Energy and Particle Confinement in the Ohmically Heated W VII-A Stellarator, Proc. 7th Int. Conf. on Plasma Physics and Contr. Nucl. Fusion Research, Innsbruck (1978) IAEA-CN-37-H-2

[2] W VII-A Team: Proc. 8th European Conf., Prague (1977), 1, 127, and 2 (1977) 236

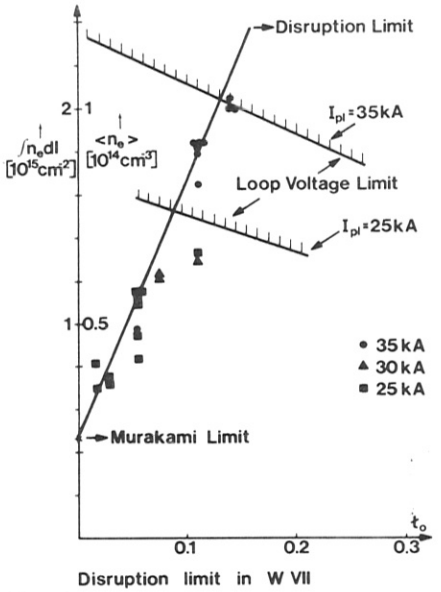

fig.1

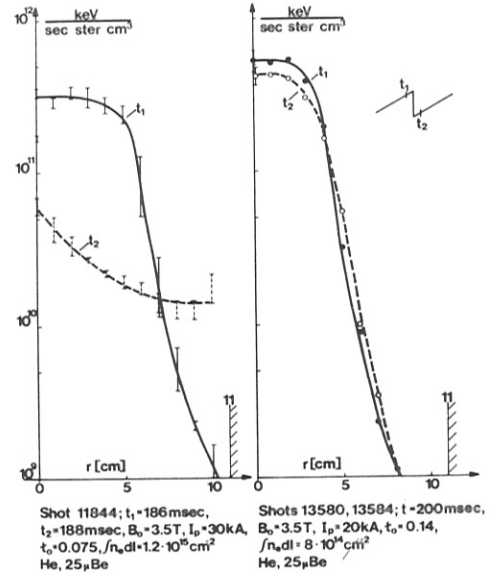

fig.2

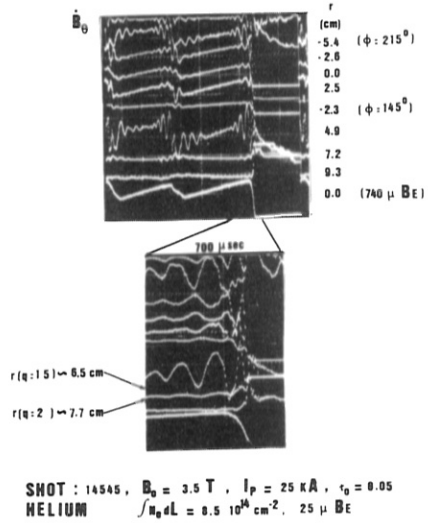

fig.3

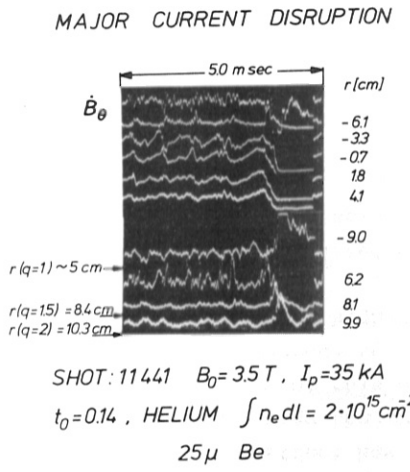

fig.4

DISRUPTIONS IN THE STELLARATOR W VII-A

- Part II -

W VII-A Team

presented by P.Smeulders

Circumstances leading to current disruptions

Except for the values of $\iota(a) \sim 0.5$, current disruptions are associated with a strong increase of the tearing modes, especially the (2,1) when either the density or the plasma current is increased. A possible explanation of the increase of the mode amplitude is given in Ref. [3]. At the same time, the q=1 surface expands with increasing electron density and with increasing $\iota(a)$. Fig. 1 shows such expanding q=1 surface as a function of the line density. Also indicated in this figure are the positions of the q=1.5 and the q=2 surfaces. (These positions are only slightly dependent on the current density radial profile). It is obvious that the diminishing distance between the islands favours their overlapping.

In the case of the increase of the density the r(q=1) expansion is likely to be caused by increased radiation cooling of the plasma edge [1]. The maximum expansion of the q=1 surface as deduced from the measurements never exceeds 6 cm.

The influence of ι_o on the disruption

The external rotational transform ι_o has a threefold influence on the disruption:

1) It puts the outer resonance surfaces on positions with flatter current gradients. Therefore, it reduces the mode amplitude as can be seen from the X-ray signals. The outer Mirnov coil signals show a similar dependence of the (2,1) mode on ι_o and $\int ndl$ [3].

2) It increases the distance between the resonant surface especially at high densities (Fig. 1).

3) It provides an additional toroidal equilibrium, like a copper shell in a tokamak (but on a longer time scale).

The second stage of the current disruption

The influence of ι_o on the toroidal equilibrium is to reduce the effect of the decrease in β_θ and l_i. In the case of soft current disruptions, some evidence of this stabilizing effect has been found (a decrease of the inward displacement during the soft disruptions with increasing ι_o). A systematic study of this effect as a function of ι_o has not been possible however due to an insufficient number of shots with soft disruptions at higher ι_o.

In W VII-A the plasma position is temporarily stabilized by the external rotational transform. Whether or not the plasma recovers (soft or hard current disruptions) depends on the availability of sufficient energy before the current starts to decay.

Soft current disruptions usually occur in W VII-A for lower ι_o, where the electron temperature is fairly high and thus the loop voltage reasonably low. The plasma energy loss due to the disruption is then mainly compensated by the flux variation in the OH transformer (with a limitation of 10 volts) and, partially, by the magnetic energy of the plasma current (only a minor drop in the plasma current occurs). The left part of Fig. 2 shows such a soft disruption at $\iota_o = 0.05$. At higher $\iota_o \geq 0.11$ and high densities, the loop voltage is already close to the 10 volt limit, due to the lower central electron temperature. Thus, the energy loss due to the disruption can only be compensated by the external magnetic energy of the plasma current which then decays on a resistive time scale. The same can happen at the end of a discharge when the available flux in the OH-transformer has been depleted (right part of Fig. 2). The limited plasma displacement can clearly be seen in the figure. In the case of the hard current disruption however the plasma is pushed further inwards, because of the decaying plasma current. The vertical field with a time constant of $\sim$ 50 msec becomes much too large.

In conclusion

A clear improvement in the maximum line density permitted by current disruption with increasing t_o has been found. In W VII-A the current disruptions that have occurred start predominantly from the q=1 or the q=2 surface. Around the time of the disruptions the following modes are observed on the X-ray signals: a (1,1) mode, at lower $t(a) < 0.5$ coupled with a (2,1) mode, and a (3,2) mode. This suggests an overlapping of up to perhaps three islands as a possible cause of the initial stage of the current disruption. A stochastical overlapping in time would explain the haphazard occurrence of such disruptions in a discharge.

The second stage seems to be governed by the flux still available in the OH-transformer. A hard current disruption seems to develop only if the flux change is insufficient to re-establish the stationary condition as in the case for a soft current disruption.

References

[1] W VII-A Team: Energy and Particle Confinement in the Ohmically Heated W VII-A Stellarator, Proc. 7th Int. Conf. on Plasma Physics and Contr. Nuclear Fusion Research, Innsbruck (1978) IAEA-CN-37-H-2.

[2] W VII-A Team: Proc. 8th European Conf., Prague (1977), 1, 127 and 2 (1977) 236.

[3] W VII-A Team: Effects of the Stellarator Field on the MHD-Mode Behaviour Close to the Disruption Limit in W VII-A. This symposium.

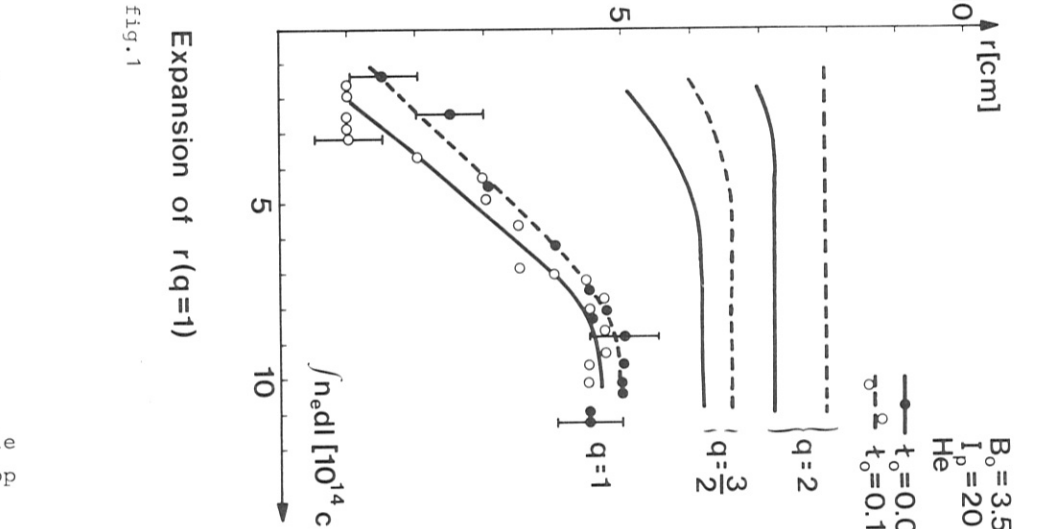

fig.1

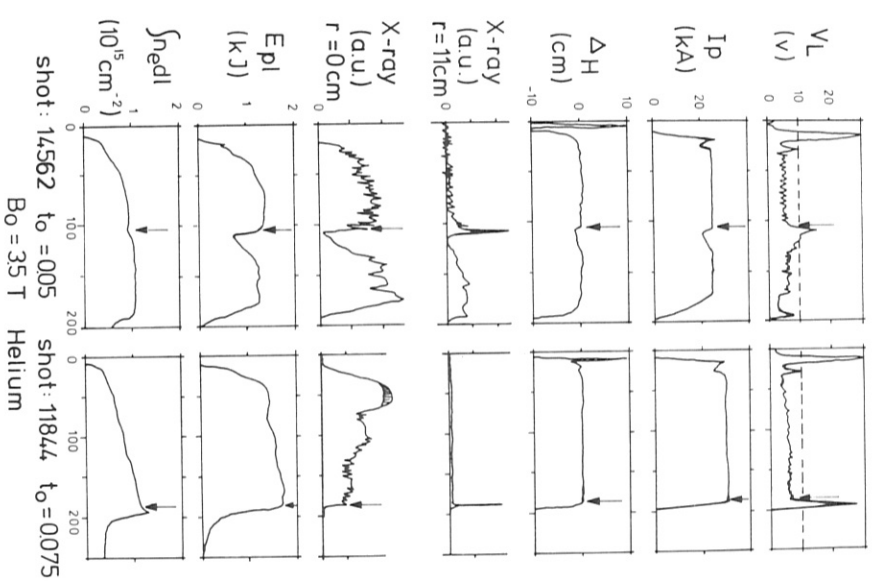

fig.2

SAWTOOTH OSCILLATIONS AND MAGNETIC ISLANDS IN THE TOSCA TOKAMAK

D C Robinson and K M McGuire*
Culham Laboratory, Abingdon, Oxon. OX14 3DB, UK
(Euratom/UKAEA Fusion Association)

ABSTRACT

Scaling from sawtooth repetition times indicate that the m=1 instability is a tearing mode. m=3 islands of width $\gtrsim$ 2 cm can cause minor disruptions. The major disruptions are caused by m=2 islands of 3 cm.

INTERNAL DISRUPTIONS

Internal disruptions or sawtooth oscillations have been observed and studied on the small tokamak TOSCA [1] (R=30 cm, a $\lesssim$ 8.5 cm, $n_e(o) = 3 \times 10^{13} cm^{-3}$, $T_e(o)$ = 300 eV). These investigations of the internal m=1, n=1 mode and the sawtooth oscillation have been extended to the effects of shaping the plasma cross-section, in particular for triangular plasmas. The internal disruptions are observed with a seven detector array of surface barrier detectors that are sensitive to soft x-rays in the photon energy range between 0.8 and 10 keV. The soft x-ray signal obtained with one of the surface barrier detectors when there is a peaked current distribution is shown in figure 1, for a circular plasma. The sawtooth oscillation represents approximately a 4% variation in temperature, its period is typically 100→200 μs. The sawtooth oscillation has a modulation superimposed on it with a frequency of 40→60 kHz. This modulation is identified, with two x-ray detectors which are at different positions in the toroidal and poloidal directions, as an m=1, n=1 mode.

A comparison of sawtooth oscillations in circular and triangular plasmas has been carried out. From the experiments, it is found that sawteeth are still present, and that their amplitude is increased with $\frac{\hat{\Delta A}}{A}$ about 20%. However, theory predicts that a certain level of triangularity should stabilise the internal ideal MHD, m=1, n=1 mode for $\hat{\beta}p \approx 1$ though it should be noted that the mode may be stable even for a circular plasma with $\hat{\beta}p \lesssim 0.3$.

m=2 DISRUPTIONS

Sawteeth oscillations are not present in all discharges on TOSCA. When a flat current distribution is present, a large amplitude m=2 mode is observed. When the amplitude of the m=2 mode reaches about $\hat{b}_r/B_\theta \sim 1\%$, ($\hat{b}_r$ is the peak radial field at the resonant surface and B_θ is the poloidal field) the plasma starts to cool as evidenced by a fall in soft x-ray emission. At 2% a minor disruption may result and at 5-6% major disruption usually occurs.

From an examination of the internal diamagnetic loop signal, a decrease in plasma energy is observed when the amplitude of the m=2 signal has reached $\hat{b}_r/B_\theta \approx 2\%$ level. In addition previous Langmuir probe measurements have shown the presence of particles at the wall correlated with the m=2 mode. Both of these observations suggest that the m=2 activity above a certain level ($\hat{b}_r/B_\theta \sim$ 3%) is correlated with a direct particle loss.

SAWTOOTH REPETITION TIME

From a comparison of the sawtooth period on other devices, it is apparent that the maximum period of the sawtooth oscillations on TOSCA is much shorter. This fact and the results from other ohmically heated tokamaks is used to obtain a scaling law for the period of the sawtooth.

Several theories have been put forward to explain the sawtooth relaxation. Resistive heating, accompanied by a reduction in q, is followed by the growth of a m=1 instability which could be an ideal MHD mode, internal resistive kink, or a tearing mode. The observations suggest that the mode must be resistive in origin. The repetition time will depend on the time scale for the reduction of q below unity and the dependence of the growth rate of the resistive mode on shear, with an allowance for diamagnetic drifts.

Solving the field diffusion equation and the heating equation for the small decrease in q below unity, we obtain $\Delta q \propto \frac{t}{\tau_h}$ (τ_h is the heating time) to a good approximation. The sawtooth repetition time is then determined by using this variation in the dependence of the growth rate on shear and assuming that heating is terminated when the m=1 island width, produced by the resistive mode grows to r_s, (r_s is radius of q=1 surface). Our results indicate that the tearing mode scaling without the inclusion of diamagnetic drift effects appears to give a good fit to the data. This scaling is somewhat similar to that obtained by Waddell et al [2].

MINOR DISRUPTIONS

Magnetic field measurements have been made in the outer regions of the plasma on TOSCA [3]. A probe consisting of 24 coils 4mm apart is used to measure simultaneously the radial, poloidal and toroidal fields. The probe can be inserted 5 cm into the plasma vertically without affecting the conductivity temperature ($\sim$ 30 eV for these measurements) or the magnetic oscillations measured with external coils. Figure 2 shows the radial distribution of the m=3 oscillating radial and poloidal field components and the arrow indicates the position of the surface where q, the safety factor, is equal to 3. The amplitude of the radial magnetic field component reaches a maximum of about 3% of the peak poloidal field. Earlier in time a m=4 perturbation with somewhat smaller

University of Oxford

amplitude is often seen. The rate of change with time of the maximum radial field is observed not to be sinusoidal in character, though the higher harmonics are reduced near the vacuum vessel wall. Soft x-ray measurements sometimes shows a similar non-sinusoidal behaviour for the m=2 mode.

If the m=3 mode increases in amplitude above about 3% , the plasma performs a minor disruption, i.e. the current density is observed to broaden in less than 10 μs. The plasma always recovers from these minor disruptions. When the m=2 mode increases in a similar way, a single larger positive going spike on the internal poloidal field is produced. We have no explanation for the 'poloidal field spike' on the basis of a simple Ohm's law, however, it may be due to a localised phenomena in the plasma near the probe. The spike is not observed outside the current carrying column.

Computed radial and poloidal fields for a tearing mode are obtained using an initial value calculation in cylindrical geometry with the measured current distribution and experimental parameters, when a m=3 mode is observed. The agreement between theory and experiment is quite good. The magnetic islands produced have a width of up to 2.0 cm for a 3% amplitude. The experimental situation is more complicated, the non-sinusoidal character shows that the magnetic islands are more elongated than the theory predicts. Experiments with both external m=2 and m=1, n=1 coils designed to deliberately interact with the islands produced by instabilities, show only small effects on the internal or m=2 disruptions,

CONCLUSIONS

The sawtooth relaxation appears to be due to resistive heating, accompanied by a reduction in q, which is followed by the growth of an m=1 instability which is due to a tearing mode. Our results show that triangularity does not suppress the internal m=1 instability. The m=3 mode causes a minor disruption when the island width is ≥ 2 cm. The m=2 islands reach 3.0 cm in size before a major disruption occurs and no other mode is usually observed in the disruptive process.

REFERENCES

[1] McGuire K M and Robinson D C, CLM-P552.

[2] Waddell B V, Jahns G L, Callen J D, and Hicks H R, Nuclear Fusion, 18, (1978) 735.

[3] Robinson D C and McGuire K M, Nuclear Fusion, 19, (1979), 115.

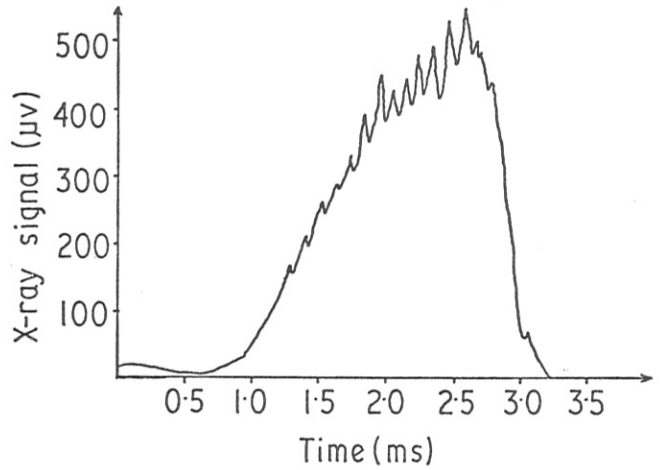

Fig. 1 Soft X-ray emission as a function of time for a circular plasma.

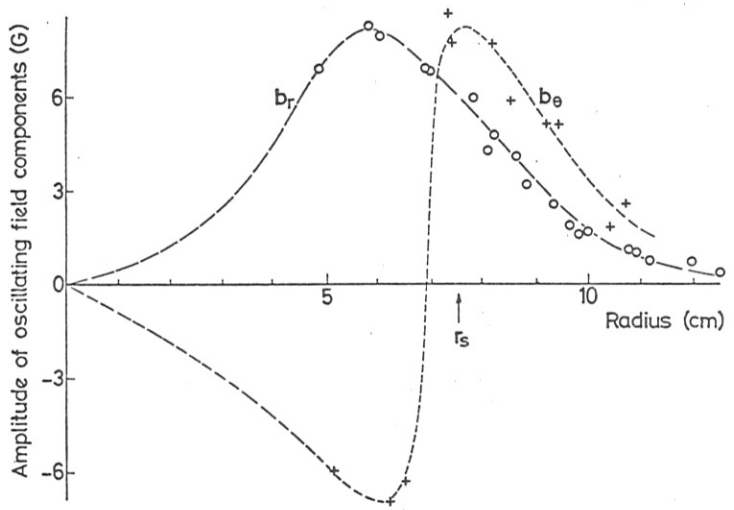

Fig. 2 Radial distribution of oscillating radial and poloidal field components. The radius at which q=3 is indicated by r_s.

TOROIDAL PUMPING OF AN INTERNAL (m = 1, n = 1) MODE BY A TEARING MODE (m = 2, n = 1)

D. Edery, R. Pellat* and J.L. Soulé

Association EURATOM-CEA sur la fusion
Département de Physique du Plasma et de la fusion contrôlée
Centres d'Etudes Nucléaires
Boîte Postale n° 6. 92260 Fontenay Aux Roses (France)

---

1) Introduction

In some Tokomak experiments [1,2] a (m = 1, n = 1) phase locked mode appears simultaneously with a (m = 2, n = 1) Tearing mode. It has been previously shown [3] that such a coupling is to be expected in toroïdal geometry.

Since many years our group [4] has been involved in computing the consequences of resonant non linear mode coupling resulting from poloïdal [5] or toroïdal modulations [6] in equilibrium configurations. Such effects are of two kinds : the first one is a "quasilinear effect" which has been used to investigate the influence of ellipticity, triangularity [5] or toroïdal curvature [6] upon the internal kink mode. That effect is of a second order in the smallness parameter (ellipticity, triangularity, inverse of aspect ratio). The same kind of quasilinear effect is used in the understanding of the cross interaction of Tearing modes in cylindrical geometry [7] if islands of different pitch do not overlap : it is in fact a renormalization of equilibrium properties.

The second kind arises when the non linear coupling drives a mode close to marginal stability ; in such a case, the effect is much stronger and may be compared to the classical resonant three waves coupling. To illustrate our point, we compute in this short note the toroidal coupling between an internal mode (m = 1, n = 1) with a Tearing mode (m = 2, n = 1). The (m = 2) mode is often proposed [8] as being responsible of the main disruption and is observed to reach large amplitudes. On the other hand the (m = 1) modes is usually close to marginal stability (q on the axis has values of order unity). Such a situation is likely to result from a combined effect of the shrinking of the current channel (produced by cold plasma on the edge or by the development of a large m = 2) and the sawtooth relaxation following an unstable internal resistive kink [3, 9]. In our previous work [3] we had taken $q \lesssim 1$, which corresponds to the Sawtooth. We consider now a simpler situation, $q \gtrsim 1$ which means that in the low β limit [6] the internal kink (ideal or resistive) is stable.

The computation can now be achieved in a quite general way if we assume $k V_A > \omega_1^* \frac{\partial}{\partial t}$ where ω^* is the standard drift frequency and $\frac{\partial}{\partial t}$ the the linear or non linear growth of the m = 2 mode.

Our computation needs two steps : we first give the general equation for the first order toroïdal coupling between two modes (m,n) and (m + 1, n).

*also Groupe de Physique Théorique de l'Ecole Polytechnique, 91128 Palaiseau, France.

That coupling results from the toroidal modulation (m = 1, n = 0) of the metrix element. We then specialize our final results to the case (m = 1, n = 1) and (m = 2, n = 1) but a similar explicit computation can be easily achieved for (m = 3, n = 1) and (m = 2, n = 1).

2) Formalism and equation for two coupled modes

When we analyse internal modes we have to separate the resonant layer (or the island) where $(m - nq) \simeq 0$ from the outside MHD region. The dynamics has to be included only in the resonant layer. Lest us consider now the MHD region. To the first order in aspect ratio and in the limit of low β plasma the coupling is well described by the toroidal equation for the perturbed poloidal flux ψ :

$$\underset{\sim}{B}_o \cdot \underset{\sim}{\nabla}\left(L\psi\right) + \frac{d}{dF}\left(R J_{o\phi}\right) \underset{\sim}{B}_{om} \cdot \underset{\sim}{\nabla}\psi = 0 \qquad (1)$$

$\underset{\sim}{B}_o$ is the equilibrium magnetic field, $\underset{\sim}{B}_{om}$ its poloidal component :

$$\underset{\sim}{B} = \underset{\sim}{\nabla}F \times \underset{\sim}{\nabla}\phi + T(F)\underset{\sim}{\nabla}\phi$$

with $$R J_{o\phi} = T\frac{dT}{dF} = -LF = -R^2 \underset{\sim}{\nabla}\cdot\left(\frac{1}{R^2}\underset{\sim}{\nabla}_m F\right)$$

$J_{o\Phi}$ is the equilibrium toroïdal current and F the equilibrium poloidal flux. To solve equation (1) it is convenient to introduce an intrinsic system of coordinates r, θ given by [6] $\frac{r^2}{2} = R_o \int_0^F \frac{q(F)dF}{T(F)}$ and $\theta = (T/q)\int_0^\ell d\ell / R^2 B_m$. The toroïdal effect only appears in the metrix elements. Equation 1 now reads :

$$\left(\frac{1}{q}\frac{\partial}{\partial\theta} + \frac{\partial}{\partial\phi}\right)\left\{\frac{1}{r}\frac{\partial}{\partial r}\left(r\,\underset{\sim}{\nabla}r\cdot\underset{\sim}{\nabla}\psi\right) + \frac{1}{r}\frac{\partial}{\partial\theta}\left(r\,\underset{\sim}{\nabla}\theta\cdot\underset{\sim}{\nabla}\psi\right) + \frac{d}{dF}\left(T\frac{dT}{dF}\right)\frac{1}{q}\frac{\partial\psi}{\partial\theta}\right. = 0$$

All the metrix elements and their derivatives can easily be expressed with the function Λ(r) [10] defined by : $B_m = \langle B_m \rangle \left[1 + \frac{r\Lambda}{R_o}\cos\theta\right]$

where $$\Lambda + 1 = \left(q/r^2\right)^2 \int_0^r r^3 dr / q^2$$

We take a Fourier representation of the poloïdal flux :

$$\psi = \sum \psi_{m,n}(r)\exp\left(im\theta - in\phi\right) \qquad (2)$$

and expand equation (1) to first order in the inverse of the aspect ratio : a mode (m, n) is coupled to a mode (m - 1, n) and a mode (m + 1, n) ; we assume, in this note a large, unstable, (m + 1, n) mode and a negligible, non resonant, (m - 1, n) mode. We then obtain :

$$\mathcal{L}_c(m,n)\xi_m = \frac{1}{T_o}\left(\frac{1}{q} - \frac{n}{m}\right)\left\{\frac{d}{dr}r^2(1+\Lambda)\frac{d\psi_{m+1}}{dr} + \frac{m+1}{2}\frac{d}{dr}\psi_{m+1}\,r\left(r\Lambda' + 2\Lambda + 3\right)\right.$$

$$\left. + \frac{mr}{2}\left(r\Lambda' + 2\Lambda + 3\right)\frac{d\psi_{m+1}}{dr} + m(m+1)(\Lambda+2)\psi_{m+1}\right\}$$

it has been convenient to introduce the Newcomb operator $\mathcal{L}_c$ in cylindrical

geometry, and the displacement ξ_m defined by $\psi_m = -\frac{T_o r}{R_o}\left(\frac{1}{q}-\frac{n}{m}\right)\xi_m$,

T_o and R_o being the values on the magnetic axis. Up to now our formalism is independent of the precise value of (m, n); we now choose [m = 1, n = 1] to illustrate the coupling in a case very important for experimental results, if moreover we take $q \gtrsim 1$ we have no singular layer at m = 1 and the MHD equation remains valid in all the plasma.

3) Toroidal pumping of the internal mode by the Tearing (2,1)

That choice allows a first integration of equation (2)

$$T_o\left(\frac{1}{q}-1\right)^2\frac{d\xi_1}{dr} = \left[\left(\frac{1}{q}-1\right)(1+\Lambda)+\left(\frac{1}{q}-\frac{1}{2}\right)\left(\frac{3}{2}+\Lambda\right)\right]\frac{d\psi_2}{dr}$$
$$-\frac{\psi_2}{r}\left[2r\left(\frac{d}{dr}\frac{1}{q}\right)(1+\Lambda)(1-q)+r\left(\frac{d}{dr}\frac{1}{q}\right)\left(\frac{3}{2}+\Lambda\right)+\Lambda\left(\frac{2}{q}-3\right)+\frac{1}{q}-1\right]$$

Knowing ψ_2 the solution is reduced to a quadrature. In TFR 400 [1], when the major disruption occurs the sawtooth has disappeared which may justify our choice of $q(0) \geq 1$. We consider a family of flat current profiles on the axis:

$$J(r) = J(0)\left[1-\left(\frac{r}{a}\right)^{2K}\right]^{\ell}$$ and select three cases which have the same q(a) = 3,3 at the limiter and close values of q on the axis.

1) $J(r) = J(0)\left[1-\left(\frac{r}{a}\right)^2\right]^2$; $q(0) \sim 1,086$

2) $J(r) = J(0)\left[1-\left(\frac{r}{a}\right)^4\right]^5$; $q(0) \sim 1,12$

3) J(r) uniform for $r \leq r_o = a/\sqrt{3}$ and zero for $a/\sqrt{3} < r \leq a$ $q(0) \sim 1,1$. In

that case one integrates exactly equation (2) and obtains inside the current channel a parabolic behaviour of ξ_1 with respect with r :

$$\frac{d}{dr}\left[\frac{T_o \xi_1}{\psi_2(r_o)}\right] = -\frac{5}{2}\,\frac{q}{1-q}\,\frac{r}{r_o^2}$$

For an explicit comparison with modulation of the poloidal magnetic field on the plasma edge. Some simplifying assumptions will be made, which may be early released.

We take the X ray signal $A = \lambda\, ne^2\, Te^2$ and neglect the possible variation of λ with the Z factor. For TFR 400 $A \sim [1-(r/a)^2]^4$. The line integrated modulation of A is easily related to the m = 1 displacement :

For ξ_1 of parabolic type one obtains $\frac{\delta A_1}{A} = -C\,\xi_1\,\frac{d\,Ln\,A}{dr}$ with C ~ 0,6; 0,7 ; 0,75 in respectively cases 1,2,3 for the current profile. We have numerically computed the quantity $T_o\,\xi_1/\psi_2(r_2)$, with $q(r_2) = 2$, which is justified by the negligible dependance of ξ_2 upon the detailed behaviour of ψ_2 for $r > r_2$. It is then straightforward to relate $\frac{\delta A_1}{A}$ to $\frac{\delta B_\theta (m=2)}{B_{\theta_o}}$ on the edge :

$$\frac{\delta A_1}{A_1} = C\,\frac{a}{q(a)R_o}\,\frac{\delta B_\theta}{B_{\theta o}}\left[\frac{a}{\psi(r_2)}\,\frac{d\psi_2}{dr}\Big|_{r=a}\right]^{-1}\frac{a\,d\ln A}{dr}\left[\frac{\xi T_o}{\psi_2(r_o)}\right] \quad (3)$$

is a numerical factor which is not easy to know because it depends upon the skin time of the copper shell and the effective boundary condition upon the mode m = 2 ; as an example in case 1 it varies between 0,75 to 2,3 if b/a varies from 3 to 1, with $\psi_2(b) = 0$.

The table of values for $\frac{\xi T_o}{\psi_2(r_o)}$ and for $\frac{\xi T_o}{\psi_2}\frac{d}{dr}$Ln A are given below :

r/a	1	2	3
0	18	24	34,8
0,1	16	23	33,7
0,2	12,2	19	30,6
0,3	8	14	25,7
0,4	4,8	8,5	18,6
0,5	2	4	9,5

r/a	1	2	3
0	0	0	0
0,1	13	18,6	27,3
0,2	20,4	31,7	51,1
0,3	21,1	37	67,8
0,4	18,3	32,4	70,9
0,5	10,7	21,3	50,6

If the current profile is flat the signal is more delocalized and the value at the center is inversely proportional to (q - 1). For a fat torus and a modulation of the poloidal field of a few per cent, the modulation of the X ray signal is also a few per cent ; in the case of TFR 400 the best agreement is achieved for a fat current (case 3) and $q - 1 \sim 0,05$. The (m = 1) X ray signal appears as a possible diagnostic of the current profile, being very sensitive by its amplitude on the axis to (q - 1) and its extension to the variation of q. If $q \to 1$, ψ_1 remains finite of order $(a/R)\psi_2$ but ξ_1 becomes divergent. It means that our expansion procedure in the inverse of the aspect ratio holds but the "resonant layer" for q = 1 will introduce dynamical and non linear effects. The reaction of the mode m = 1 upon the m = 2 has been found negligible.

As a conclusion, a large m = 1, n = 1 internal mode may be driven by a Tearing m = 2, n = 1 during the main disruption in agreement with experimental results of TFR 400. During this conference a similar behaviour has been reported by the Kurchatov team. It has also been reported that modes are often observed with $(m - nq) \neq 0$ with follows the property of toroidal coupling with small aspect ratio.

Our effect is much smaller in the case of a torus with a large aspect ratio and for the Stellerator WIIIA. The cylindrical sawtooth should be the dominant m = 1 mode.

References

1) Equipe TFR, Nuclear Fusion, 17, 6, 1977.
2) S.V. Mirnov - V.G. Merezhkin, This symposium.
3) M.N. Bussac and Al, Proc. of the 6th , International Conference of Berchtesgaden 1976. 1IAEA, Vienna (1971) 607.
4) M.N. Bussac, D. Edery, G. Laval, R. Pellat, J.L. Soulé
5) D.Edery and Al, Physics of Fluids, Vol.19, No2(1976)
6) M.N. Bussac and Al, Phys. Rev. Lett., Vol 35, No 24 1638 (1975)
7) H.P. Furth , This symposium
8) R.B. White and Al, Phys. Rev. Lett. Vol 39, No 25 (1977)
9) B. Coppi and Al, Sov. J. Plasma Physics 2 (1973) 533.
10) A.A. Ware and Al, The Physics of Fluids, 9, 956 (1966).

Author Index